Mechanisms and Effects of NAD+ Modulation in Inflammation and Aging

Mechanisms and Effects of NAD^+ Modulation in Inflammation and Aging

A dissertation presented

by

Michael Benjamin Schultz

to

The Division of Medical Sciences

in partial fulfilment of the requirements

for the degree of

Doctor of Philosophy

in the subject of

Biological and Biomedical Sciences

Harvard University

Cambridge, Massachusetts

May 2019

Dissertation Advisor: Professor David A. Sinclair Michael Benjamin Schultz

Mechanisms and Effects of NAD^+ Modulation in Inflammation and Aging

Abstract

Levels of nicotinamide adenine dinucleotide (NAD^+) fall during aging for reasons that are not fully understood. Caloric restriction, the most effective intervention to slow aging, prevents this fall, and pharmacological restoration of NAD^+ levels slows or reverses many aspects of age-related disease.

In Chapter 2, I identify the enzyme PARP14, induced by inflammation, as a novel driver of declining NAD^+ levels. As chronic inflammation is a conserved characteristic of aging, we examined the effect of inflammatory stimuli on NAD^+ levels in bone marrow-derived macrophages. Toll-like receptor agonists were found to induce a drop in NAD^+ levels. Through pharmacological and genetic approaches, we identified PARP14 as necessary for such NAD^+ destruction. We also identified a potent, synthetic NAD^+ precursor, nicotinamide riboside hydride. PARP14 levels increase during sepsis and PARP14 inhibition or deletion restored NAD^+ to normal levels in spleens of septic mice. PARP14 also increased during aging, and PARP14 inhibition restored splenic NAD^+ to youthful levels. Our results suggest that PARP14 inhibitors and potent synthetic NAD^+-precursors are promising drug candidates for the treatment of age-related diseases.

In Chapter 3, I explore the interaction between NAD^+ levels and expression levels of the sirtuin gene family on aspects of aging. Sirtuins are NAD^+ sensors that promote health and longevity. We boosted the expression of the entire sirtuin gene family with adeno-associated viral vectors in 20-month old mice, in combination with dietary supplementation with the NAD^+

precursor NMN. We observed a protection from body weight loss, a protection from muscle weight loss, and a trend towards increased longevity.

In Chapter 4, I describe approaches to estimate biological age based on non-invasive assessment of frailty. We used the frailty index (FI) to assess frailty longitudinally in mice until their natural deaths, and created a model to predict chronological age, termed FRIGHT Age, and a model to predict mortality, termed the AFRAID score. These models may be useful as early indicators of the effectiveness of aging interventions.

Taken together, this dissertation provides new insight into novel regulatory mechanisms and effects of NAD^+ dynamics during inflammation and aging.

Acknowledgments

I would like to thank many people for their support, without which this dissertation would not have been possible. I am truly grateful for all the generosity, inspiration, guidance, and fond memories they have afforded me.

First, I would like thank my thesis advisor, Professor David Sinclair, for welcoming me into his lab and teaching me how to be a scientist. You have always encouraged me to take on challenging, impactful projects, and have taught me the resolve and vision required to push past difficulties. It has been a pleasure and a privilege to learn from and work with you. I am also grateful for the amazing team and community which you have built in the lab and beyond. Our lab meetings are always dynamic, and the lab environment is one that promotes constant growth and learning. I will also always fondly remember the fireworks at the lab's summer parties and Sandra's (equally dangerous) fire punch at the lab's holiday parties!

I owe a large debt of gratitude to Michael Bonkowski. Among the many skills you've taught me are Western blots, mouse genotyping, and how to catch striper in Boston harbor! You have been a huge mentor to me both in lab and in life. The wisdom you've imparted will forever stay with me (and will always be heard in your own voice). I am pleased to call you a friend and to see your and Meg's growing family.

I'd like to thank my fellow graduate students in the Sinclair lab. Those senior to me, Ana Gomes, Alvin Ling, and Thomas Bochaton, served as role model and mentors. Ana and Thomas, even after you left it was so wonderful to continue to receive your mentorship via our regular Skype calls. I have been privileged to welcome as colleagues Yuancheng Lu, Michael Cooney, João Amorim, and Patrick Griffin. The lab is immeasurably stronger scientifically, and an immeasurably more fun place to work, due to your presence in it.

The Sinclair lab staff, Luis, Susan and Karolina, contribute so much to the lab. Your often unsung work gives the rest of us the privilege to focus on our projects. Susan, I will always remember the birthday cake you surprised me with during my first week as a rotation student. Luis, thanks to you the lab has become more organized and efficiently run each year that I've been here. Unlike the lab, your empanadas never had any room for improvement. Karolina, I only wish you had joined the lab earlier in my Ph.D., as you have been a such huge help to all of us.

I'd like to thank every person who has passed through the Sinclair lab during my time there. I've learned something from each of you. I'd especially like to thank Po Hien Ear and Neha Garg, who were mentors for me early in my Ph.D., and Alice Kane who has been an amazing mentor to me these past two years. I've also had the enviable opportunity to work with a talented group of summer students and undergraduates over the course of my Ph.D. Andrew Portuguese, Kristen Simmons, Alex Colville, Brianna Kaplan, Doyle Lokitiyakul, and Yiming Cai, thank you all for choosing to invest your time working with me. The "back bay" just isn't the same without any of you around.

Thank you to the members of my dissertation advisory committee (DAC), Professors Andrew Lassar, Raul Mostoslavsky, Keith Blackwell, and Dianne Mathis. You have given me helpful, insightful advice throughout my graduate career. Andrew also taught one of the most fascinating courses, Vertebrate Development, which I have ever taken. Raul has been a part of my Ph.D. from nearly the beginning, serving on my prequalifying exam committee, on my DAC, and now as chair of my thesis exam committee. I would also like to thank the other members of my thesis exam committee, Professors Jay Mitchell, Amy Wagers, and Steve Helfand. Thank you for taking the time to read my dissertation and for serving as examiners.

Kate, Maria, Danny, and Anne have done an incredible job running the BBS program. From organizing recruitment and the Provincetown retreat to keeping track of all of us spread across Boston and Cambridge, I don't know how you possibly do it. Thank you also to Catherine Dubreuil who runs the Therapeutics Graduate Program, which has provided me with an academic community within the wider expanse of Harvard Medical School. Also, thank you to Yvonne White, who mentored me during an internship in industry, in which I learned a great deal.

I would not have made it to graduate school without inspirational mentors while I was an undergraduate student: Sarah Elgin, Yehuda Ben-Shahar, Liviu Mirica, Kathy Hafer, and Chris Shaffer at Washington University in St. Louis; Phillip Laible and Deborah Hanson at Argonne National Lab; and Stefan Gründer, Stefan Dürnagel, and Marc Assmann at RWTH Aachen. Thank you all for facilitating my first forays into scientific research.

I would not have made it through graduate school without many great friends in the BBS program. Martin Fan, Ryan Alexander, Evgeny Kiner, Jacob Layer, Sanchez Jarrett, Arial Aspiras, Colin Platt, and so many others, thank you for all the fond memories, from sailing and bike rides to trying not to lose all my money at poker.

Last, but not least, thank you to my parents and family. I won the family lottery the day I was born. You inspired my curiosity and interest in science at an early age. Thank you for your unconditional love and support.

Table of Contents

Chapter 1: Introduction

Eos and Tythonis (~470 BCE), British Museum, London

"[Eos] went with a request to [Zeus] asking that [Tythonis] become immortal... Too bad that her thinking was disconnected!... She should have asked for adolescence and a stripping away of baneful old age. Well, for a while [Tythonis] held onto adolescence... [until] the first strands of gray hair started growing from his beautiful head and his noble chin... When hateful old age was pressing hard on him with all its might, and he couldn't move his limbs, much less lift them up... [Eos] put him in her chamber and closed the shining doors over him. From there his voice pours out, it never seems to end, and he has no strength at all."

- Homeric hymn to Aphrodite, translated by Gregory Nagy

Parts of this introduction were adapted from:

Schultz, M.B., and Sinclair, D.A. (2016). When Stem Cells Grow Old: Phenotypes and Mechanisms of Stem Cell Aging. Development. *143*, 3-14.

Schultz, M.B., and Sinclair, D.A. (2016). Why NAD^+ Declines During Aging: It's Destroyed. Cell Metabolism. *23*, 965-966.

Schultz, M.B., Rinaldi, C., Lu, Y., Amorim, J., and Sinclair, D.A. Molecular and Cellular Characterization of SIRT1 Allosteric Activators. Methods Mol. Biol. (*in revision*).

Evolutionary theories of aging

Aging is a phenomenon in living systems characterized by a progressive decline in physiological functions and an associated increase in mortality. It is a process so pervasive that biologists once thought it the inevitable result of accumulated damage over time, an idea first distilled in the Wear and Tear Theory of aging (Weismann, 1882). The lifespans of living systems, however, are not directly analogous to those of durable goods like cars that simply break down with increasing use. Living systems maintain homeostasis and have the ability to repair themselves. As extreme examples of this fact, some organisms have flat or even decreasing mortality with increasing age, such as the hydra and the desert tortoise, respectively (Jones et al., 2014). When viewed through the lens of Darwinian evolution, the fact that aging occurs at all appears to be a confounding paradox, or at best a negligent oversight; perpetual longevity ought to be selected for, as it would allow an organism many more opportunities to reproduce and pass on its own genes. So if aging is not an inevitability of all living systems, why has natural selection not fixed it yet?

Theories that reconcile aging with Darwinian evolution focus on the idea of trade-offs. Two such theories predominate. The first is the Disposable Soma Theory, proposed by Thomas Kirkwood in 1977 (Kirkwood, 1977). Here, 'soma' refers to somatic tissue, as opposed to the germline. Kirkwood's insight is that since only the germline will propagate *ad infinitum*, investments of resources and energy to maintain the somatic tissue will not improve genetic fitness if they come at the expense of further germline propagation. Aging arises because organisms invest their resources preferentially in growth and reproduction, instead of investing in tissue maintenance and repair. One prominent demonstration of this theory is Steven Austad's ecological research on the longevity of two populations of opossums on the Virginia coast (Austad, 1993).

Those on the mainland have a 50% extrinsic mortality rate due to predation, which puts selective pressure on them to grow and reproduce quickly, at the expense of their longevity. A related, isolated population on a nearby island, where predation is non-existent, has faced less pressure to grow and reproduce quickly, allowing for selection of a gene pool that promotes more investment of biological resources in health and longevity. As such, the island opossums display smaller litter sizes and longer lifespans.

The Antagonistic Pleiotropy theory of aging, proposed by George Williams in 1957, applies the idea of trade-offs directly to genes (Williams, 1957). Williams conjectured that genes with pleiotropic functions, beneficial early in life and detrimental late in life, will still be selected for despite their late life detriments, and thus will drive aging. For example, genes that drive inflammation will protect an animal from infection in order to survive to its reproductive years, but over time inflammation will also promote diseases of aging such as cardiovascular disease and cancer.

One implication of these theories is that aging in living systems is not an absolute inevitability. It is a side-effect of optimizing for growth, reproduction, and survival early in life, not an iron-clad law of thermodynamics. When conditions arise in which enhanced longevity promotes genetic fitness, natural selection is able to produce mechanisms to maintain health for years or decades (or even centuries).

With an aging population in the U.S. and around the world, it behooves our society to better understand mechanisms that promote longevity and health in advanced age. Currently, many think of the various diseases of aging as disparate islands with separate etiologies and opportunities for therapeutic intervention. Yet age is the biggest risk factor for them all, so if one disease is cured in isolation, the next one in line will rapidly develop, in a grim game of whack-a-mole. As a result,

if cancer were to be cured completely, average life expectancy from birth in the U.S. would rise by only 3.2 years, or if heart disease were eliminated in isolation, life expectancy would only rise by 3.5 years (Olshansky et al., 1990). The alternative approach is to understand the underlying mechanisms that are shared among the diseases of aging, in order to develop interventions that delay the onset of many age-related diseases simultaneously. Through this approach, we stand a chance to unlock the benefits of healthy aging and long life.

Caloric restriction and nutrient sensors in aging

As in many fields, finding a tractable experimental framework requires creativity. In the field of aging biology, multiple approaches have proved fruitful in identifying genes and molecular mechanisms that regulate aging. Molecular genetics was first applied to biogerontology through the identification of long-lived mutants in organisms with very short lifespans, such as DAF-2 mutant *C. elegans* worms (Friedman and Johnson, 1988; Kenyon et al., 1993) and SIR2 transgenic yeast (Kaeberlein et al., 1999). Other productive approaches have included identifying longevity mechanisms present in long-lived species such as naked mole rats (reviewed in Tian et al., 2017) and humans (reviewed in Milman and Barzilai, 2015), and identifying differences between young and old animals of the same species – even surgically linking the circulatory systems of young and old animals to identify biologically active factors whose levels rise or fall with age (Conboy et al., 2005; Loffredo et al., 2013)

Yet perhaps the most widespread strategy for understanding the biological basis of aging has come from research on the most effective intervention to extend healthspan and lifespan – caloric restriction (CR). Reducing the caloric intake of an animal, or a yeast cell, by as much as 40%, while still providing nutrients in sufficient quantities to prevent malnutrition, reproducibly

extends lifespan (Weindruch and Sohal, 1997). This phenomenon was first identified experimentally in rats in the 1930s where it extended maximum lifespan by a remarkable 40% (McCay et al., 1935), and has since been shown to extend maximum lifespan in yeast, worms, flies, mice, and monkeys (Mattison et al., 2017; reviewed in Taormina and Mirisola, 2014). CR not only extends lifespan, but also reduces the incidence of all age-related diseases, suggesting that CR curbs the rate of aging itself (reviewed in Omodei and Fontana, 2011). As with aging, CR's effect on longevity at first appears to be an evolutionary paradox: why would *reduced* consumption of energy resources allow an organism to *better* maintain homeostasis? The evolutionary trade-off theories can explain this too – especially the Disposable Soma theory. In times of moderate famine, where there is enough food to stay alive but not enough to raise offspring, the evolutionarily optimal strategy is to forestall growth and reproduction and maintain health until times are better. Indeed, while CR suppresses fertility in the short term, it extends the ability to remain fertile to an older age when animals later re-enter an *ad libitum* state (Selesniemi et al., 2008).

For a variety of reasons, it is generally not recommended for humans to practice CR. However, identification of the molecular sensors and effectors of the CR response that mediate its health and longevity benefits could lead to the development of pharmacological CR mimetics that would confer the benefits of CR to those still consuming normal diets. Four major categories of CR mediators, often called nutrient sensors, have been studied in-depth: the growth hormone/insulin/insulin-like growth factor (IGF) axis, which senses hormonal signals that promote growth and energy expenditure; AMP-activated protein kinase (AMPK), which senses levels of 5' adenosine monophosphate (AMP), a metabolite prevalent when cellular energy is low; the target of rapamycin (TOR) pathway, which senses levels of anabolic amino acids; and the

sirtuins, which sense levels of NAD^+, a marker of the cellular redox state. These pathways have complex interactions with each other representing both positive and negative feedback (**Fig. 1.1**). Each also has examples of transgenic or knockout animals or pharmacological activators or inhibitors that have been shown to extend lifespan and healthspan (Baur et al., 2006; Bonkowski et al., 2006; Harrison et al., 2009; Mair et al., 2011). Recently, another molecular mechanism that mediates the CR response has been identified – hydrogen sulfide production (Hine et al., 2015;

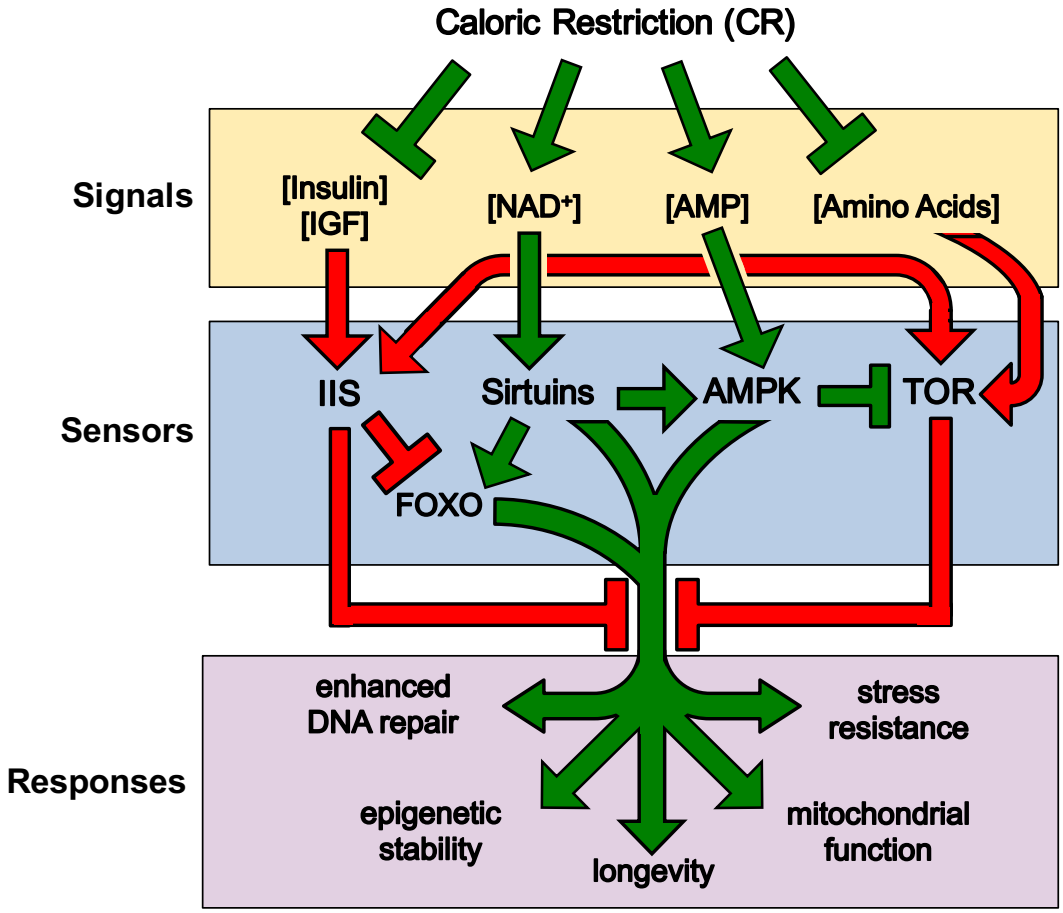

Figure 1.1: The molecular effects of caloric restriction. Caloric restriction causes reduced levels of insulin, IGF, and amino acids, and increased levels of NAD^+ and AMP. These changes are sensed by the insulin-IGF signaling (IIS) pathway, target of rapamycin (TOR), sirtuins, and AMP kinase (AMPK), resulting in enhanced DNA repair, stability of the epigenome, stress resistance, oxidative metabolism, and ultimately, longevity. Green arrows represent interactions that promote longevity and related phenotypes, and red arrows are interactions that suppress these phenotypes (from Schultz and Sinclair, 2016).

Longchamp et al., 2018). It will be interesting to know how this pathway, and others yet undiscovered, propagate CR sensing and to what degree they interact with other nutrient sensing pathways to enhance health and longevity.

The sirtuins

Sirtuins are a family of NAD^+-dependent lysine deacylases that regulate health and longevity as effectors of the CR response. Their eponym is the yeast enzyme Silent Information Regulator 2 (SIR2) which was the first longevity gene to be identified in that species (Kaeberlein et al., 1999). SIR2 is chromatin bound, where it deacetylates histones to suppress transcription, especially at mating type loci, rDNA, and telomeres (Kennedy et al., 1997). It also participates in DNA damage repair (Mills et al., 1999). These functions give it a central role in proper maintenance of the genome and epigenome (Oberdoerffer et al., 2008; Sinclair and Guarente, 1997). In the years after its identification as a longevity factor in yeast, overexpression of its homologs in *C. elegans* and *D. melanogaster* were also shown to extend longevity (Rogina and Helfand, 2004; Tissenbaum and Guarente, 2001; Viswanathan and Guarente, 2011; Whitaker et al., 2013).

In mammals, SIR2 has seven homologs, the sirtuins ("SIR2-ins"). They vary by their enzymatic activities, their protein targets, and their cellular localizations. The most common enzymatic activity of sirtuins is deacetylation, but some enzymes such as SIRT4, SIRT5, and SIRT6 can also remove long-chain fatty acids and even act as ADP-ribosyltransferases (Du et al., 2011; Haigis et al., 2006; Jiang et al., 2013; Liszt et al., 2005). All seven share a common enzymatic core domain, and a dependence on the coenzyme nicotinamide adenine dinucleotide

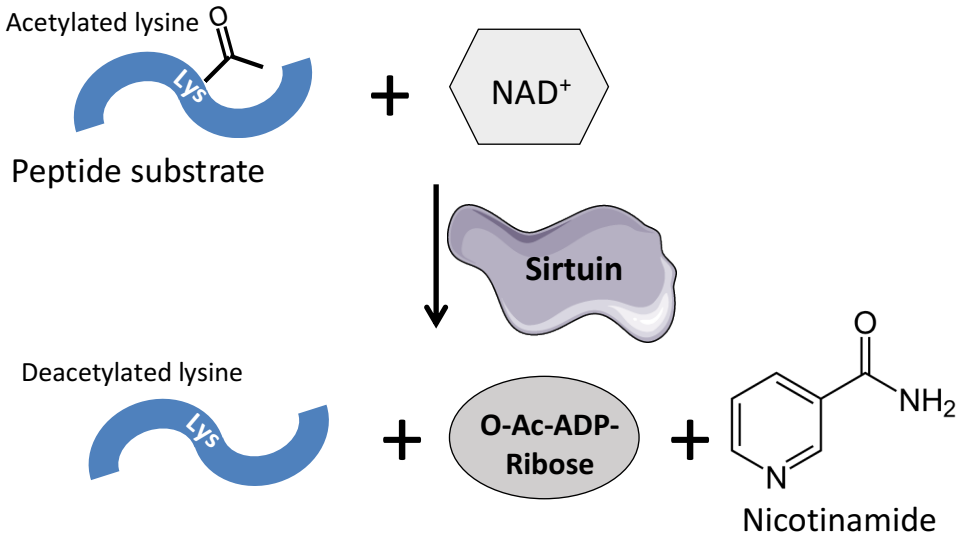

Figure 1.2: The enzymatic function of sirtuins. Sirtuins require two substrates, a peptide with an acylated lysine, and NAD^+. Sirtuins remove the acyl group (shown here as an acetyl group) from the lysine and add it to the ADP-ribose from the NAD^+ molecule, forming O-acyl-ADP ribose, free nicotinamide, and a deacylated lysine in the process (adapted from Schultz et al., Methods in Mol. Biol., in revision).

(NAD^+) (**Fig. 1.2**) (Imai et al., 2000). In general, sirtuins promote DNA repair, epigenetic maintenance, mitochondrial function, cell survival, insulin sensitivity, and reduced inflammation (reviewed in Haigis and Sinclair, 2010). Notable targets include histones, p53, NF-κB, PGC-1α, IRS-2 and SOD2, whose activity they modify by removing post-translational modifications (Bause et al., 2013; Luo et al., 2001; Rodgers et al., 2005; Yeung et al., 2004; Zhang et al., 2009). Many studies have shown that sirtuins protect against a variety of age-related diseases, especially against metabolic and inflammatory diseases (reviewed in Bonkowski and Sinclair, 2016). At least one member, SIRT1, is also required for the benefits of calorie restriction (Chen et al., 2008; Cohen et al., 2004; Li et al., 2019; Mercken et al., 2014). To date, overexpression of two sirtuins, SIRT1 in the brain and whole-body SIRT6, have been shown to extend median and maximum lifespan in a mammal (Kanfi et al., 2012; Satoh et al., 2013). Additionally, pharmacological activators of

SIRT1 extend lifespan in wild-type mice (Chen et al., 2008; Cohen et al., 2004; Li et al., 2019; Mercken et al., 2014a; Mitchell etl al., 2014). In Chapter 3, I explore whether overexpression of all the sirtuins in combination, along with increased levels of their substrate NAD^+, may have additive or even synergistic effects on health and longevity.

NAD^+ metabolism

NAD^+, and its reduced form NADH, are best known for their roles as coenzymes in redox reactions, linking the catabolic processes of glycolysis and the TCA cycle to oxidative phosphorylation. In the last two decades, however, another perhaps equally important role for NAD^+ has been uncovered, as a signaling molecule. From fungi to metazoans, an increase in intracellular levels of NAD^+ directs cells to make adjustments to ensure survival, including increasing energy production and utilization, boosting cellular repair, and coordinating circadian rhythms (reviewed in Rajman et al., 2018). NAD^+ levels are converted to signals by various enzymes that have evolved to sense NAD^+, including the sirtuin deacylases (SIRT1–7) and poly-ADP-ribose polymerases (PARPs). They can sense NAD^+ fluctuations because, unlike the enzymes of glycolysis and the TCA cycle, their dissociation constants for NAD^+ are close to physiological concentrations (Cantó et al., 2015).

NAD^+ levels steadily decline during aging. By the time a mouse or human is middle-aged, levels of NAD^+ have fallen to half of youthful levels, with resulting loss of sirtuin and PARP activity (Wang and Miao, 2017; Zhou et al., 2016). NAD^+ levels are also affected by dietary interventions: a high fat diet will result in reduced NAD^+ levels even in youth, and CR prevents NAD^+ levels from falling in old age (Gomes et al., 2013; Yoshino et al., 2011). These phenomena

do not seem to be the result of increased reduction to NADH, as there is not a concomitant increase in levels of that metabolite. Thus, the reasons for why NAD^+ levels fall during aging are unclear.

Lower levels of NAD^+ must logically be caused by an increase in consumption, a decrease in production, or some combination thereof. More than 5% of annotated gene products are predicted to bind NAD(P) (Hua et al., 2014). Most either use NAD^+ as a redox donor/acceptor, or bind to it without catalyzing an enzymatic reaction, as does DBC1, leaving it available for future use (Li et al., 2017). A few enzymes, including sirtuins, hydrolyze NAD^+ into nicotinamide and some form of ADP-ribose, thus rendering it unavailable unless resynthesized. However, sirtuins, which require a protein substrate to carry out their reactions, are not likely processive enough to have a major impact on cellular NAD^+ levels. A few NAD^+-hydrolyzing enzymes are sufficiently active to dramatically alter intracellular levels of NAD^+. One such example is CD38, a cell surface protein which hydrolyzes NAD^+ into nicotinamide and cyclic-ADP ribose. Deletion or pharmacological inhibition of CD38 raises NAD^+ levels in aged mice and improves mitochondrial function, glucose sensitivity, and cardiac function (Camacho-Pereira et al., 2016; Tarragó et al., 2018). Another prominent NAD^+ hydrolase is poly-ADP ribose polymerase 1 (PARP1), which hydrolyzes NAD^+ to produce nicotinamide and long polymers of poly-ADP ribose (PAR). Treatment with PARP inhibitors in mice on a high fat diet also raises NAD^+ levels and improves mitochondrial function, glucose sensitivity, and liver function (Bai et al., 2011; Gariani et al., 2017). In recent years, a novel NAD^+ hydrolase, SARM1, has been identified in neurons. Its deletion protects neurons from degeneration, presumably through an NAD^+-dependent mechanism (Gerdts et al., 2015). In Chapter 2, I add one more hydrolase to this list: PARP14.

In animals, NAD^+ can be produced *de novo* from tryptophan, or salvaged from nicotinamide in a two-step process. The *de novo* pathway was recently shown to regulate steady

state NAD^+ levels in mice, as inhibition or deletion of an enzyme that shunts an intermediate away from NAD^+ synthesis raised its levels and improved mitochondrial function (Katsyuba et al., 2018). However, since nicotinamide is energetically expensive to produce, in most cases, its salvage is the basis for the predominant pathway to generate NAD^+. In the first step of the NAD^+ salvage pathway, nicotinamide and phosphoribosyl pyrophosphate (PRPP) are reacted to form nicotinamide mononucleotide (NMN) by the enzyme nicotinamide phosphoribosyltransferase (NAMPT). From there, NMN reacts with ATP to form a molecule of NAD^+, catalyzed by one of the three nicotinamide mononucleotide adenylyltransferase (NMNAT) enzymes. Overexpression of the first salvage enzyme, NAMPT, in mouse skeletal muscle prevents the levels of NAD^+ from falling during aging, resulting in improved exercise capacity (Frederick et al., 2016). Overexpression of the second salvage enzyme, NMNAT, in fruit flies extends lifespan and improves movement capacity (Liu et al., 2018). These data suggest that flux through biosynthetic pathways is insufficient to maintain optimal NAD^+ levels during aging.

With so many candidates for why NAD^+ levels fall during aging, a hybrid model seems to best fit the current data: due to DNA damage, inflammation, and other insults that enhance NAD^+ consumption, the body's demand for NAD^+ simply outstrips its ability to supply the metabolite (**Fig. 1.3**).

Regardless of the cause for the decline, it is clear that preserving NAD^+ levels during aging greatly improves health. Several studies have shown this by treating mice with NAD^+-hydrolase inhibitors or NAD^+ precursors. Observed effects include increased insulin sensitivity, reversal of mitochondrial dysfunction, reduced stem cell senescence, increased muscle vasculature and running endurance, protection from Alzheimer's-like neurodegeneration, and extension of lifespan (Bai et al., 2011; Das et al., 2018; Gomes et al., 2013; Hou et al., 2018; Yoshino et al., 2011; Zhang

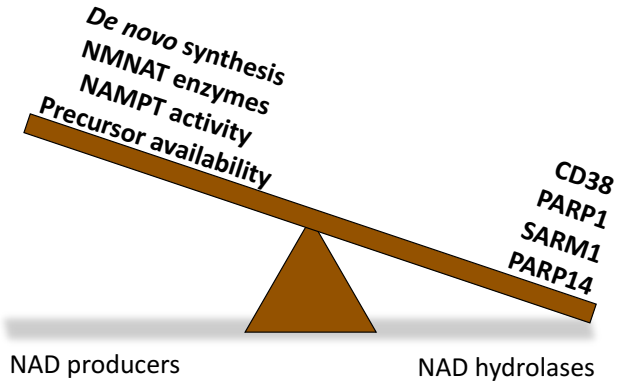

Figure 1.3: Hybrid model for decline in NAD^+ levels during aging. Rather than a single cause for low NAD^+ during aging, its drop may be due to multiple cooperative factors: increased inflammation leads to CD38 and PARP14 expression, increased DNA damage leads to increased PARP1 activation, and damage in neurons leads to SARM1 activation. Together, these phenomena outstrip the body's ability to restore NAD^+ through biosynthetic pathways, leading to a drop in steady state levels.

et al., 2016). NAD^+ precursors are currently in early phase human clinical trials for the treatment of age-related diseases (Dellinger et al., 2017).

PARPs

The poly(ADP-ribose) polymerases (PARPs) are a family of seventeen proteins in humans. Except for PARP13 which is catalytically dead, the PARPs bind to and hydrolyze NAD^+, converting it into nicotinamide and linking the ADP-ribose to an acceptor protein or to a growing oligomer or polymer of ADP-ribose. PARP1 is by far the most active member of the PARP family accounting for the vast majority of basal PARP activity (Shieh et al., 1998). Its high activity is due to the fact that it links together polymers of hundreds of NAD^+ molecules into polyADP-ribose (PAR), a molecule that was at first thought to be polyA RNA when it was discovered (Kraus, 2015). PARP1 is also the most studied member of the PARP family due to its prominent role in DNA repair and cancer. In order to prevent PARP1 from depleting NAD^+ to lethally low levels during acute DNA damage, an inhibitor, DBC1, has evolved to sense the low NAD^+ levels and

limit PARP1's activity (Li et al., 2017). Pharmacological PARP inhibitors are of great clinical interest in oncology, as PARP1 inhibition is synthetically lethal with BRCA depletion in tumors with genomic instability (Malyuchenko et al., 2015). PARP1 activity increases during aging, likely due to increased basal DNA damage (Li et al., 2017). Beyond its role in DNA repair, PARP1 also regulates gene expression, cooperating with NF-κB to promote transcription of pro-inflammatory genes (Oliver et al., 1999).

The other members of the PARP family were identified due to their homology with PARP1. Most are not, however, functionally poly-ADP-ribose polymerases. Rather, most possess mono-ADP-ribose transferase (mART) activity. This limits how much they can impact cellular NAD^+ levels as, like sirtuins, they can only hydrolyze one NAD^+ molecule per protein substrate. In Chapter 2, I identify PARP14 as a major NAD^+ hydrolase in Toll-like receptor- (TLR) activated macrophages. While PARP14 has not previously been identified as a major regulator of NAD^+ metabolism, it has been linked to inflammation, although its role in inflammation is still unclear. Some studies support a pro-inflammatory role for PARP14 (Caprara et al., 2018; Cho et al., 2013; Iansante et al., 2015; Mehrotra et al., 2013, 2015), while others identify anti-inflammatory effects (Goenka et al., 2007; Iwata et al., 2016; Krishnamurthy et al., 2017). PARP14's impact on both metabolism and inflammation may be context dependent, and more research is necessary to build a clear model of its function and effects.

Inflammation and aging

One of the hallmarks of aging is altered intercellular communication, and chief among the categories of dysregulated messages are those that mediate inflammation (López-Otín et al., 2013). Even in the absence of infection or insult, inflammation increases during aging, a phenomenon

that is so robust it has been termed "inflamm-aging" (Franceschi et al., 2000; Walford, 1969). This age-related inflammation is marked by increased macrophage infiltration into tissues, increased amounts of pro-inflammatory cytokines in serum and tissues, and an increase in transcriptional activation of inflammatory pathways in cells. From an evolutionary context, inflammatory signaling is a prime example of Antagonistic Pleiotropy; it is beneficial in allowing an animal to survive to a reproductive age as inflammation helps ward off lethal infections. Over longer periods of time, however, low basal rates of inflammation engender dysfunction and increase disease risk. Indeed, many age-related diseases such as diabetes, cancer, neurodegeneration, and cardiovascular disease have a major inflammatory component to their etiology.

It is not yet clear why inflammation increases during aging, but several prominent hypotheses have been put forward. One hypothesis is that this inflammation is a result of the accumulation of senescent cells during aging, which secrete pro-inflammatory cytokines such as IL-6 and IL-8 as part of the senescence-associated secretory phenotype (SASP) to improve immune surveillance (Coppé et al., 2008). Indeed, treatment of human adipose explants with molecules that selectively kill senescent cells, termed senolytics, reduced secretion of these cytokines (Xu et al., 2018). A second hypothesis is that during aging, the epithelium of the intestine becomes leaky, allowing for bacterial products to enter the bloodstream sufficient to cause systemic low-grade inflammation. Such a phenomenon has been observed in fruit flies (Regan et al., 2016). A final hypothesis is that metabolic changes during aging such as increased succinate, fatty acids, and cholesterol promote a pro-inflammatory state (Tannahill et al., 2013; Youm et al., 2013). Low NAD^+ levels may also predispose the development of aberrant inflammation.

Biomarkers of aging

Supreme Court Justice Potter Stewart referred to obscenity as difficult to define but "I know it when I see it" (Jacobellis v. Ohio, 1964). Our current definition of aging is similar. The field has a long list of measures associated with aging, but no way to assess aging directly. Perhaps this is because there is no agreed upon understanding about what aging inherently is, there is only agreement on its outcomes. Chief among these outcomes is death, but even an extension of survival is not a clear measure of aging. Death can be caused by age-independent events, which when removed, do not affect the rate or onset of aging, and thus largely manifest themselves at the population level as an extension of median lifespan with little impact on maximum lifespan. Only a slowing of the rate or a delay of the onset of aging can robustly extend maximum lifespan, which is why an extension of maximum lifespan is among the top indicators that an intervention has affected aging itself (Finch and Pike, 1996). However, maximum lifespan has major drawbacks – it must be assessed at the population level, and only once most of the population has died.

A true biomarker of aging would track with an individual's "biological age," a term nearly as nebulous as the definition of aging. In practical terms, a biomarker of aging should be able to predict an individual's chronological age and life expectancy, two terms that have clear, quantitative definitions. It should also be able to predict the outcome of other age-sensitive tests, and its measurement should be sufficiently non-invasive as to not alter life expectancy or the outcomes of subsequent tests (Butler et al., 2004).

In recent years, DNA methylation has largely fulfilled such criteria (Hannum et al., 2013; Horvath, 2013; Meer et al., 2018). Characteristic increases or decreases in methylation of specific CpGs are assembled into a linear model to generate a prediction of biological age. Such models are referred to as DNA methylation clocks and are generally consistent across tissues and

organisms. They also are able to predict age acceleration and abatement from genetic and dietary interventions (Maegawa et al., 2017; Petkovich et al., 2017). Current drawbacks of these methylation clocks are cost, time, and the requirement for blood or tissue.

While a molecular clock has the advantage of being more proximal to the driver of aging, whatever it may be (e.g. chromatin modifications), a combination of gross, phenotypic biomarkers can also serve as a predictor of age and health. The Frailty Index (FI) is such an aggregate measurement, combining the unweighted score of up to 70 measurements of age-related physiological deficits in humans, or 31 measurements in mice, including hearing loss, weight loss, and impaired gait (Rockwood et al., 2017; Whitehead et al., 2014). FI correlates with age and mortality in humans (Ravindrarajah et al., 2013) and mice (Rockwood et al., 2017; Whitehead et al., 2014). In mice, it has the advantage of being free to assess and quick (1-2 minutes). In Chapter 4, I describe the tracking of FI longitudinally in mice until their natural deaths, and the construction of predictive models of age and life expectancy based on those data. This demonstrates that FI can be used as a phenotypic aging clock.

REFERENCES

Austad, S. (1993). Retarded senescence in an insular population of Virginia opossums (Didelphis virginiana). J Zool *229*, 695–708.

Bai, P., Cantó, C., Oudart, H., Brunyánszki, A., Cen, Y., Thomas, C., Yamamoto, H., Huber, A., Kiss, B., Houtkooper, R.H., et al. (2011). PARP-1 inhibition increases mitochondrial metabolism through SIRT1 activation. Cell Metab. *13*, 461–468.

Baur, J.A., Pearson, K.J., Price, N.L., Jamieson, H.A., Lerin, C., Kalra, A., Prabhu, V.V., Allard, J.S., Lopez-Lluch, G., Lewis, K., et al. (2006). Resveratrol improves health and survival of mice on a high-calorie diet. Nature *444*, 337–342.

Bause, A.S., Matsui, M.S., and Haigis, M.C. (2013). The protein deacetylase SIRT3 prevents oxidative stress-induced keratinocyte differentiation. J. Biol. Chem. *288*, 36484–36491.

Bonkowski, M.S., and Sinclair, D.A. (2016). Slowing ageing by design: the rise of NAD+ and sirtuin-activating compounds. Nat. Rev. Mol. Cell Biol. *17*, 679–690.

Bonkowski, M.S., Rocha, J.S., Masternak, M.M., Al Regaiey, K.A., and Bartke, A. (2006). Targeted disruption of growth hormone receptor interferes with the beneficial actions of calorie restriction. Proc. Natl. Acad. Sci. U.S.A. *103*, 7901–7905.

Butler, R.N., Sprott, R., Warner, H., Bland, J., Feuers, R., Forster, M., Fillit, H., Harman, S.M., Hewitt, M., Hyman, M., et al. (2004). Biomarkers of aging: from primitive organisms to humans. J. Gerontol. A Biol. Sci. Med. Sci. *59*, B560–7.

Camacho-Pereira, J., Tarragó, M.G., Chini, C.C.S.C., Nin, V., Escande, C., Warner, G.M., Puranik, A.S., Schoon, R.A., Reid, J.M., Galina, A., et al. (2016). CD38 Dictates Age-Related NAD Decline and Mitochondrial Dysfunction through an SIRT3-Dependent Mechanism. Cell Metab. *23*, 1127–1139.

Cantó, C., Menzies, K.J., and Auwerx, J. (2015). NAD(+) Metabolism and the Control of Energy Homeostasis: A Balancing Act between Mitochondria and the Nucleus. Cell Metab. *22*, 31–53.

Caprara, G., Prosperini, E., Piccolo, V., Sigismondo, G., Melacarne, A., Cuomo, A., Boothby, M., Rescigno, M., Bonaldi, T., and Natoli, G. (2018). PARP14 Controls the Nuclear Accumulation of a Subset of Type I IFN-Inducible Proteins. J. Immunol. *200*, 2439–2454.

Chen, D., Bruno, J., Easlon, E., Lin, S.-J.J., Cheng, H.-L.L., Alt, F.W., and Guarente, L. (2008). Tissue-specific regulation of SIRT1 by calorie restriction. Genes Dev. *22*, 1753–1757.

Cho, S.H., Raybuck, A., Wei, M., Erickson, J., Nam, K.T., Cox, R.G., Trochtenberg, A., Thomas, J.W., Williams, J., and Boothby, M. (2013). B cell-intrinsic and -extrinsic regulation of antibody responses by PARP14, an intracellular (ADP-ribosyl)transferase. J. Immunol. *191*, 3169–3178.

Cohen, H.Y., Miller, C., Bitterman, K.J., Wall, N.R., Hekking, B., Kessler, B., Howitz, K.T., Gorospe, M., de Cabo, R., and Sinclair, D.A. (2004). Calorie restriction promotes mammalian cell survival by inducing the SIRT1 deacetylase. Science *305*, 390–392.

Conboy, I.M., Conboy, M.J., Wagers, A.J., Girma, E.R., Weissman, I.L., and Rando, T.A. (2005). Rejuvenation of aged progenitor cells by exposure to a young systemic environment. Nature *433*, 760–764.

Coppé, J.-P.P., Patil, C.K., Rodier, F., Sun, Y., Muñoz, D.P., Goldstein, J., Nelson, P.S., Desprez, P.-Y.Y., and Campisi, J. (2008). Senescence-associated secretory phenotypes reveal cell-nonautonomous functions of oncogenic RAS and the p53 tumor suppressor. PLoS Biol. *6*, 2853–2868.

Das, A., Huang, G.X., Bonkowski, M.S., Longchamp, A., Li, C., Schultz, M.B., Kim, L.-J.J., Osborne, B., Joshi, S., Lu, Y., et al. (2018). Impairment of an Endothelial NAD+-H2S Signaling Network Is a Reversible Cause of Vascular Aging. Cell *173*, 74–89.e20.

Dellinger, R.W., Santos, S.R., Morris, M., Evans, M., Alminana, D., Guarente, L., and Marcotulli, E. (2017). Repeat dose NRPT (nicotinamide riboside and pterostilbene) increases NAD+ levels in humans safely and sustainably: a randomized, double-blind, placebo-controlled study. NPJ Aging Mech Dis *3*, 17.

Du, J., Zhou, Y., Su, X., Yu, J.J., Khan, S., Jiang, H., Kim, J., Woo, J., Kim, J.H., Choi, B.H., et al. (2011). Sirt5 is a NAD-dependent protein lysine demalonylase and desuccinylase. Science (New York, N.Y.) *334*, 806–809.

Finch, C.E., and Pike, M.C. (1996). Maximum life span predictions from the Gompertz mortality model. J. Gerontol. A Biol. Sci. Med. Sci. *51*, B183–94.

Franceschi, C., Bonafè, M., Valensin, S., Olivieri, F., De Luca, M., Ottaviani, E., and De Benedictis, G. (2000). Inflamm-aging. An evolutionary perspective on immunosenescence. Annals of the New York Academy of Sciences *908*, 244–254.

Frederick, D.W., Loro, E., Liu, L., Davila, A., Chellappa, K., Silverman, I.M., Quinn, W.J., Gosai, S.J., Tichy, E.D., Davis, J.G., et al. (2016). Loss of NAD Homeostasis Leads to Progressive and Reversible Degeneration of Skeletal Muscle. Cell Metabolism *24*, 269–282.

Friedman, D.B., and Johnson, T.E. (1988). Three mutants that extend both mean and maximum life span of the nematode, Caenorhabditis elegans, define the age-1 gene. J Gerontol *43*, B102–9.

Gariani, K., Ryu, D., Menzies, K.J., Yi, H.-S.S., Stein, S., Zhang, H., Perino, A., Lemos, V., Katsyuba, E., Jha, P., et al. (2017). Inhibiting poly ADP-ribosylation increases fatty acid oxidation and protects against fatty liver disease. J. Hepatol. *66*, 132–141.

Gerdts, J., Brace, E.J., Sasaki, Y., DiAntonio, A., and Milbrandt, J. (2015). SARM1 activation triggers axon degeneration locally via NAD^+ destruction. Science *348*, 453–457.

Goenka, S., Cho, S.H., and Boothby, M. (2007). Collaborator of Stat6 (CoaSt6)-associated poly(ADP-ribose) polymerase activity modulates Stat6-dependent gene transcription. J. Biol. Chem. *282*, 18732–18739.

Gomes, A.P., Price, N.L., Ling, A.J., Moslehi, J.J., Montgomery, M.K., Rajman, L., White, J.P., Teodoro, J.S.S., Wrann, C.D., Hubbard, B.P., et al. (2013). Declining NAD(+) induces a pseudohypoxic state disrupting nuclear-mitochondrial communication during aging. Cell *155*, 1624–1638.

Haigis, M., and Sinclair, D. (2010). Mammalian Sirtuins: Biological Insights and Disease Relevance. Annual Review of Pathology: Mechanisms of Disease *5*.

Haigis, M.C., Mostoslavsky, R., Haigis, K.M., Fahie, K., Christodoulou, D.C., Murphy, A.J., Valenzuela, D.M., Yancopoulos, G.D., Karow, M., Blander, G., et al. (2006). SIRT4 inhibits glutamate dehydrogenase and opposes the effects of calorie restriction in pancreatic beta cells. Cell *126*, 941–954.

Hannum, G., Guinney, J., Zhao, L., Zhang, L., Hughes, G., Sadda, S., Klotzle, B., Bibikova, M., Fan, J.-B.B., Gao, Y., et al. (2013). Genome-wide methylation profiles reveal quantitative views of human aging rates. Mol. Cell *49*, 359–367.

Harrison, D.E., Strong, R., Sharp, Z.D., Nelson, J.F., Astle, C.M., Flurkey, K., Nadon, N.L., Wilkinson, J.E., Frenkel, K., Carter, C.S., et al. (2009). Rapamycin fed late in life extends lifespan in genetically heterogeneous mice. Nature *460*, 392–395.

Hine, C., Harputlugil, E., Zhang, Y., Ruckenstuhl, C., Lee, B.C., Brace, L., Longchamp, A., Treviño-Villarreal, J.H., Mejia, P., Ozaki, C.K., et al. (2015). Endogenous hydrogen sulfide production is essential for dietary restriction benefits. Cell *160*, 132–144.

Horvath, S. (2013). DNA methylation age of human tissues and cell types. Genome Biol. *14*, R115.

Hua, Y.H., Wu, C.Y., Sargsyan, K., and Lim, C. (2014). Sequence-motif detection of NAD(P)-binding proteins: discovery of a unique antibacterial drug target. Scientific Reports *4*, 6471.

Hou, Y., Lautrup, S., Cordonnier, S., Wang, Y., Croteau, D.L., Zavala, E., Zhang, Y., Moritoh, K., O'Connell, J.F., Baptiste, B.A., et al. NAD+ supplementation normalizes key Alzheimer's features and DNA damage responses in a new AD mouse model with introduced DNA repair deficiency. Proc. Natl. Acad. Sci. U.S.A. *115*, E1876–E1885.

Iansante, V., Choy, P.M., Fung, S.W., Liu, Y., Chai, J.-G.G., Dyson, J., Del Rio, A., D'Santos, C., Williams, R., Chokshi, S., et al. (2015). PARP14 promotes the Warburg effect in hepatocellular carcinoma by inhibiting JNK1-dependent PKM2 phosphorylation and activation. Nat Commun *6*, 7882.

Imai, S., Armstrong, C.M., Kaeberlein, M., and Guarente, L. (2000). Transcriptional silencing and longevity protein Sir2 is an NAD-dependent histone deacetylase. Nature *403*, 795–800.

Iwata, H., Goettsch, C., Sharma, A., Ricchiuto, P., Goh, W.W., Halu, A., Yamada, I., Yoshida, H., Hara, T., Wei, M., et al. (2016). PARP9 and PARP14 cross-regulate macrophage activation via STAT1 ADP-ribosylation. Nat Commun *7*, 12849.

Jacobellis v. Ohio, 378 U.S. 184 (1964).

Jiang, H., Khan, S., Wang, Y., Charron, G., He, B., Sebastian, C., Du, J., Kim, R., Ge, E., Mostoslavsky, R., et al. (2013). SIRT6 regulates TNF-α secretion through hydrolysis of long-chain fatty acyl lysine. Nature *496*, 110–113.

Jones, O.R., Scheuerlein, A., Salguero-Gómez, R., Camarda, C.G., Schaible, R., Casper, B.B., Dahlgren, J.P., Ehrlén, J., García, M.B.B., Menges, E.S., et al. (2014). Diversity of ageing across the tree of life. Nature *505*, 169–173.

Kaeberlein, M., McVey, M., and Guarente, L. (1999). The SIR2/3/4 complex and SIR2 alone promote longevity in Saccharomyces cerevisiae by two different mechanisms. Genes Dev. *13*, 2570–2580.

Kanfi, Y., Naiman, S., Amir, G., Peshti, V., Zinman, G., Nahum, L., Bar-Joseph, Z., and Cohen, H.Y. (2012). The sirtuin SIRT6 regulates lifespan in male mice. Nature *483*, 218–221.

Katsyuba, E., Mottis, A., Zietak, M., De Franco, F., van der Velpen, V., Gariani, K., Ryu, D., Cialabrini, L., Matilainen, O., Liscio, P., et al. (2018). De novo NAD+ synthesis enhances mitochondrial function and improves health. Nature *563*, 354–359.

Kennedy, B.K., Gotta, M., Sinclair, D.A., Mills, K., McNabb, D.S., Murthy, M., Pak, S.M., Laroche, T., Gasser, S.M., and Guarente, L. (1997). Redistribution of silencing proteins from telomeres to the nucleolus is associated with extension of life span in S. cerevisiae. Cell *89*, 381–391.

Kenyon, C., Chang, J., Gensch, E., Rudner, A., and Tabtiang, R. (1993). A C. elegans mutant that lives twice as long as wild type. Nature *366*, 461–464.

Kirkwood, T.B. (1977). Evolution of ageing. Nature *270*, 301–304.

Kraus, W.L. (2015). PARPs and ADP-Ribosylation: 50 Years … and Counting. Molecular Cell *58*, 902–910.

Krishnamurthy, P., Da-Silva-Arnold, S., Turner, M.J., Travers, J.B., and Kaplan, M.H. (2017). Poly-ADP ribose polymerase-14 limits severity of allergic skin disease. Immunology *152*, 451–461.

Li, J., Bonkowski, M.S., Moniot, S., Zhang, D., Hubbard, B.P., Ling, A.J., Rajman, L.A., Qin, B., Lou, Z., Gorbunova, V., et al. (2017). A conserved NAD+ binding pocket that regulates protein-protein interactions during aging. Science (New York, N.Y.) *355*, 1312–1317.

Li, L., Chen, Z., Zhao, K., and Zeng, Z. (2019). [Role of deacetylase sirtuins in sepsis: beneficial or harmful?]. Zhonghua Wei Zhong Bing Ji Jiu Yi Xue *31*, 23–28.

Liszt, G., Ford, E., Kurtev, M., and Guarente, L. (2005). Mouse Sir2 homolog SIRT6 is a nuclear ADP-ribosyltransferase. The Journal of Biological Chemistry *280*, 21313–21320.

Liu, X., Liu, M., Tang, C., Xiang, Z., Li, Q., Ruan, X., Xiong, K., and Zheng, L. (2018). Overexpression of Nmnat improves the adaption of health span in aging Drosophila. Exp. Gerontol. *108*, 276–283.

Loffredo, F.S., Steinhauser, M.L., Jay, S.M., Gannon, J., Pancoast, J.R., Yalamanchi, P., Sinha, M., Dall'Osso, C., Khong, D., Shadrach, J.L., et al. (2013). Growth differentiation factor 11 is a circulating factor that reverses age-related cardiac hypertrophy. Cell *153*, 828–839.

Longchamp, A., Mirabella, T., Arduini, A., MacArthur, M.R., Das, A., Treviño-Villarreal, J.H., Hine, C., Ben-Sahra, I., Knudsen, N.H., Brace, L.E., et al. (2018). Amino Acid Restriction Triggers Angiogenesis via GCN2/ATF4 Regulation of VEGF and H2S Production. Cell *173*, 117–129.e14.

López-Otín, C., Blasco, M.A., Partridge, L., Serrano, M., and Kroemer, G. (2013). The hallmarks of aging. Cell *153*, 1194–1217.

Luo, J., Nikolaev, A.Y., Imai, S., Chen, D., Su, F., Shiloh, A., Guarente, L., and Gu, W. (2001). Negative control of p53 by Sir2alpha promotes cell survival under stress. Cell *107*, 137–148.

Maegawa, S., Lu, Y., Tahara, T., Lee, J.T., Madzo, J., Liang, S., Jelinek, J., Colman, R.J., and Issa, J.-P.J. (2017). Caloric restriction delays age-related methylation drift. Nat Commun *8*, 539.

Mair, W., Morantte, I., Rodrigues, A.P., Manning, G., Montminy, M., Shaw, R.J., and Dillin, A. (2011). Lifespan extension induced by AMPK and calcineurin is mediated by CRTC-1 and CREB. Nature *470*, 404–408.

Malyuchenko, N.V., Kotova, E.Y., Kulaeva, O.I., Kirpichnikov, M.P., and Studitskiy, V.M. (2015). PARP1 Inhibitors: antitumor drug design. Acta Naturae *7*, 27–37.

Mattison, J.A., Colman, R.J., Beasley, T.M., Allison, D.B., Kemnitz, J.W., Roth, G.S., Ingram, D.K., Weindruch, R., de Cabo, R., and Anderson, R.M. (2017). Caloric restriction improves health and survival of rhesus monkeys. Nat Commun *8*, 14063.

McCay, C.M., Crowell, M.F., and Maynard, L.A. (1935). The effect of retarded growth upon the length of life span and upon the ultimate body size. Nutrition (Burbank, Los Angeles County, Calif.) *5*, 155–71; discussion 172.

Meer, M.V., Podolskiy, D.I., Tyshkovskiy, A., and Gladyshev, V.N. (2018). A whole lifespan mouse multi-tissue DNA methylation clock. Elife *7*.

Mehrotra, P., Hollenbeck, A., Riley, J.P., Li, F., Patel, R.J., Akhtar, N., and Goenka, S. (2013). Poly (ADP-ribose) polymerase 14 and its enzyme activity regulates T(H)2 differentiation and allergic airway disease. J. Allergy Clin. Immunol. *131*, 521–31.e1–12.

Mehrotra, P., Krishnamurthy, P., Sun, J., Goenka, S., and Kaplan, M.H. (2015). Poly-ADP-ribosyl polymerase-14 promotes T helper 17 and follicular T helper development. Immunology *146*, 537–546.

Mercken, E.M., Hu, J., Krzysik-Walker, S., Wei, M., Li, Y., McBurney, M.W., de Cabo, R., and Longo, V.D. (2014a). SIRT1 but not its increased expression is essential for lifespan extension in caloric-restricted mice. Aging Cell *13*, 193–196.

Mercken, E.M., Mitchell, S.J., Martin-Montalvo, A., Minor, R.K., Almeida, M., Gomes, A.P., Scheibye-Knudsen, M., Palacios, H.H., Licata, J.J., Zhang, Y., et al. (2014b). SRT2104 extends survival of male mice on a standard diet and preserves bone and muscle mass. Aging Cell *13*, 787–796.

Mills, K.D., Sinclair, D.A., and Guarente, L. (1999). MEC1-dependent redistribution of the Sir3 silencing protein from telomeres to DNA double-strand breaks. Cell *97*, 609–620.

Milman, S., and Barzilai, N. (2015). Dissecting the Mechanisms Underlying Unusually Successful Human Health Span and Life Span. Cold Spring Harb Perspect Med *6*, a025098.

Mitchell, S.J., Martin-Montalvo, A., Mercken, E.M., Palacios, H.H., Ward, T.M., Abulwerdi, G., Minor, R.K., Vlasuk, G.P., Ellis, J.L., Sinclair, D.A., et al. (2014). The SIRT1 activator SRT1720 extends lifespan and improves health of mice fed a standard diet. Cell Rep *6*, 836–843.

Nagy, G., Homeric Hymn to Aphrodite. (available at http://www.uh.edu/~cldue/texts/aphrodite.html)

Oberdoerffer, P., Michan, S., McVay, M., Mostoslavsky, R., Vann, J., Park, S.-K.K., Hartlerode, A., Stegmuller, J., Hafner, A., Loerch, P., et al. (2008). SIRT1 redistribution on chromatin promotes genomic stability but alters gene expression during aging. Cell *135*, 907–918.

Oliver, F.J., Ménissier-de Murcia, J., Nacci, C., Decker, P., Andriantsitohaina, R., Muller, S., de la Rubia, G., Stoclet, J.C., and de Murcia, G. (1999). Resistance to endotoxic shock as a consequence of defective NF-kappaB activation in poly (ADP-ribose) polymerase-1 deficient mice. EMBO J. *18*, 4446–4454.

Olshansky, S.J., Carnes, B.A., and Cassel, C. (1990). In search of Methuselah: estimating the upper limits to human longevity. Science *250*, 634–640.

Omodei, D., and Fontana, L. (2011). Calorie restriction and prevention of age-associated chronic disease. FEBS Lett. *585*, 1537–1542.

Petkovich, D.A., Podolskiy, D.I., Lobanov, A.V., Lee, S.-G.G., Miller, R.A., and Gladyshev, V.N. (2017). Using DNA Methylation Profiling to Evaluate Biological Age and Longevity Interventions. Cell Metab. *25*, 954–960.e6.

Rajman, L., Chwalek, K., and Sinclair, D.A. (2018). Therapeutic Potential of NAD-Boosting Molecules: The In Vivo Evidence. Cell Metabolism *27*, 529–547.

Ravindrarajah, R., Lee, D.M., Pye, S.R., Gielen, E., Boonen, S., Vanderschueren, D., Pendleton, N., Finn, J.D., Tajar, A., O'Connell, M.D., et al. (2013). The ability of three different models of frailty to predict all-cause mortality: results from the European Male Aging Study (EMAS). Arch Gerontol Geriatr *57*, 360–368.

Regan, J.C., Khericha, M., Dobson, A.J., Bolukbasi, E., Rattanavirotkul, N., and Partridge, L. (2016). Sex difference in pathology of the ageing gut mediates the greater response of female lifespan to dietary restriction. Elife *5*, e10956.

Rockwood, K., Blodgett, J.M., Theou, O., Sun, M.H., Feridooni, H.A., Mitnitski, A., Rose, R.A., Godin, J., Gregson, E., and Howlett, S.E. (2017). A Frailty Index Based On Deficit Accumulation Quantifies Mortality Risk in Humans and in Mice. Sci Rep *7*, 43068.

Rodgers, J.T., Lerin, C., Haas, W., Gygi, S.P., Spiegelman, B.M., and Puigserver, P. (2005). Nutrient control of glucose homeostasis through a complex of PGC-1alpha and SIRT1. Nature *434*, 113–118.

Rogina, B., and Helfand, S.L. (2004). Sir2 mediates longevity in the fly through a pathway related to calorie restriction. Proc. Natl. Acad. Sci. U.S.A. *101*, 15998–16003.

Satoh, A., Brace, C.S., Rensing, N., Cliften, P., Wozniak, D.F., Herzog, E.D., Yamada, K.A., and Imai, S.-I. (2013). Sirt1 extends life span and delays aging in mice through the regulation of Nk2 homeobox 1 in the DMH and LH. Cell Metab. *18*, 416–430.

Schultz, M.B., and Sinclair, D.A. (2016). When Stem Cells Grow Old: Phenotypes and Mechanisms of Stem Cell Aging. Development. *143*, 3-14.

Schultz, M.B., and Sinclair, D.A. (2016). Why NAD^+ Declines During Aging: It's Destroyed. Cell Metabolism. *23*, 965-966.

Schultz, M.B., Rinaldi, C., Lu, Y., Amorim, J., and Sinclair, D.A. Molecular and Cellular Characterization of SIRT1 Allosteric Activators. Methods Mol. Biol. (*in revision*).

Selesniemi, K., Lee, H.-J.J., and Tilly, J.L. (2008). Moderate caloric restriction initiated in rodents during adulthood sustains function of the female reproductive axis into advanced chronological age. Aging Cell *7*, 622–629.

Shieh, W.M., Amé, J.C., Wilson, M.V., Wang, Z.Q., Koh, D.W., Jacobson, M.K., and Jacobson, E.L. (1998). Poly(ADP-ribose) polymerase null mouse cells synthesize ADP-ribose polymers. The Journal of Biological Chemistry *273*, 30069–30072.

Sinclair, D.A., and Guarente, L. (1997). Extrachromosomal rDNA circles--a cause of aging in yeast. Cell *91*, 1033–1042.

Tannahill, G.M., Curtis, A.M., Adamik, J., Palsson-McDermott, E.M., McGettrick, A.F., Goel, G., Frezza, C., Bernard, N.J., Kelly, B., Foley, N.H., et al. (2013). Succinate is an inflammatory signal that induces IL-1β through HIF-1α. Nature *496*, 238–242.

Taormina, G., and Mirisola, M.G. (2014). Calorie restriction in mammals and simple model organisms. Biomed Res Int *2014*, 308690.

Tarragó, M.G., Chini, C.C.S.C., Kanamori, K.S., Warner, G.M., Caride, A., de Oliveira, G.C., Rud, M., Samani, A., Hein, K.Z., Huang, R., et al. (2018). A Potent and Specific CD38 Inhibitor Ameliorates Age-Related Metabolic Dysfunction by Reversing Tissue NAD+ Decline. Cell Metab. *27*, 1081–1095.e10.

Tian, X., Seluanov, A., and Gorbunova, V. (2017). Molecular Mechanisms Determining Lifespan in Short- and Long-Lived Species. Trends Endocrinol. Metab. *28*, 722–734.

Tissenbaum, H.A., and Guarente, L. (2001). Increased dosage of a sir-2 gene extends lifespan in Caenorhabditis elegans. Nature *410*, 227–230.

Viswanathan, M., and Guarente, L. (2011). Regulation of Caenorhabditis elegans lifespan by sir-2.1 transgenes. Nature 477, E1–E2.

Walford, R. (1969). The Immunologic Theory of Aging. Immunological Reviews *2*, 171–171.

Wang, P., and Miao, C.-Y.Y. (2017). Reply to Moon and Minhas: Teasing apart NAD+ metabolism in inflammation: commentary on Zhou et al. (2016). Br J Pharmacol 173: 2352-2368. British Journal of Pharmacology *174*, 2962–2963.

Weindruch, R., and Sohal, R.S. (1997). Caloric intake and aging. The New England Journal of Medicine *337*, 986–994.

Weismann, A. (1882). Ueber die Dauer des Lebens.

Whitaker, R., Faulkner, S., Miyokawa, R., Burhenn, L., Henriksen, M., Wood, J.G., and Helfand, S.L. (2013). Increased expression of Drosophila Sir2 extends life span in a dose-dependent manner. Aging (Albany NY) *5*, 682–691.

Whitehead, J.C., Hildebrand, B.A., Sun, M., Rockwood, M.R., Rose, R.A., Rockwood, K., and Howlett, S.E. (2014). A clinical frailty index in aging mice: comparisons with frailty index data in humans. J. Gerontol. A Biol. Sci. Med. Sci. *69*, 621–632.

Williams, G.C. (1957). Pleiotropy, Natural Selection, and the Evolution of Senescence . Evolution *11*, 398–411.

Xu, M., Pirtskhalava, T., Farr, J.N., Weigand, B.M., Palmer, A.K., Weivoda, M.M., Inman, C.L., Ogrodnik, M.B., Hachfeld, C.M., Fraser, D.G., et al. (2018). Senolytics improve physical function and increase lifespan in old age. Nat. Med. *24*, 1246–1256.

Yeung, F., Hoberg, J.E., Ramsey, C.S., Keller, M.D., Jones, D.R., Frye, R.A., and Mayo, M.W. (2004). Modulation of NF-kappaB-dependent transcription and cell survival by the SIRT1 deacetylase. EMBO J. *23*, 2369–2380.

Yoshino, J., Mills, K.F., Yoon, M.J., and Imai, S. (2011). Nicotinamide mononucleotide, a key NAD(+) intermediate, treats the pathophysiology of diet- and age-induced diabetes in mice. Cell Metab. *14*, 528–536.

Youm, Y.-H.H., Grant, R.W., McCabe, L.R., Albarado, D.C., Nguyen, K.Y., Ravussin, A., Pistell, P., Newman, S., Carter, R., Laque, A., et al. (2013). Canonical Nlrp3 inflammasome links systemic low-grade inflammation to functional decline in aging. Cell Metab. *18*, 519–532.

Zhang, D., Li, S., Cruz, P., and Kone, B.C. (2009). Sirtuin 1 functionally and physically interacts with disruptor of telomeric silencing-1 to regulate alpha-ENaC transcription in collecting duct. J. Biol. Chem. *284*, 20917–20926.

Zhang, H., Ryu, D., Wu, Y., Gariani, K., Wang, X., Luan, P., D'Amico, D., Ropelle, E.R., Lutolf, M.P., Aebersold, R., et al. (2016). NAD^+ repletion improves mitochondrial and stem cell function and enhances life span in mice. Science *352*, 1436–1443.

Zhou, C.-C.C., Yang, X., Hua, X., Liu, J., Fan, M.-B.B., Li, G.-Q.Q., Song, J., Xu, T.-Y.Y., Li, Z.-Y.Y., Guan, Y.-F.F., et al. (2016). Hepatic NAD(+) deficiency as a therapeutic target for non-alcoholic fatty liver disease in ageing. British Journal of Pharmacology *173*, 2352–2368.

Chapter 2: PARP14 hydrolyzes NAD^+ during TLR-induced inflammation and aging

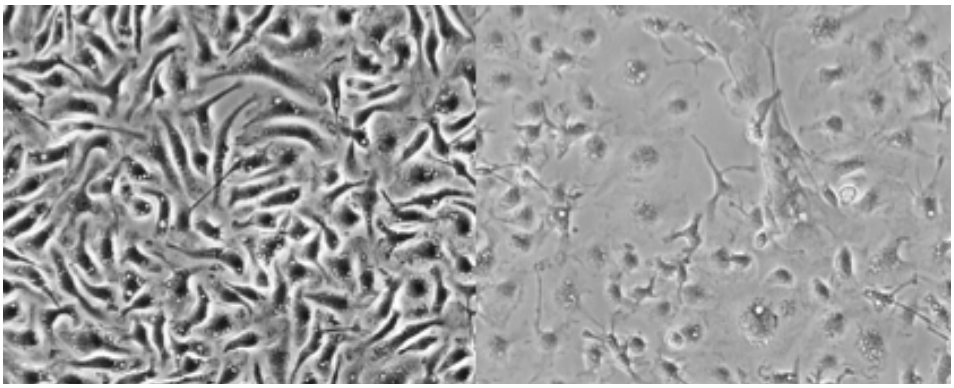

Mouse bone marrow-derived macrophages before and after LPS stimulation

"The precise function of the co-enzyme is even more obscure than its chemical nature."

-Arthur Harden, on the discovery of NAD^+, 1914

This chapter is based on the following manuscript, in preparation:

Schultz, M.B., Bochaton, T., Bonkowski, M.S., Li., J.,Alam, M.P., Kane, A., Gomes, A., Cai, Y., Lokitikayul, D., Colville, A., Tombline, G., Goldfarb, A., Gorbonova, V., Migaud, M., and Sinclair, D.A. (*in preparation*). NAD^+ restoration by PARP14 inhibition and nicotinamide riboside hydride in inflammation and aging.

ABSTRACT

Activated immune cells undergo profound metabolic reprogramming which facilitates inflammation. The role of one essential metabolite, nicotinamide adenine dinucleotide (NAD^+), in inflammation is incompletely characterized. NAD^+, a critical cofactor in redox reactions, is also a signaling molecule whose levels fluctuate in response to circadian rhythm, diet, and aging. Through activation of enzymes that are attuned to these fluctuations, such as sirtuins and poly-ADP-ribose polymerases (PARPs), high NAD^+ levels promote efficient DNA repair, chromatin modifications, and mitochondrial function, which together foster insulin sensitivity, vascular health, and longevity. Here, we report that inflammation induced by Toll-like receptor (TLR) stimulation engenders a precipitous depletion of intracellular NAD^+ in macrophages. We sought to understand the cause of this depletion, which we determined is due to hydrolysis of the NAD^+ molecule, rather than reduction or decreased synthetic flux. Through pharmacological and genetic means, we identified the enzyme PARP14 as necessary for such NAD^+ destruction. We also identified a highly potent, synthetic NAD^+ precursor, nicotinamide riboside hydride (NRH), which is able to restore NAD^+ levels even in the face of PARP14-driven hydrolysis. Restoration of NAD^+ levels by NRH supplementation or PARP14 inhibition restores PARP1 activity, based on level of poly-ADP-ribose. PARP14 levels increase during LPS-induced septic shock and aging in the spleen, and PARP14 inhibition raised NAD^+ levels in both contexts, demonstrating that PARP14 is partially responsible for the decline in NAD^+ levels in inflammation and aging. In addition to identifying PARP14 as a new major regulator of NAD^+ metabolism, our results suggest that PARP14 inhibitors and potent NAD^+-precursors such as NRH are promising drug candidates to treat inflammatory and age-related diseases.

INTRODUCTION

Activation of macrophages, lymphocytes, and other immune cells towards a pro-inflammatory stance requires vast shifts in cellular metabolism to support pathogen clearance. Such shifts put demands on glycolytic (Tannahill et al., 2013) and mitochondrial (Ron-Harel et al., 2016) pathways to fulfill the energetic and biosynthetic needs of the cell. The metabolite nicotinamide adenine dinucleotide (NAD^+) plays a critical role in cellular metabolism, most notably as an electron acceptor in redox reactions. NAD^+ also acts as a signaling molecule, supporting the activities of sirtuins deacylases, ADP-ribosyl transferases, and mediating protein-protein interactions (Li et al., 2017; Rajman et al., 2018; Verdin, 2015). In activated macrophages, demand for NAD^+ requires ongoing biosynthetic pathways to maintain steady state levels. Inhibition of either the NAD^+ salvage pathway (Cameron et al., 2019; Van Gool et al., 2009; Halvorsen et al., 2015; Schilling et al., 2012; Venter et al., 2014) or the NAD^+ *de novo* pathway (Minhas et al., 2019) leads to macrophage dysfunction. At least one pathogen, *Mycobacterium tuberculosis*, targets NAD^+ for degradation in order to blunt immune cell function (Pajuelo et al., 2018; Tak et al., 2019).

As animals age, NAD^+ metabolism becomes dysregulated, resulting in steady state NAD^+ levels dropping by half by middle age (Gomes et al., 2013; Zhou et al., 2016). Increased inflammation during aging may drive this dysregulation, as the expression of the NAD^+-consuming enzyme CD38 (Camacho-Pereira et al., 2016) and the activity of the NAD^+-consuming enzyme PARP1 (Li et al., 2017) increase during aging and are enhanced by inflammatory stimuli (Amici et al., 2018; Liaudet et al., 2002). Increased consumption from these and other enzymes appears to outpace the body's capacity for synthesis (Frederick et al.; Katsyuba et al.). Lowered NAD^+ levels contribute to many age-related maladies including insulin resistance (Yoshino et al.,

2011), vascular disease (Das et al., 2018), and neurodegeneration (Gerdts et al., 2015; Hou et al., 2018), and limit longevity (Zhang et al., 2016).

In this study, we show that NAD^+ is rapidly hydrolyzed in macrophages in response to Toll-like receptor (TLR) stimuli such as lipopolysaccharide (LPS), and we identify that the enzyme PARP14 is necessary for this hydrolysis. PARP14 has previously been implicated in immune cell function as a regulator of STAT6 signaling in response to IL-4 (Cho et al., 2009, 2011; Goenka and Boothby, 2006; Goenka et al., 2007; Iwata et al., 2016; Krishnamurthy et al., 2017; Mehrotra et al., 2011; Riley et al., 2013), of interferon signaling (Caprara et al., 2018; Higashi et al., 2019), and of tissue factor expression (Iqbal et al., 2014). Its role as a regulator of cellular NAD^+ levels was not previously appreciated. In addition, we describe a highly potent NAD^+-boosting molecule, nicotinamide riboside hydride (NRH). We also present evidence that PARP14 activity contributes to low NAD^+ levels during sepsis and aging.

RESULTS

NAD^+ is hydrolyzed after TLR stimulation

To study the effects of inflammation on steady state NAD^+ levels, we stimulated murine bone marrow-derived macrophages (BMDMs) with lipopolysaccharide (LPS, 100 ng/mL) for increasing lengths of time, up to 48 hours, and measured the concentrations of NAD^+ and NAD^+ hydride (NADH). Remarkably, we observed that NAD^+ levels were massively depleted over the first six hours of LPS stimulation. After this initiation phase, longer periods of LPS stimulation resulted in a slow restoration of NAD^+ levels, perhaps an adaptation to prolonged activation (**Fig. 2.1a**). We did not observe a contaminant increase in NADH levels, suggesting that reduction of NAD^+ was not the cause of the apparent depletion. LPS initiates inflammation through activation

of Toll-like receptor (TLR) 4. We found that P3CSK4, a TLR2 agonist, also caused a depletion of intracellular NAD^+ (**Fig. 2.1b**), as did palmitic acid (**Fig. 2.1c**), a saturated fatty acid and TLR4 agonist (Nicholas et al., 2017). This latter finding has implications for the etiology of metabolic syndrome, as high fat diets increase inflammation and reduce NAD^+ levels (Yoshino et al., 2011; Cantó et al., 2012). Interferon gamma (IFNγ) and interleukin-4 (IL-4), both of which activate macrophages through TLR-independent signaling cascades, did not induce an NAD^+ depletion, and in fact raised NAD^+ levels over 48 hours of stimulation (**Fig. 2.1d-e**). Thus, inflammation-induced NAD^+ depletion appears to be TLR dependent.

To verify this NAD^+ depletion observation, we employed two additional methods to assess NAD^+ levels in response to LPS. First, we used a genetically-encoded fluorescent NAD^+-sensor which can be targeted to specific intracellular compartments (Cambronne et al., 2016) in RAW264.7 immortalized macrophages, and observed a depletion of NAD^+ after six hours of LPS treatment, and a partial restoration after 24 hours, in the nucleus, the cytoplasm, and the mitochondria (**Fig. 2.1f-g**). This suggests either that NAD^+ is destroyed throughout the cell, or that NAD^+ levels are in a dynamic equilibrium among the organelles. Additionally, we performed polar mass spectrometry metabolomics in BMDMs, which also corroborated our description of NAD^+ dynamics (**Fig. 2.1i-j**).

Figure 2.1: NAD^+ and NADH levels in response to stimuli. (A) 48-hour timecourse of NAD^+ and NADH levels in BMDMs treated with LPS (100 ng/mL), (B) P3CSK4 (10 μg/mL), (C) Palmitic acid (0.5 mM), (D) IFNγ (100 ng/mL), and (E) IL-4 (20 ng/mL). (F) Fluorescence image and quantified relative levels by flow cytometry for RAW264.7 cells treated with LPS, stably expressing an NAD^+-sensor targeted to the nucleus, (G) cytoplasm, or (H) mitochondria. (I) Overview of NAD^+ metabolic pathways. (J) Mass spectrometry based metabolomics for NAD metabolites form BMDMs treated with LPS for 0 or 6 hours.

Figure 2.1 continued.

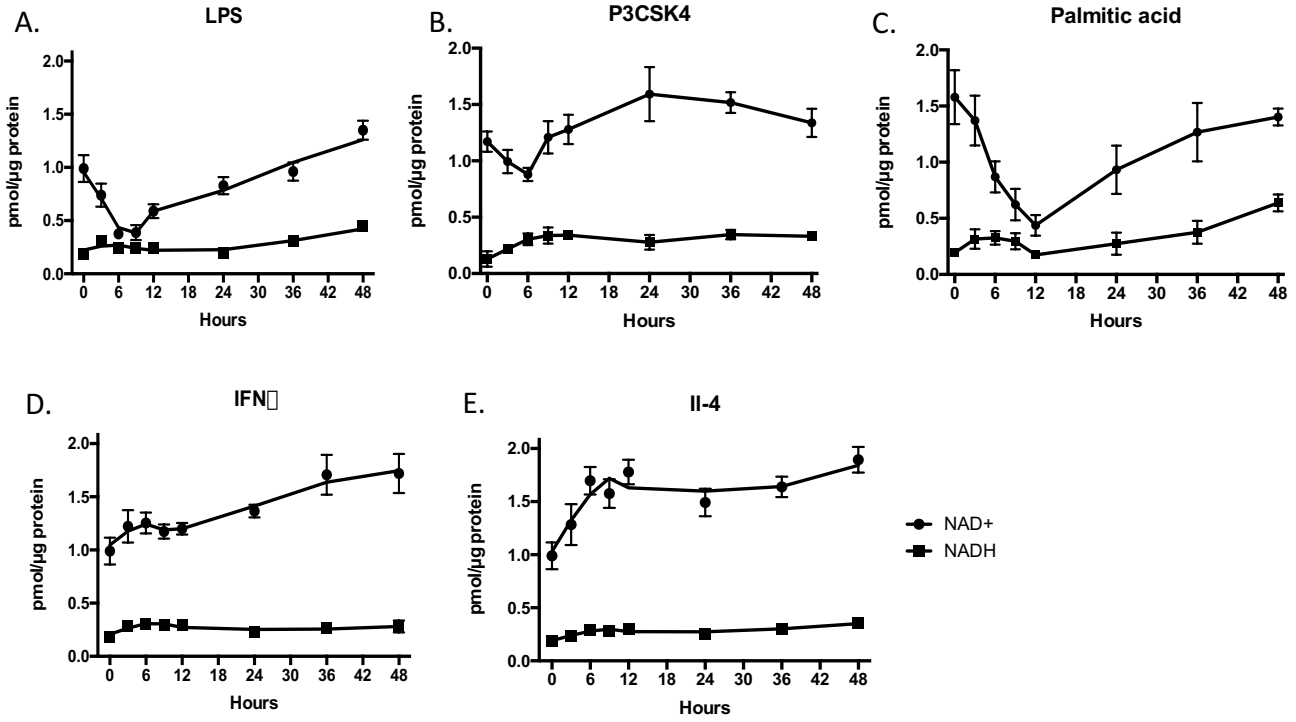

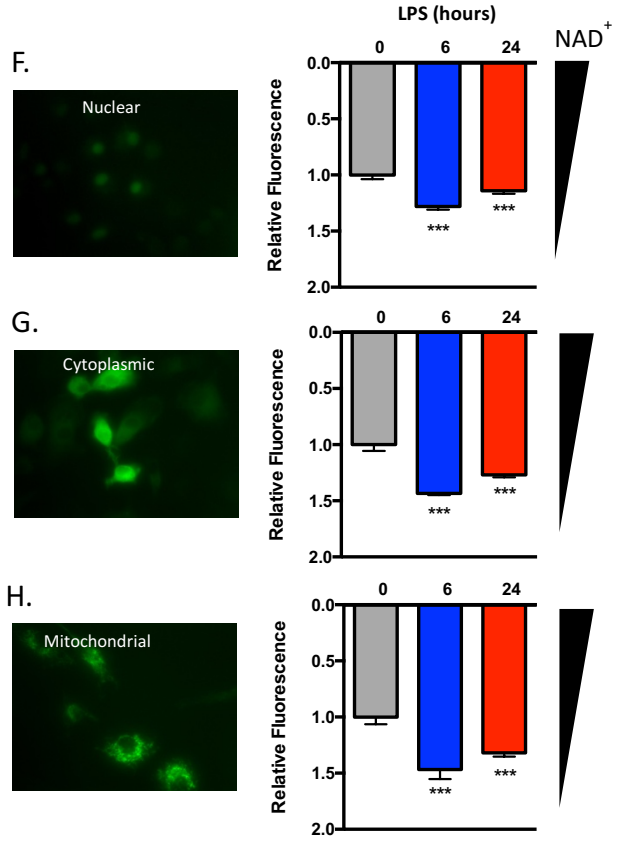

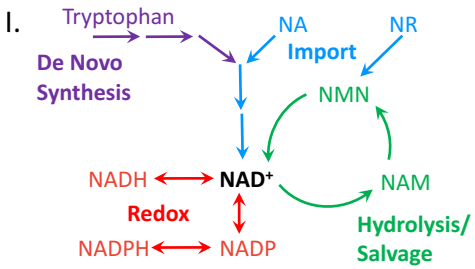

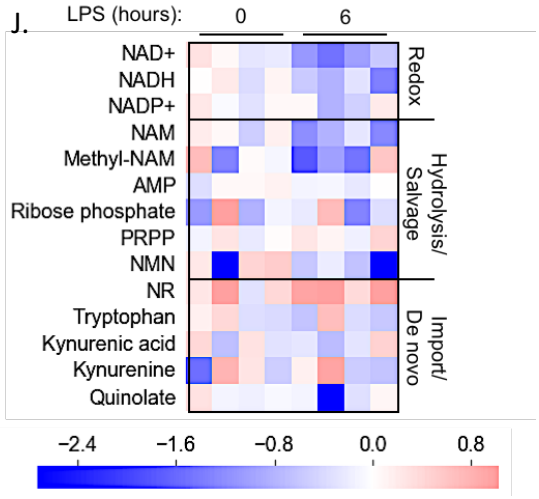

A PARP enzyme is responsible for LPS-induced NAD^+ hydrolysis

We hypothesized that an NAD^+ hydrolase was responsible for the fall in NAD^+ levels. The most apparent candidate was the enzyme CD38, as it is well-known to be induced under inflammatory conditions and is a highly active NAD^+ hydrolase (Amici et al., 2018; Camacho-Pereira et al., 2016). However, the potent CD38 inhibitor GSK-78c, which had an IC_{50} of 7 nM with recombinant mouse CD38 *in vitro*, did not protect NAD^+ levels from falling in LPS-stimulated macrophages, even at a concentration of 10 μM (**Fig. 2.2a-b**) (Haffner et al., 2015).

We next widened our search by measuring the RNA levels of enzymes involved in NAD^+ consumption and production, in order to implicate one or several as the driver of LPS-induced NAD^+ depletion (**Fig. 2.2c**). While CD38 levels were massively elevated by LPS, the increase did not begin until after six hours, demonstrating that the kinetics of CD38 induction were temporally incongruous with those of the NAD^+ depletion. We did, however, observe a large increase in the RNA levels of multiple members of the PARP family after six hours of LPS treatment, in particular for PARPs 7, 9, 10, 11, 12, and 14. Levels of these enzymes were moderately lower at 24 hours compared to six hours, demonstrating an expression pattern inversely correlated to NAD^+ levels. We also observed an increase in the levels of the NAD^+-synthetic enzymes NAMPT, and NMNAT1 and 2, which may account for the recovery in NAD^+ levels over longer periods of LPS stimulation.

To test if one or multiple of these PARPs were responsible for the initial drop, we treated macrophages with two pan-PARP inhibitors, 3-aminobenzimide and PJ-34. These drugs modestly raised NAD^+ levels in the absence of LPS, and completely ablated the drop in NAD^+ levels following LPS stimulation (**Fig. 2.2d**). While we observed no increase in PARP1 RNA levels, PARP1 accounts for the vast majority of basal PARP hydrolase activity in many cells, so we could

not easily dismiss it as the culprit enzyme (Shieh et al., 1998). Several additional experiments led us to rule it out. When PARP1 was immunoprecipitated from LPS-stimulated macrophages and its activity assayed *in vitro*, its activity tracked with falling NAD^+ levels, with almost no PARP1 activity observed when the enzyme was immunoprecipitated from macrophages treated with LPS for six hours (**Fig. 2.2e**). While this result was initially surprising, as NAD^+ is provided in the *in vitro* assay, we found PARP1 bound to its inhibitor DBC1 when NAD^+ levels were low, thus explaining the enzyme's low activity (**Fig. 2f**) (Li et al., 2017). We also observed that levels of poly-ADP ribose (PAR), the product of PARP1 activity, fell with LPS stimulation (**Fig. 2.2g**). If PARP1 were the responsible enzyme, we would expect levels of PAR to increase. The protein levels of both PARP1 and CD38 tracked with their RNA levels: PARP1 protein levels were decreased with LPS stimulation, and CD38 levels were increased but only after NAD^+ levels were already low (**Fig. 2.2g**).

As further evidence in support of our hypothesis that a PARP enzyme other than PARP1 was responsible for the fall in NAD^+ levels, we found that the small molecule OUL35 modestly raised NAD^+ levels in the absence of LPS, and completely ablated the drop in NAD^+ levels following LPS-stimulation in a dose-dependent manner (**Fig. 2.2h**). OUL35 is a potent PARP10 inhibitor, with activity against other PARP enzymes including PARPs 4 and 14 (Venkannagari et al., 2016). Importantly, OUL35 did not inhibit activity of PARP1, even at a concentration of 1 mM (**Fig. 2.2i**). Thus, we concluded that one or multiple PARP enzymes other than PARP1 were responsible.

Figure 2.2: Expression and activity of NAD^+-associated enzymes. (A) Dose-response curve of rmCD38 activity in the presence of GSK-78c, as measured by the etheno-NAD assay. (B) NAD^+ levels in BMDMs treated with LPS (100 ng/mL) for six hours and increasing doses of GSK-78c. (C) RNA levels of genes associated with NAD metabolism in BMDMs treated with LPS for six or 24 hours. (D) NAD^+ levels in BMDMs treated with LPS for six hours without or with 3-aminobenzimide (5 mM) or PJ-34 (10 μM). (E) Activity of immunoprecipitated PARP1 from BMDMs treated with LPS for 0, 3, 6, or 24 hours, as measured by PARylation of a histone substrate *in vitro*. (F) Western blot of levels of PARP1 and DBC1 in lysate from LPS-treated BMDMs from input and immunoprecipitant with a PARP1 antibody. (G) Western blot from BMDMs treated with LPS for PAR, PARP1, CD38, and Actin. (H) NAD^+ levels in BMDMs treated without or with LPS, and increasing doses of OUL35. (I) PARP1 activity *in vitro* in the absence or presence of PJ-34 and OUL35.

Figure 2.2 continued.

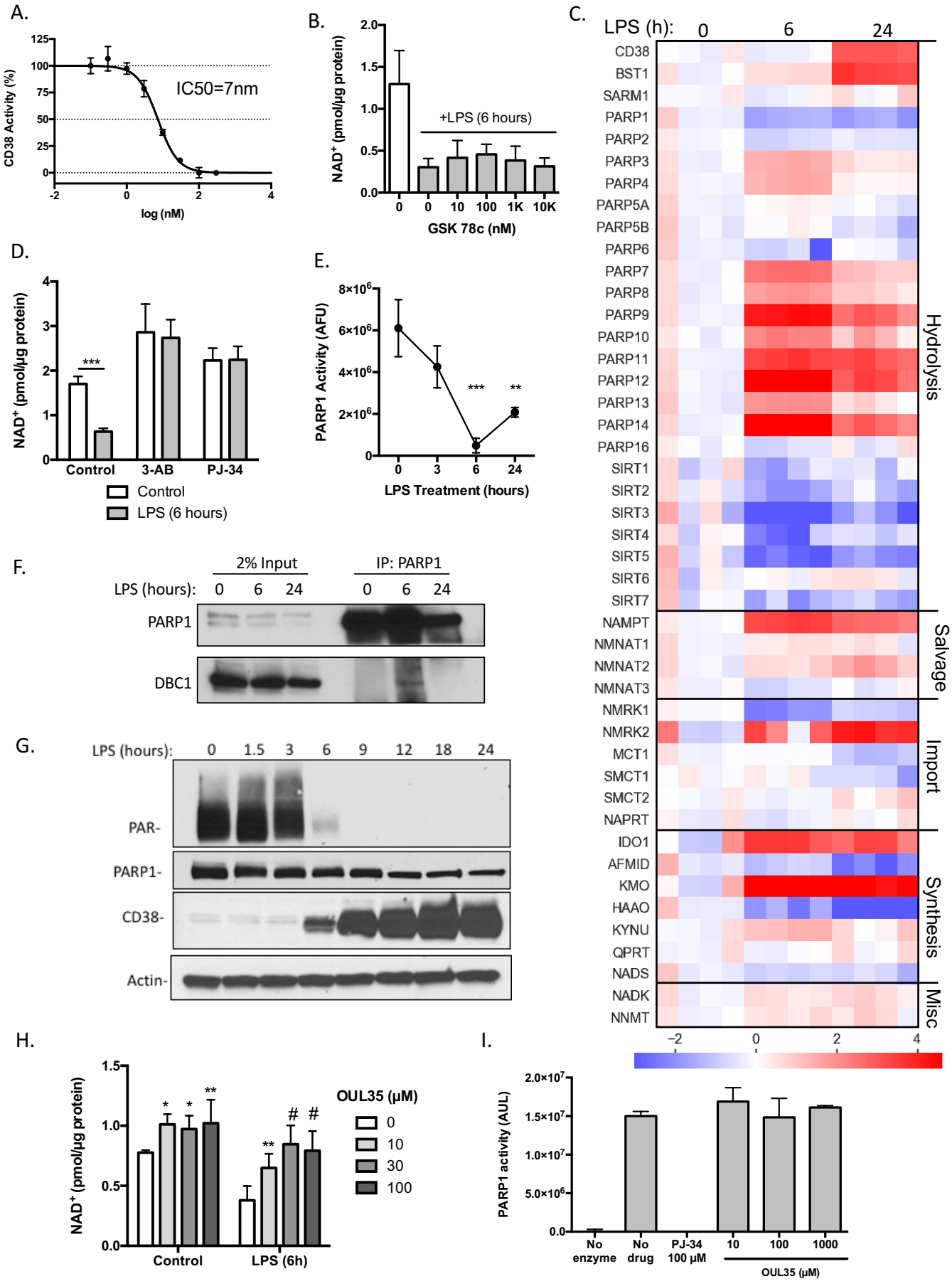

PARP14 is necessary for LPS-induced NAD^+ hydrolysis

To determine if a single PARP enzyme was responsible, we used CRISPR/Cas9 in RAW264.7 cells to generate multiple cell lines with either PARP 7, 9, 10, 11, 12, or 14 knocked out. Three to four compound heterozygous knock out cell lines were identified for each PARP by PCR screening and DNA sequencing (**Fig. 2.3a**). When stimulated with LPS for six hours, the level of NAD^+ fell in all cell lines except for those lacking PARP14, identifying PARP14 as solely necessary among these enzymes for the LPS-induced fall in NAD^+ levels (**Fig. 2.3b**). In both RAW264.7 cells and in BMDMs, LPS induced an increase in PARP14 protein levels (**Fig. 2.3c-d**). To verify that other well-known NADases were not responsible, we obtained knockout mice for PARP1, CD38, SARM1, and PARP14. While BMDMs deficient in each of the first three enzymes did have slightly elevated NAD^+ levels at individual time points in an LPS timecourse, all still displayed an initial drop in NAD^+ levels. Only for PARP14 knockout cells did NAD^+ levels remain steady (**Fig. 2.3e**). These results clearly demonstrate that PARP14 is necessary for the LPS induced fall in NAD^+ levels. However, PARP14 is not sufficient in all contexts to induce a fall in NAD^+ levels, as interferon gamma also induced its expression but did not lower NAD^+ levels (**Fig. 2.3f-g**). A second, yet-unidentified permissive signal must be induced by LPS, allowing for NAD^+ depletion.

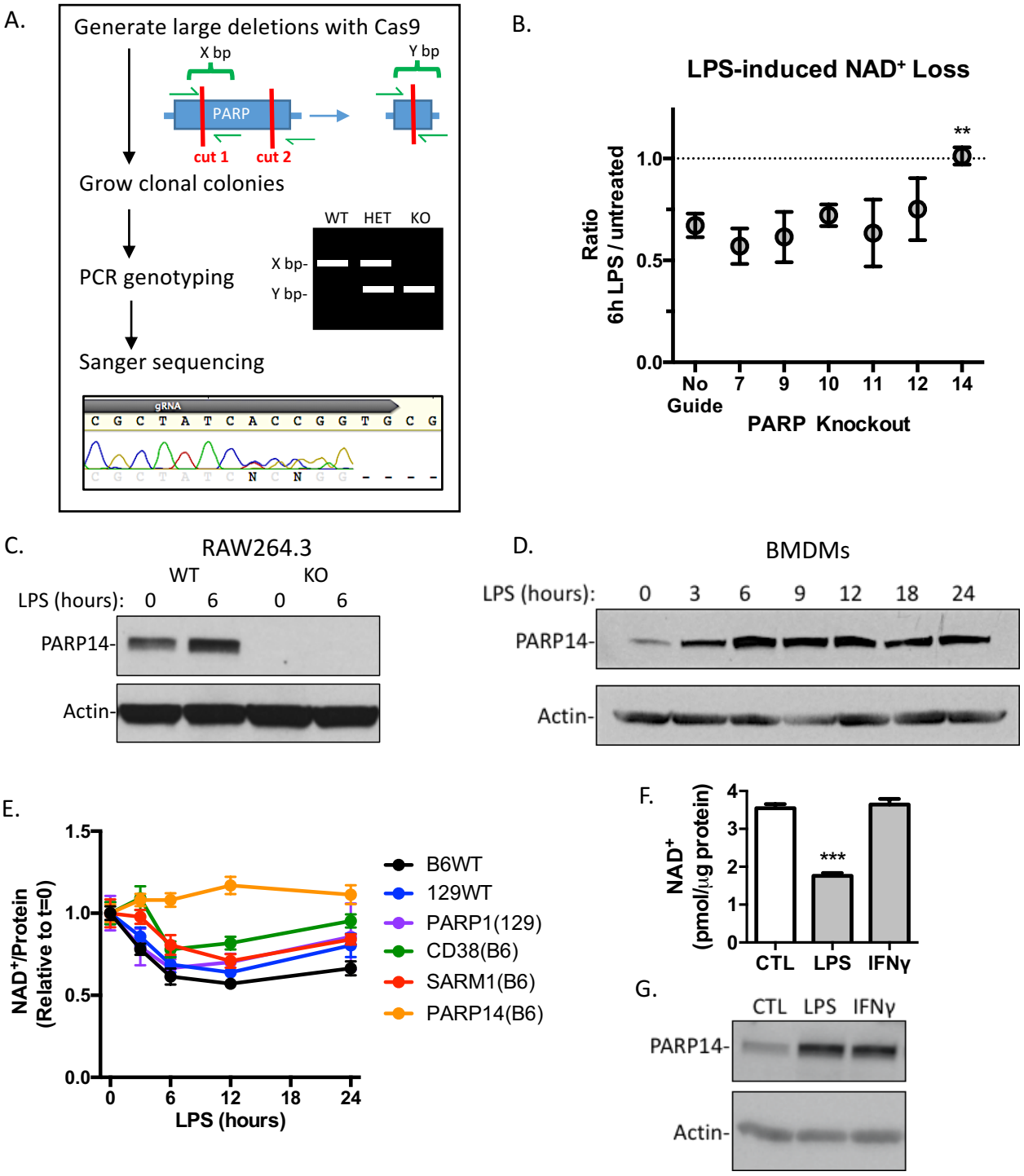

Figure 2.3: Identification of PARP14 as necessary for LPS-induced NAD$^+$ hydrolysis. (A) Overview of process to generate and identify clonal PARP knockout cell lines in RAW264.7 immortalized macrophages. (B) Ratio of NAD$^+$ levels in LPS-treated (100 ng/mL, 6 hours) cells to NAD$^+$ levels in untreated cells. Each point is the average of at least three independent cell lines. (C) PARP14 levels in WT and PARP14 knockout RAW264.7 cells without and with LPS. (D) PARP14 levels in BMDMs treated with LPS. (E) NAD$^+$ levels in LPS-treated BMDMs in WT (C57/Bl6 and 129 strains), PARP1 KO, CD38 KO, SARM1 KO, and PARP14 KO mice. (F) NAD$^+$ levels and (G) PARP14 protein levels in BMDMs treats with LPS or IFNγ (100 ng/mL).

Mechanism of PARP14-dependent NAD^+ hydrolysis

We next sought to understand the mechanism by which PARP14 engenders such a decrease in steady state NAD^+ levels. It is indeed surprising that PARP14 would drive this phenomenon, as PARP14's reported enzymatic activity is as a mono-ADP ribosyl transferase (ADPRT), and thus it would be difficult for the enzyme to achieve the activity required to deplete so large a quantity of NAD^+ (Vyas et al., 2013). One hypothesis is that PARP14, under the right conditions, could be a highly active ADPRT, indiscriminately post-translationally modifying copious target proteins. To test this hypothesis, we performed mass spectrometry-based proteomics on wild-type and PARP14 knockout BMDMs treated with LPS for six hours, enriched for peptides containing post-translational modifications with phosphates on a titanium oxide column, and analyzed peptides with an ADPR modification. Peptides with a ribose-phosphate (ribP) modification were also included in the analysis, as this modification is likely a result of degraded ADPR following hydrolysis of the pyrophosphate. Surprisingly, we found more unique proteins with an ADPR or ribP modification in knock out cells than in the wild-type cells. While not a quantitative assay, these data do not provide evidence to support a massive increase in ADPRylation that would account for the NAD^+ depletion (**Fig. 2.4a-b**). This modest increase in ADPRylated unique proteins associated with PARP14 deletion is likely due to the fact that knockout cells have much higher NAD^+ levels, allowing other ADPRTs to function.

Among the proteins identified as ADP-ribosylated in wild-type cells but not in knockout cells were Akt1, Rictor, NF-κB, and PARP14 itself. We performed cluster analysis on the list of proteins identified as ADP-ribosylated in the wild-type cells but not in the knockout cells. Many of the identified clusters involved RNA biology, suggesting that PARP14 may have a role in RNA processing and homeostasis (**Fig. 2.4c**).

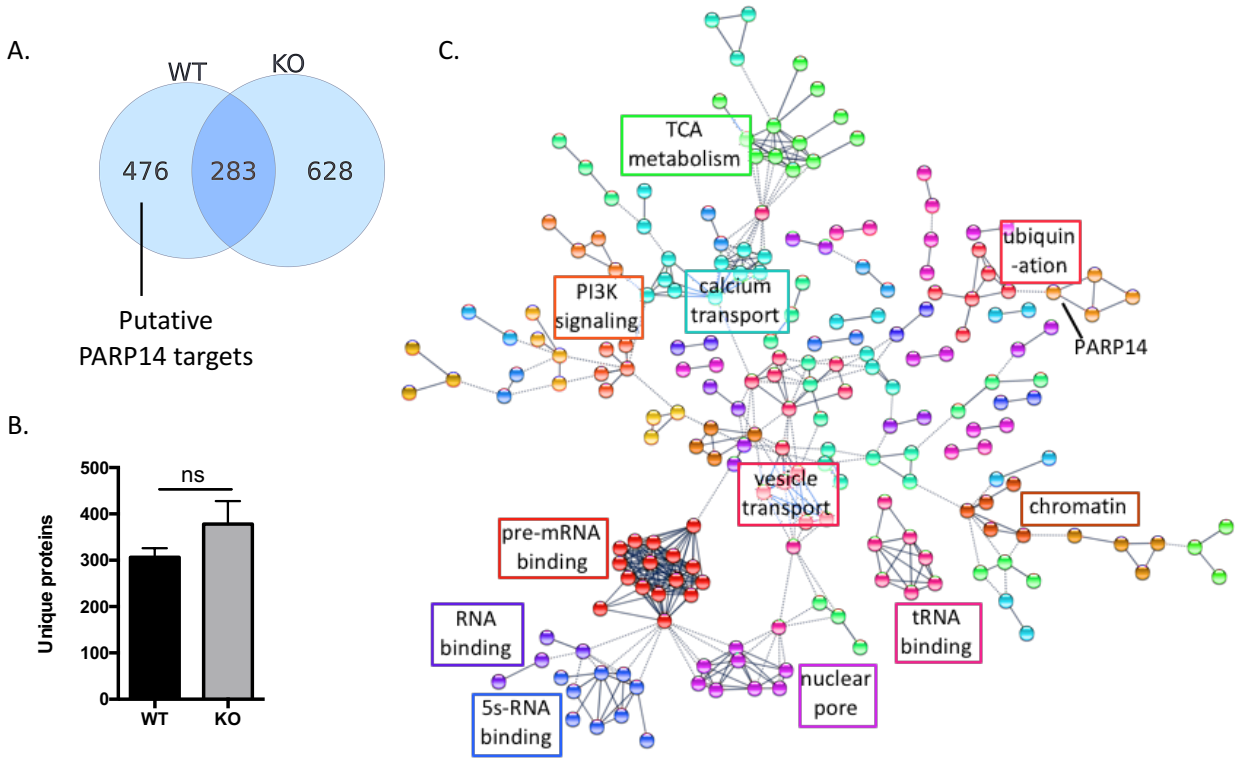

Figure 2.4: Mass spectrometry-based proteomics for ADPR and ribP PTMs. (A) Venn diagram of unique proteins found in wild type and PARP14 knock out BMDMs treated with LPS (100 ng/mL) for six hours. (B) Number of unique proteins per biological replicate (N=3). (C) STRING interactome map of PARP14 targets, with clusters labeled by gene ontology enrichment analysis.

Our next two hypotheses to account for how PARP14 could drive NAD^+ consumption were inspired by an evaluation of PARP14's domains (**Fig. 2.5a**). PARP14's enzymatic activity is driven by its C-terminal PARP domain, shared among all PARP family members. It is also a Macro-PARPs (along with PARP9 and PARP15) in that it contains Macro domains, which bind to and in some cases hydrolyze ADP-ribose. PARP14's first Macro domain is predicted to have such hydrolase activity based on a homology comparison to Macro domain-containing proteins with ADP-ribose hydrolase activity, such as MacroD1, and Macro domain containing proteins without such activity, such as histone macro-H2A.1 (Jankevicius et al., 2013). This observation led to the hypothesis that PARP14 may be auto-ADP-ribosylating itself via its PARP domain and then removing the ADP-ribose via its first Macro domain, leading to high NAD hydrolase processivity.

PARP14 also contains an N-terminal RNA-recognition motif (RRM). This led to the hypothesis that PARP14 may be ADP-ribosylating nucleic acids rather than proteins. This hypothesis fits in line with the mass spectrometry clustering analysis, which found that PARP14 may modify many RNA-binding proteins. Furthermore, PARP2 and PARP3 were recently shown to be able to ADP-ribosylate the terminal phosphates of DNA, increasing the plausibility that PARP14 may directly ADP-ribosylate a nucleic acid (Belousova et al., 2018; Zarkovic et al., 2018). PARP14 has also been shown to localize to RNA stress granules (Leung et al., 2011) and to regulate the stability of a specific mRNA, albeit not via direct ADPRylation (Iqbal et al., 2014).

To test these hypotheses, we overexpressed wild-type or mutant PAPR14 constructs in human embryonic kidney 293T cells, in comparison to GFP on the same backbone as a control (**Fig. 2.5b-c**). Overexpression of wild type PARP14 massively depleted cellular NAD^+, demonstrating that the permissive signal which allows PARP14 to deplete NAD^+ in LPS treated macrophages is likely constitutively active in 293T cells. The catalytically inactive PARP14 mutant G888W had no effect on NAD^+ levels, demonstrating that the PARP domain is necessary

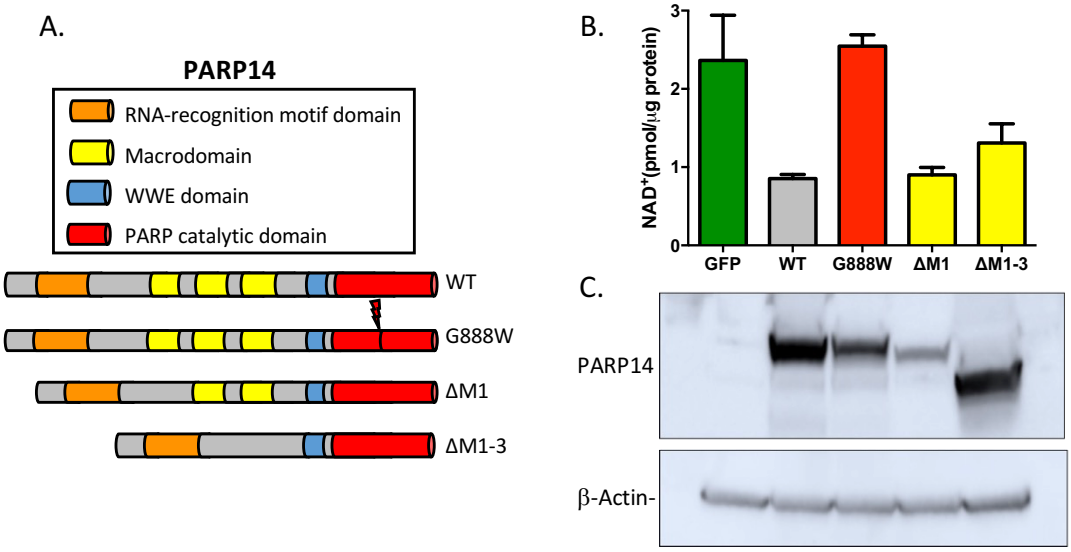

Figure 2.5:Activity of PARP14 mutants in 293T cells. (A) Diagram of PARP14 domains and mutants tested. (B) NAD^+ levels and (C) PARP14 protein levels in human embryonic kidney 293T cells overexpressing wildtype or mutant PARP14.

for activity. PARP14 mutants missing either the first Macro domain (ΔM1) or all three of its Macro domains (ΔM1-3) still retained most of their activity, suggesting that the Macro domains do not play a large role in the enzyme's NAD^+-hydrolase function. At present, we cannot reject the nucleic acid ADPRylation hypothesis. Experiments to measure the activity of a PARP14 mutant missing the RNA recognition motif, and to probe PARP14's activity *in vitro* with the addition of various substrates, are ongoing in order to test this hypothesis.

NRH is a highly potent NAD-precursor

We next sought to identify the consequences on macrophage function from such a depletion of intracellular NAD^+. To address this, we identified multiple methods to maintain NAD^+ levels during LPS stimulation. This can be done genetically, with PARP14 knockout (KO) BMDMs, or pharmacologically with a PARP14 inhibitor. It can also be done with supplementation of an NAD^+ precursor. We compared the efficacy of four NAD^+ precursors in macrophages: nicotinamide mononucleotide (NMN), nicotinamide riboside (NR), nicotinic acid riboside (NAR), and NR hydride (NRH) (**Fig. 2.3a-d**). While all were able to raise NAD^+ levels, NRH had surprising efficacy, even at micromolar concentrations (**Fig 2.3e-f**). As a synthetic metabolite, it may escape natural mechanisms of regulation or destruction. Or, as the only precursor without a charge on its pyridine ring, it may permeate cell membranes more rapidly.

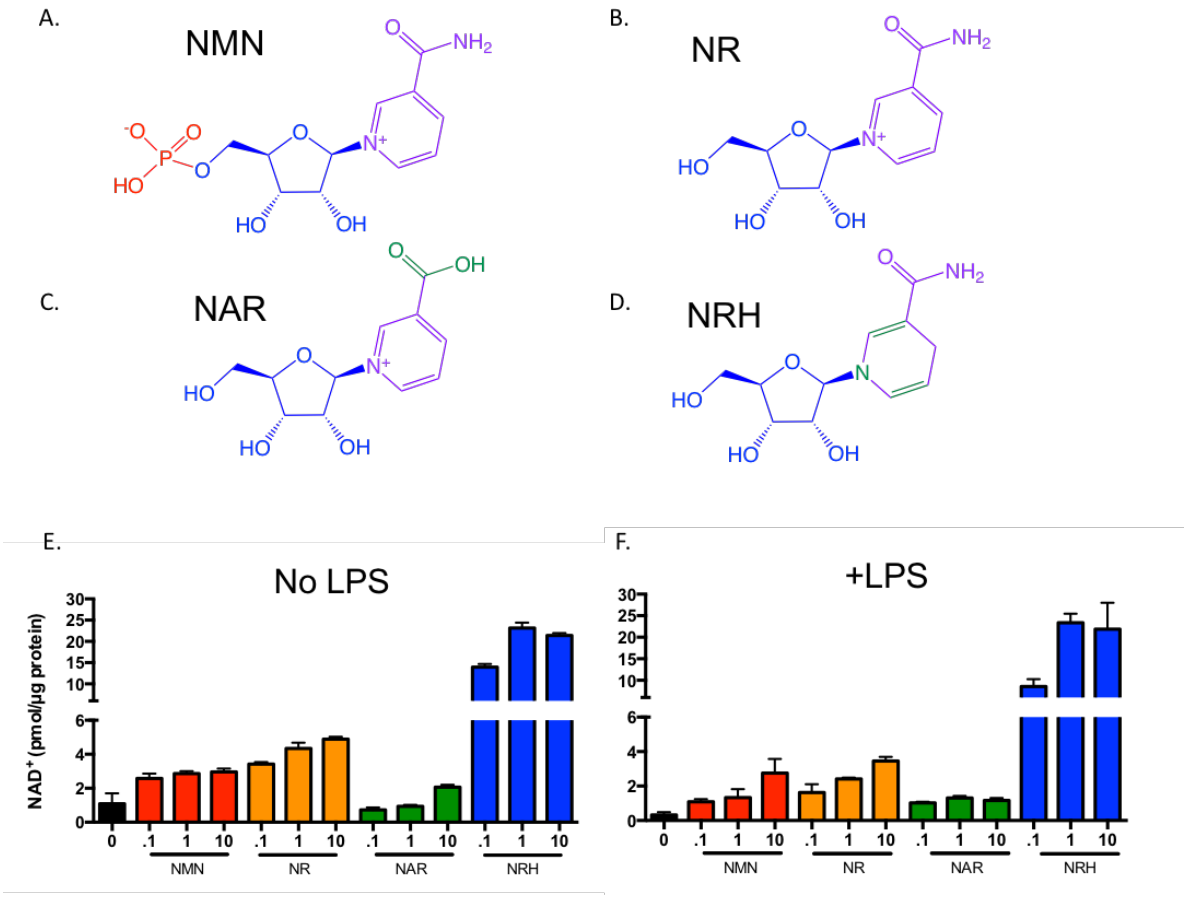

Figure 2.6: Comparison of NAD$^+$ precursor efficacy in BMDMs. (A) Chemical structure of nicotinamide mononucleotide (NMN), (B) nicotinamide riboside (NR), (C) nicotinic acid riboside (NAR), and (D) NR hydride (NRH). Structures are colored by chemical group: blue for ribose, purple for nicotinamide or related group, red for phosphate, and green for modifications to the nicotinamide group. (E) NAD$^+$ levels in BMDMs treated with NAD$^+$ precursors without or (F) with LPS (100 ng/mL) for six hours.

NAD^+ depletion engenders loss of PARylation

Using multiple approaches to maintain NAD^+ levels, we explored the effect of NAD^+ depletion on macrophage function. When comparing cytokine secretion between wild-type and PARP14 knockout cells, TNFα levels were unchanged, while IL-6 and IL-1β secretion were slightly depressed (**Fig. 2.7a-c**). However, pharmacological modulation of NAD^+ levels did not phenocopy these results. IL-6 levels were unchanged by OUL35 and NRH treatment, and IL-1β levels were in fact slightly increased by NRH treatment. This last finding suggests that IL-1β secretion may be sensitive to NAD^+ levels below or above physiological levels.

We also observed no consistent effect on phagocytosis, mitochondrial number and membrane potential, or ROS production. One consistent effect we did observe was a loss of PAR, likely due to a loss of PARP1 activity, which could be restored with PARP14 depletion, inhibition with OUL35, or NAD^+ repletion with NRH (**Fig 2.7g-h**). We are currently exploring the effect of NAD^+ depletion on the activity of other enzymes such as sirtuins.

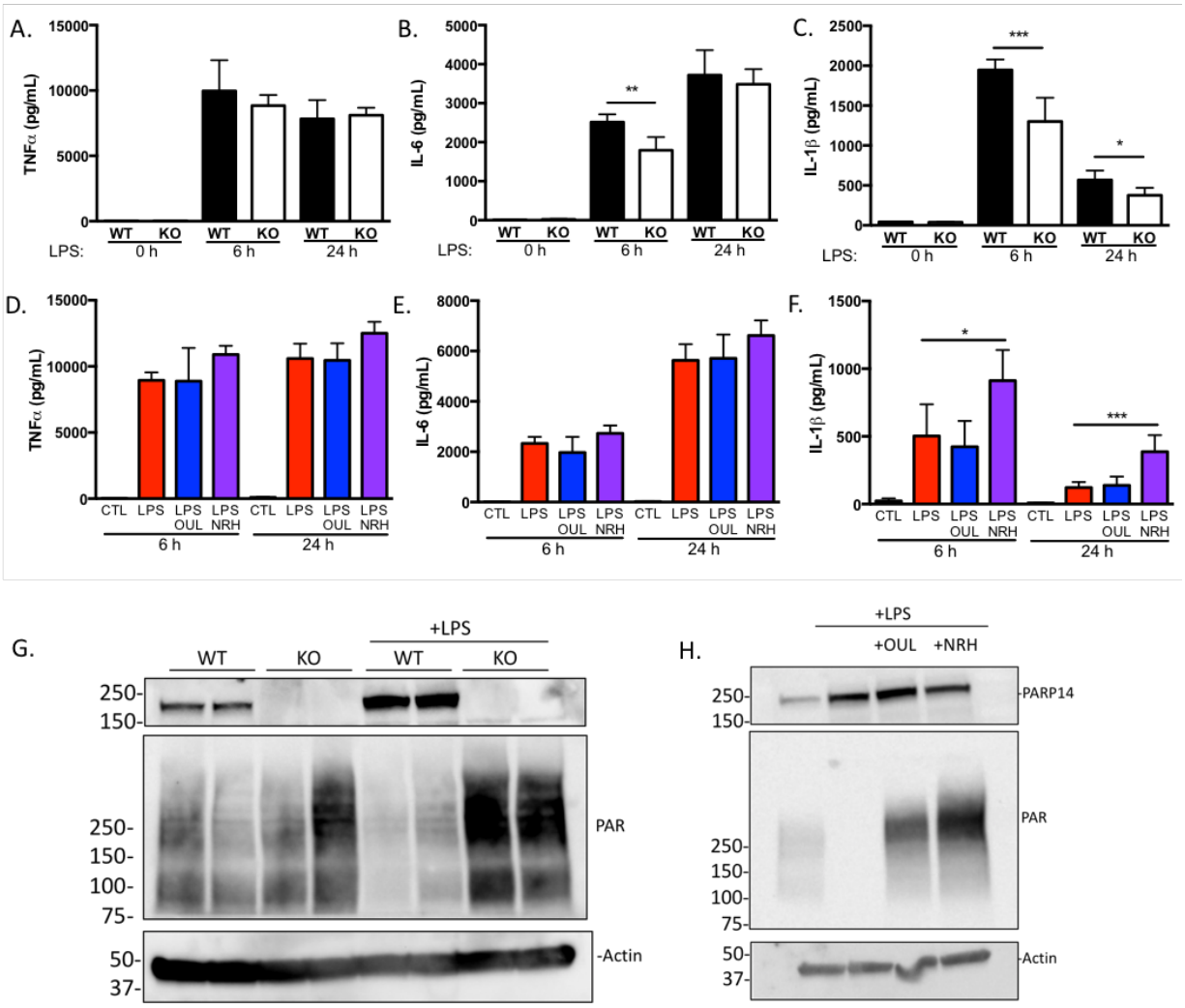

Figure 2.7: Effects of NAD$^+$ modulation in BMDMs. (A) TNFα, (B) IL-6, and (C) IL-1β (with 30 min nigericin treatment) secretion in PARP14 wild-type and knockout BMDMs stimulated with LPS. (D) TNFα, (E) IL-6, and (F) IL-1β (with 30 min nigericin treatment) secretion in BMDMs treated with OUL35 (30 μM) or NRH (100 μM). (G) PARylation levels in PARP14 wild-type and knockout BMDMs treated with LPS. (F) PARylation levels in wild-type BMDMs treated with LPS, OUL35, and NRH for six hours.

PARP14 depletes splenic NAD^+ in sepsis and aging

We extended our findings to a model of LPS-induced septic shock, wherein a single intraperitoneal LPS injection induces an often lethal cytokine storm. We observed that six hours after LPS injection, PARP14 protein levels were elevated in the spleen, an organ with a large population of resident macrophages (**Fig. 2.8a**). This increase in PARP14 expression was associated with a depletion of NAD^+ levels, a phenomenon that does not occur in PARP14 knockout animals (**Fig. 2.8b**). Co-injection of LPS with OUL35 or NRH was also sufficient to

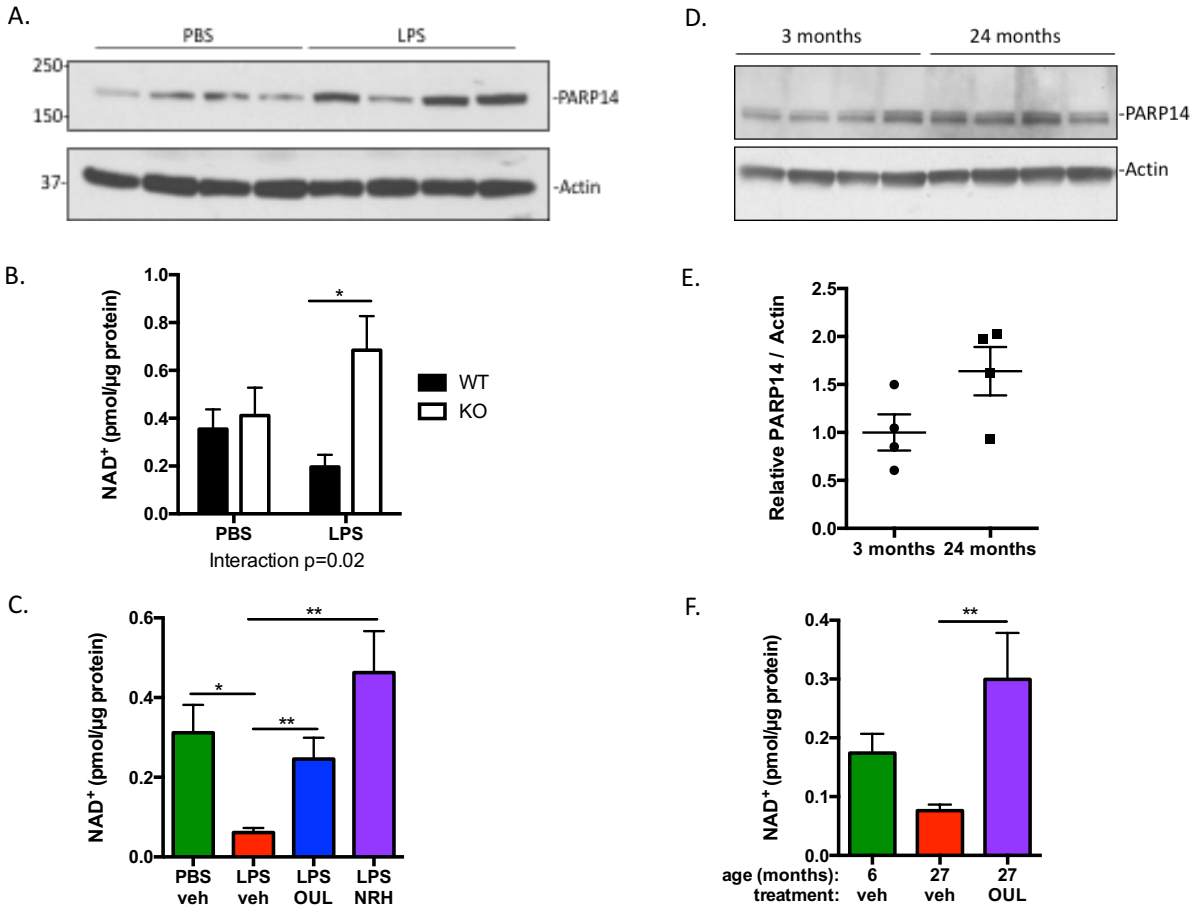

Figure 2.8: PARP14's effect on splenic NAD^+ levels. (A) PARP14 protein levels in the spleen 6-hours after LPS injection (15 mg/kg). (B) NAD^+ levels in PARP14 wild-type and KO mouse injected with PBS vehicle or LPS. (C) NAD^+ levels in wild-type mice injected with LPS, and co-injected with either vehicle (veh), OUL35 (200 mg/kg) or NRH (200 mg/kg). (D-E) PARP14 protein levels in young and aged mice. (F) NAD^+ levels in young mice and aged mice injected with vehicle (veh), and in aged mice injected with OUL35 (200 mg/kg) for two hours.

maintain splenic NAD^+ levels (**Fig. 2.8c**). However, neither PARP14 knockout mice, nor mice injected with OUL35 or NRH, had a survival benefit over wild-type or vehicle-injected animals.

We also observed an increase in PARP14 protein levels in the aging spleen (**Fig. 2.8d-e**). This is associated with a drop in NAD^+ levels, as has been observed in other tissues during aging. To test if PARP14 was a driver of low splenic NAD^+ during aging, we injected OUL35 into 27-month old mice, which raised NAD^+ levels to those seen in young mice (**Fig. 2.8f**). This implicates PARP14 induction, likely due to age-related inflammation, as a novel cause of low NAD^+ levels in aged tissues.

DISCUSSION

From yeast to humans, aging is associated with a drop in NAD^+ levels, which limits the activity of sirtuins and PARPs and contributes to the etiology of many age-related diseases. This has been previously attributed to increased DNA damage driving PARP1 activity (Bai et al., 2011), to increased CD38 levels (Camacho-Pereira et al., 2016), and to insufficient levels/activity of NAD^+-producing enzyme NAMPT (Frederick et al., 2016). We identified another enzyme as a driver of low NAD^+ levels: inflammation-induced PARP14. Interestingly, PARP14 was recently identified by another group as one of only sixteen genes whose levels consistently increase with age across multiple tissues (Benayoun et al., 2019). These data suggest that, as inflammation increases during aging, increased PARP14 levels may enhance NAD^+ hydrolysis, contributing to decreased levels of the metabolite.

Taken together, our findings reveal in PARP14 a novel highly active inflammation-induced suppressor of intracellular NAD^+ levels, that limits the activity of other NAD^+-utilizing enzymes. Recently several PARP14 inhibitors have been developed, with varying specificities and

pharmacokinetic properties (Holechek et al., 2018; Peng et al., 2017; Yoneyama-Hirozane et al., 2017). These and other molecules targeting PARP14, along with highly potent NAD^+-precursors such as NRH, represent enticing candidate molecules to treat inflammatory and age-related diseases.

MATERIALS AND METHODS

Cell culture

Bone barrow-derived macrophages were generated from bone marrow collected from the femurs and tibias of mice, differentiated for 7-10 days in RPMI 1640 supplemented with 10% heat-inactivated fetal bovine serum (FBS), 10% L929 cell (ATCC) conditioned media, and 1% penicillin/streptomycin (pen/strep) (Gibco). Media was changed on day 3, at which point non-adherent cells were removed, and subsequently every 2 days.

RAW264.7 cells (ATCC) and HEK 293T cells were cultured in DMEM supplemented with 10% FBS and 1% pen/strep. All cell lines and primary cultures were grown in a 37°C humidified incubator at 5% CO_2, and were regularly tested for mycoplasma. LPS (Sigma-Aldrich), P3CSK4 (Abcam), palmitic acid (Sigma-Aldrich), IFNγ (R&D Systems), IL-4 (R&D Systems), 3-aminobenzimide (Sigma-Aldrich), PJ-34 (Sigma-Aldrich), OUL35 (Sigma-Aldrich), and NMN (GeneHarbor) were added in the concentrations describes in the figure legends. NR and NAR were received from Dr. David Livingston (MetroBiotech), and NRH was received from Professor Marie Migaud (University of South Alabama, Mobile, AL).

NAD^+ Measurements

NAD^+ and NADH were measured with a commercially available kit (Promega). Cells and tissue were homogenized and lysed in a 1:1 solution of PBS and 0.2 N NaOH containing 1% (w/v) dodecltrimethylammonium bromide (Sigma-Aldrich), on ice, and centrifuged maximum speed for 5 min at 4°C to remove insoluble materials. For tissues, lysates were pre-normalized to protein concentration before NAD^+/NADH measurements. For NAD^+ measurements, 15 µL of lystate was pH-adjusted with the addition of 7 µL of 0.4 N HCl; for NADH measurements, 15 µL of lysate

was used and the pH was left basic. Samples were heated at 60°C for 15 min to destroy NADH or NAD^+, respectively, based on pH. After a 10 min incubation at room temperature to allow for cooling, the NAD^+ samples were neutralized with 7 µL of 0.5 M Tris base (Sigma-Aldrich). For NADH samples, 7 µL of 0.4 HCl and 7 µL of 0.5 M Tris base were added to neutralize the samples and match the buffer composition of the NAD^+ samples. Finally, 15 µL of each sample was mixed with 15 µL of a mixture containing lactate, lactate dehydrogenase, proluciferin, and an NADH-dependent proluciferin reductase, in a white half-area 96-well plate (Vidugiriene et al., 2014). A standard curve of NAD^+ at known concentrations, from 4 µM to 7 nM, made in the same final buffer composition as the samples, was also incubated with the enzyme mixture. Luminesce was measured approximately every ten minutes for up to one hour, until standard curve became saturated. NAD^+ or NADH levels were inferred by luminescence compared against the standard curve, and were normalized to protein concentration, measured with the bicinchoninic acid assay on the original lysates (Thermo Fisher Scientific).

NAD^+ Biosensor

The plasmids for the NAD^+ biosensor, localized to various cell compartments, were a kind gift from Xiaolu Cambronne and Michael S. Cohen (Oregon Health & Science Univrsity, Portland, OR). The plasmids were packaged into lentiviruses by standard protocols. In brief, each plasmid was transfected into HEK 293T cells with the lentiviral packaging plasmids pMDG.2 and psPAX2, using X-treme GENE HP transfection reagion (Roche). Media was changed 1 day after transfection, and media containing lentivirus was collected on days 2 and 3 post-transfection, filtered with a 0.2 micron filtered, and delivered to RAW264.7 immortalized macrophages (ATCC). Cells were selected with puromycin (2 µg/mL). After incubation with LPS, fluorescence

was measured by flow cytometry on an LSRII flow cytometer (BD). Cells were gated to exclude debris and doublets. Values were calculated for median fluorescence in the FTIC channel.

Mass spectrometry

For mass spectrometry-based metabolomics, cells were lysed in 80% methanol (v/v) and centrifuged (maximum speed for 5 m) to remove insoluble materials. Supernatants were transferred to a fresh tubes and solvent was removed with a SpeedVac concentrator. Samples were resuspended in water and analyzed on a QTRAP 5500 LC-MS/MS System (SCIEX).

Sample preparation for analysis of post-translational ADPR modifications was based on methods previously described (Matic et al., 2012; Villen et al, 2008). BMDMs were washed twice with PBS and collected after incubation with trypsin and mechanical scraping, followed by two more PBS washes and spins. After re-pelleting, PBS was aspirated and the cell pellets were snap-frozen in liquid nitrogen and stored at -80°C until further processing. Pellets were resuspended in lysis buffer (50 mM HEPES, 75 mM NaCl, 3% SDS, 1 mM NaF, 1 mM beta-glycerophosphate, 1 mM sodium orthovanadate, 10 mM sodium pyrophosphate, 1 mM PMSF, protease inhibitors (Roche), pH 8.5), passed through a 21 gauge needle 20 times, and sonicated (5x 20 sec with one min between pulses, on ice). Cellular debris was removed by centrifugation (max speed 5 min), and lysate concentrations were normalized using the BCA assay.

To reduce the proteins, samples were incubated with DTT (10 mM final concentration) at 50°C for 1 hour. Alkylation was carried out via addition of iodoacetamide (15 mM final concertation) and incubation in the dark at RT for 1 hour. Unreacted iodoacetamide was quenched by adding an additional 25 μL of 0.5 M DTT. Proteins were precipitated with methanol-chloroform and dried overnight in a chemical hood at RT. Proteins were resuspended in 1 mL of

50 mM ammonium bicarbonate (pH 7.0) via vortexing and incubation at 55°C, and digested by adding 50 µg of MS-grade trypsin (Thermo-Pierce) followed by incubation 37°C overnight. Trypsin was quenched by adding 6 µL of 100% trifluoroacetic acid. Samples were desalted in Sep-pak C018 columns (Waters), eluted with 70% acetonitrile, and dried via SpeedVac.

ADP-ribosylated and phospho-ribosylated peptides were enriched on TiO_2 beads. Proteins were resuspended in 2 M lactic acid and 50% acetonitrile, vortexed, and centrifuged (max speed for 5 min) to remove insoluble material. Supernatant was added to beads and vortexed for 1 hour. Beads were washed 3x with 2 M lactic acid and 50% acetonitrile and 3x with 50% acetonitrile and 0.1% trifluoroacetic acid, then eluted 2x with 0.5 mL each of 50 mM potassium phosphate, pH 10, via vortexing for 5 m. Beads were pelleted and supernatant collected. 0.5 mL of 1% triofluoracetic acid was added and samples were dried in a SpeedVac. Proteins were resuspended in 5% acetonitrile and 0.1% formic acid.

Samples were measured on an Orbitrap LC-MS (Thermo Fisher Scientific) by collision-induced dissociation and by higher energy collision dissociation with ion trap. Analysis was directed at identification of ADP-ribose and ribose-phosphate modifcations. Network analysis of unique proteins was performed with on the STRING database (Szklarcyk et al., 2019).

Gene expression

Total mRNA was isolated from cells using the E.Z.N.A. Total RNA Kit (Omega Bio-tek), and converted to cDNAs using the iScript Reverse Transcription Supermix (BioRad). qPCR was performed with 25 ng of cDNA LightCycler SYBR Green I Mastermix (Roche) by manufacturer's instructions. Relative mRNA expression levels were calculated with the ΔΔCt method relative to β-Actin. The primer sequences used are reported in **Table 2.1**.

Western blots

SDS-PAGE was performed by standard procedures and detected with ECL reagent (GE Healthcare). Antibodies for β-Actin (Cell Signaling), CD38 (R&D Systems), DBC1 (Bethyl Laboratories), PAR (Millipore Sigma), PARP1 (Cell Signaling), and PARP 14 (Santa Cruz Biotechnology) were used at a 1:1000 dilution.

Generation of CRISPR knockouts

RAW264.7 cell lines were transduced with lentiviruses packaged by standard methods containing Cas9 and two guide RNAs flanking each gene. Cells were selected with puromycin (2 μg/mL) and clonal colonies were generated by limiting dilution. Crude genomic DNA was isolated by digesting cell pellets with proteinase K in 10 mM Tris pH 8, 100 mM NaCl, 25 mM EDTA, and 0.5% SDS, followed by washes with isopropanol and 70% ethanol, after which PCR genotyping was performed. Bands of interest were isolated by gel extraction (Omega Bio-tek) and analyzed by Sanger sequencing. Sequences for guide RNAs and genotyping primers are reported in **Table 2.2** and **Table 2.3**. Three to four clonal colonies for each gene were identified.

Animals

All experiments were conducted according to protocols approved by the Institutional Animal Care and Use Committee (Harvard Medical School).

PARP14 knockout mice were a kind gift from Professor Masanori Aikawa (Brigham and Womens Hospital, Harvard Medical School, Boston, MA). CD38 knockout mice were a kind gift from Eduardo Chini (Mayo Chinic, Rochester, MN). PARP1 and SARM1 knockout mice were

purchased from the Jackson Laboratory (Bar Harbor, ME). Aged mice were ordered from the National Institute on Aging (Bethesda, MD).

Sepsis was induced by intraperitoneal injection (I.P.) of 15 mg/kg of LPS in 0.9% NaCl. OUL35 and NRH applied by I.P. injection in 40% (w/v) 2-hydroxyproply-beta-cyclodextrin (Sigma-Aldrich) and 1% medium viscosity carboxymethylcelluloose (Sigma-Aldrich) in PBS.

Statistical analysis

Data were analyzed by a two-tailed unpaired Student's t-test or by a one-way ANOVA with multiple comparisons corrections when appropriate. Statistical tests were performed with GraphPad Prism. Data are presented as means ± SD for *in vitro* replicates or SEM for *in vivo* replicates.

Table 2.1: RT-qPCR primers

Gene	Forward Primer	Reverse Primer
CD38	TCTCTAGGAAAGCCCAGATCG	AGAAAAGTGCTTCGTGGTAGG
BST1	AGGGACAAGTCACTGTTCTGG	AACTTTGCCATACAGCACGTC
SARM1	TTCCTTGGCTCCAGAAATGCT	GACCCTGAGTTCCTCCGGTA
PARP1	GGTCTTTAAGAGCGACGCTTAT	TTCTGTGTCTTGACCATGCAC
PARP2	GCAACAGAAGACGACTCTCCT	CAGCCATAGGCCCTTTTCTCT
PARP3	ATCGCTCCAAAACGAAAGGC	CACGGATGACCCGATTATCAG
PARP4	TCATACCACCTAAGTTGGGTCC	AGCAAAGCTACCTGAGAAAGC
PARP5A	GTCTACTCCGTTACACCTGGC	TGAAGAGGTACAAGTCCACCTTT
PARP5B	CGCCCGAGAAGGTGAACAG	TTTGCACCGTTCTGAAGAAGAT
PARP6	TATTGTGTTGAGGCTACGGTTTT	CTTCCTTATTCGATGGCTGGAAA
PARP7	GCCAGACTGTGTAGTACAGCC	GGGTTCCAGTTCCCAATCTTTT
PARP8	CACTTCCGAAACCACTTCGC	GGCAGTCTTTCTCGGCTCTT
PARP9	AGGACGCCAAAGGGATCTG	CCGGCTCCATAAACTGGGT
PARP10	GACACCCCGTGCAGACTTG	CCACCACACGTACTGCTCG
PARP11	GTGGACGACATGGACACATCG	GAATGTTGGTATCCGGCTGAA
PARP12	CAACCTGAGTGTGTTGAGGAC	CACCTTTGTTGTAGTGTAGGCAT
PARP13	AAGCAGAGACCGCTTCCATC	GTCCCCAGGTACTTGAACTTCT
PARP14	AGCAGTGGATCAGAAAAGACAG	GTCAGCACCATCTCGGATACT
PARP16	CCAAAGGAGAACGAGACCTAATC	AGGCCATTGTGAATGATGGAG
SIRT1	TGATTGGCACCGATCCTCG	CCACAGCGTCATATCATCCAG
SIRT2	CCACGGCACCTTCTACACATC	CACCTGGGAGTTGCTTCTGAG
SIRT3	GGCTCTATACACAGAACATCGAC	TAGCTGTTACAAAGGTCCCGT
SIRT4	GGCGACGTGTTCCTCACTG	ACAAAGTCAACCTTGTCTGGG
SIRT5	CCAGTTGTGTTGTAGACGAAAGC	TTCCGAAAGTCTGCCATATTTGA
SIRT6	CCTGGTCAGCCAGAACGTAG	TACTGCGTCTTACACTTGGGA
SIRT7	GCACTTGGTTGTCTACACGG	TGTCCATACTCCATTAGGACCC
NAMPT	GAATGTCTCCTTCGGTTCTGG	TCAGCAACTGGGTCCTTAAAC
NMNAT1	TCTTCTTGTACGCATCACCGA	TGGCTCTTTTAACCCCATCAC
NMNAT2	ATGACCGAGACCACAAAGACC	ATCCCGCCAATCACAATAAATCT
NMNAT3	TCACCCGTCAATGACAGCTAT	CACCCGAATCCAGTCAGATGT
NMRK1	TGGAATTGGTGGTGTGACAAA	TATGACGCTGCAGTTGGGAA
NMRK2	TGACTTCTTCAAGCCCCAGG	GCGTGCAAACTTGTGTGGAT
MCT1	ACGCCGGAGTCTTTGGATTT	GGCAGCATTCCACAATGGTC
SMCT1	GCCCCTTGAAACCTATGGCT	CAGTGGAGTCCTTTCCGCAT
SMCT2	TCCTCTGGAATTGGCGTGTT	CAAAGCTACAGGGCCAAAGC
NAPRT	TGCTCACCGACCTCTATCAGG	GCGAAGGAGCCTCCGAAAG
IDO1	TGGCGTATGTGTGGAACCG	CTCGCAGTAGGGAACAGCAA
AFMID	TTGGGAACTTCGTGCAGATAGG	CAGTTTCTCCCCTTCGCCATC
KMO	AAGTTGATGTGTACGAAGCTAGG	AGGGCCAAGTTAATGCTCCTT
HAAO	GAACGCCGTGTGAGAGTGAA	CCAACGAACATGATTTTGAGCTG
KYNU	CCTTCGCCTCTTGAGCTTCC	AGAGCAACCCTCTCATCTGTT
QPRT	GGGGCTGACCTGGTAATGC	TGGGGAATCTGGCTTTAAGTGTA
NADS	GTGGGGATGCCTATAATGCAC	TCCCGGTAGTTGCCTTCGT
NADK	CCACAACGGCCTCAGTGAAA	CTCTGTCGATCACCACTTCATTT
NNMT	TGTGCAGAAAACGAGATCCTC	AGTTCTCCTTTTACAGCACCCA
β-Actin	TGGCGCTTTTGACTCAGGAT	GGGATGTTTGCTCCAACCAA

Table 2.2: gRNAs for CRISPR knockout generation

Name	5' cut guide sequence	3' cut guide sequence
PARP7	TACCATACTCACCAAGAGAA(TGG)	TGGCATGAGAAGGCCCCCTC(CGG)
PARP9	TGGAATCGCTATCACCGGTG(CGG)	TGCAATACGGTGTGCAGAGT(CGG)
PARP10	GTCCTCCACCCGAGCGACGG(TGG)	GGAGTTCCAAGATGTGGTGC(GGG)
PARP11	GGAAACAGCGCCTAATAAAG(AGG)	GAACACATTCCAGATTCATG(GGG)
PARP12	GAAGAGCGGCTAACTTACCT(TGG)	TGGTACTAGTGCCAACTTCG(TGG)
PARP14	CGTGCTGGGTTCCCCGGCTC(CGG)	GCATCTCTTCCATGGGACAG(AGG)

Table 2.3: PCR primers for identification of CRISPR knockouts

Name	Sequence
PARP 7 common	TGGAAACAGTGTTACTGACTTCT
PARP 7 WT	GGACAAGGCAGTTATTTCGCA
PARP 7 KO	AAGCTTCCCTTGAGCTTGTGTTT
PARP 9 common	CCACTGACTCTGCTAGCCTG
PARP 9 WT	AGGTTGTTTCAGCAGGTCCC
PARP 9 KO	TGCTCAGAGAGTCTTCAGAAGGACC
PARP 10 common	CCCCCAGAAATACCAGATGAGC
PARP 10 WT	GCTCAGTCGGACACCATGTA
PARP 10 KO	GAACTCACTCGAACAATGCGG
PARP 11 common	GCACTCGAGCAAGAAACATGG
PARP 11 WT	ACATCTGTCCCTGTGGTGTG
PARP 11 KO	TACTCTGCACTGTGTGCTGC
PARP 12 common	CAGTTCAGGTCCTGTGTCACCA
PARP 12 WT	CGGACCCACACAAGAATGACTA
PARP 12 KO	TTTGCCATAGGATGTGCCGT
PARP 14 common	GGAGATTGGTCGTCAGTTCGG
PARP 14 WT	TTCTGGGGCGTTTTCCCAAG
PARP 14 KO	GAACCTTGACTCAATGCCGTA

REFERENCES

Amici, S.A., Young, N.A., Narvaez-Miranda, J., Jablonski, K.A., Arcos, J., Rosas, L., Papenfuss, T.L., Torrelles, J.B., Jarjour, W.N., and Guerau-de-Arellano, M. CD38 Is Robustly Induced in Human Macrophages and Monocytes in Inflammatory Conditions. Front Immunol *9*, 1593.

Bai, P., Cantó, C., Oudart, H., Brunyánszki, A., Cen, Y., Thomas, C., Yamamoto, H., Huber, A., Kiss, B., Houtkooper, R.H., et al. PARP-1 inhibition increases mitochondrial metabolism through SIRT1 activation. Cell Metab. *13*, 461–468.

Belousova, E.A., Ishchenko, A.A.A., and Lavrik, O.I. Dna is a New Target of Parp3. Sci Rep *8*, 4176.

Benayoun, B.A.A., Pollina, E.A., Singh, P.P., Mahmoudi, S., Harel, I., Casey, K.M., Dulken, B.W., Kundaje, A., and Brunet, A. Remodeling of epigenome and transcriptome landscapes with aging in mice reveals widespread induction of inflammatory responses. Genome Res. *29*, 697–709.

Camacho-Pereira, J., Tarragó, M.G., Chini, C.C.S.C., Nin, V., Escande, C., Warner, G.M., Puranik, A.S., Schoon, R.A., Reid, J.M., Galina, A., et al. CD38 Dictates Age-Related NAD Decline and Mitochondrial Dysfunction through an SIRT3-Dependent Mechanism. Cell Metab. *23*, 1127–1139.

Cambronne, X.A., Stewart, M.L., Kim, D., Jones-Brunette, A.M., Morgan, R.K., Farrens, D.L., Cohen, M.S., and Goodman, R.H. Biosensor reveals multiple sources for mitochondrial NAD^+. Science *352*, 1474–1477.

Cameron, A.M., Castoldi, A., Sanin, D.E., Flachsmann, L.J., Field, C.S., Puleston, D.J., Kyle, R.L., Patterson, A.E., Hässler, F., Buescher, J.M., et al. Inflammatory macrophage dependence on NAD+ salvage is a consequence of reactive oxygen species-mediated DNA damage. Nat. Immunol. *20*, 420–432.

Cantó, C., Houtkooper, R.H., Pirinen, E., Youn, D.Y., Oosterveer, M.H., Cen, Y., Fernandez-Marcos, P.J., Yamamoto, H., Andreux, P.A.A., Cettour-Rose, P., et al. The NAD(+) precursor nicotinamide riboside enhances oxidative metabolism and protects against high-fat diet-induced obesity. Cell Metab. *15*, 838–847.

Caprara, G., Prosperini, E., Piccolo, V., Sigismondo, G., Melacarne, A., Cuomo, A., Boothby, M., Rescigno, M., Bonaldi, T., and Natoli, G. PARP14 Controls the Nuclear Accumulation of a Subset of Type I IFN-Inducible Proteins. J. Immunol. *200*, 2439–2454.

Cho, S.H., Goenka, S., Henttinen, T., Gudapati, P., Reinikainen, A., Eischen, C.M., Lahesmaa, R., and Boothby, M. PARP-14, a member of the B aggressive lymphoma family, transduces survival signals in primary B cells. Blood *113*, 2416–2425.

Cho, S.H., Ahn, A.K., Bhargava, P., Lee, C.-H.H., Eischen, C.M., McGuinness, O., and Boothby, M. Glycolytic rate and lymphomagenesis depend on PARP14, an ADP ribosyltransferase of the B aggressive lymphoma (BAL) family. Proc. Natl. Acad. Sci. U.S.A. *108*, 15972–15977.

Das, A., Huang, G.X., Bonkowski, M.S., Longchamp, A., Li, C., Schultz, M.B., Kim, L.-J.J., Osborne, B., Joshi, S., Lu, Y., et al. Impairment of an Endothelial NAD+-H2S Signaling Network Is a Reversible Cause of Vascular Aging. Cell *173*, 74–89.e20.

Frederick, D.W., Loro, E., Liu, L., Davila, A., Chellappa, K., Silverman, I.M., Quinn, W.J., Gosai, S.J., Tichy, E.D., Davis, J.G., et al. Loss of NAD Homeostasis Leads to Progressive and Reversible Degeneration of Skeletal Muscle. Cell Metab. *24*, 269–282.

Gerdts, J., Brace, E.J., Sasaki, Y., DiAntonio, A., and Milbrandt, J. SARM1 activation triggers axon degeneration locally via NAD^+ destruction. Science *348*, 453–457.

Goenka, S., and Boothby, M. Selective potentiation of Stat-dependent gene expression by collaborator of Stat6 (CoaSt6), a transcriptional cofactor. Proc. Natl. Acad. Sci. U.S.A. *103*, 4210–4215.

Goenka, S., Cho, S.H., and Boothby, M. Collaborator of Stat6 (CoaSt6)-associated poly(ADP-ribose) polymerase activity modulates Stat6-dependent gene transcription. J. Biol. Chem. *282*, 18732–18739.

Gomes, A.P., Price, N.L., Ling, A.J., Moslehi, J.J., Montgomery, M.K., Rajman, L., White, J.P., Teodoro, J.S.S., Wrann, C.D., Hubbard, B.P., et al. Declining NAD(+) induces a pseudohypoxic state disrupting nuclear-mitochondrial communication during aging. Cell *155*, 1624–1638.

Van Gool, F., Gallí, M., Gueydan, C., Kruys, V., Prevot, P.-P.P., Bedalov, A., Mostoslavsky, R., Alt, F.W., De Smedt, T., and Leo, O. Intracellular NAD levels regulate tumor necrosis factor protein synthesis in a sirtuin-dependent manner. Nat. Med. *15*, 206–210.

Haffner, C.D., Becherer, J.D., Boros, E.E., Cadilla, R., Carpenter, T., Cowan, D., Deaton, D.N., Guo, Y., Harrington, W., Henke, B.R., et al. Discovery, Synthesis, and Biological Evaluation of Thiazoloquin(az)olin(on)es as Potent CD38 Inhibitors. J. Med. Chem. *58*, 3548–3571.

Halvorsen, B., Espeland, M.Z., Andersen, G.Ø., Yndestad, A., Sagen, E.L., Rashidi, A., Knudsen, E.C., Skjelland, M., Skagen, K.R., Krohg-Sørensen, K., et al. Increased expression of NAMPT in PBMC from patients with acute coronary syndrome and in inflammatory M1 macrophages. Atherosclerosis *243*, 204–210.

Harden, A. (1914). Alcoholic Fermentation (Longmans, Green and Company).

Higashi, H., Maejima, T., Lee, L.H., Yamazaki, Y., Hottiger, M.O., Singh, S.A., and Aikawa, M. A Study into the ADP-Ribosylome of IFN-γ-Stimulated THP-1 Human Macrophage-like Cells Identifies ARTD8/PARP14 and ARTD9/PARP9 ADP-Ribosylation. J. Proteome Res. *18*, 1607–1622.

Holechek, J., Lease, R., Thorsell, A.-G.G., Karlberg, T., McCadden, C., Grant, R., Keen, A., Callahan, E., Schüler, H., and Ferraris, D. Design, synthesis and evaluation of potent and selective inhibitors of mono-(ADP-ribosyl)transferases PARP10 and PARP14. Bioorg. Med. Chem. Lett. *28*, 2050–2054.

Hou, Y., Lautrup, S., Cordonnier, S., Wang, Y., Croteau, D.L., Zavala, E., Zhang, Y., Moritoh, K., O'Connell, J.F., Baptiste, B.A., et al. NAD+ supplementation normalizes key Alzheimer's features and DNA damage responses in a new AD mouse model with introduced DNA repair deficiency. Proc. Natl. Acad. Sci. U.S.A. *115*, E1876–E1885.

Iqbal, M.B., Johns, M., Cao, J., Liu, Y., Yu, S.-C.C., Hyde, G.D., Laffan, M.A., Marchese, F.P., Cho, S.H., Clark, A.R., et al. PARP-14 combines with tristetraprolin in the selective posttranscriptional control of macrophage tissue factor expression. Blood *124*, 3646–3655.

Iwata, H., Goettsch, C., Sharma, A., Ricchiuto, P., Goh, W.W., Halu, A., Yamada, I., Yoshida, H., Hara, T., Wei, M., et al. PARP9 and PARP14 cross-regulate macrophage activation via STAT1 ADP-ribosylation. Nat Commun *7*, 12849.

Jankevicius, G., Hassler, M., Golia, B., Rybin, V., Zacharias, M., Timinszky, G., and Ladurner, A.G. A family of macrodomain proteins reverses cellular mono-ADP-ribosylation. Nat. Struct. Mol. Biol. *20*, 508–514.

Katsyuba, E., Mottis, A., Zietak, M., De Franco, F., van der Velpen, V., Gariani, K., Ryu, D., Cialabrini, L., Matilainen, O., Liscio, P., et al. De novo NAD+ synthesis enhances mitochondrial function and improves health. Nature *563*, 354–359.

Krishnamurthy, P., Da-Silva-Arnold, S., Turner, M.J., Travers, J.B., and Kaplan, M.H. Poly-ADP ribose polymerase-14 limits severity of allergic skin disease. Immunology *152*, 451–461.

Leung, A.K., Vyas, S., Rood, J.E., Bhutkar, A., Sharp, P.A., and Chang, P. Poly(ADP-ribose) regulates stress responses and microRNA activity in the cytoplasm. Mol. Cell *42*, 489–499.

Li, J., Bonkowski, M.S., Moniot, S., Zhang, D., Hubbard, B.P., Ling, A.J., Rajman, L.A., Qin, B., Lou, Z., Gorbunova, V., et al. A conserved NAD+ binding pocket that regulates protein-protein interactions during aging. Science *355*, 1312–1317.

Liaudet, L., Pacher, P., Mabley, J.G., Virág, L., Soriano, F.G., Haskó, G., and Szabó, C. Activation of poly(ADP-Ribose) polymerase-1 is a central mechanism of lipopolysaccharide-induced acute lung inflammation. Am. J. Respir. Crit. Care Med. *165*, 372–377.

Matic, I., Ahel, I., and Hay, R.T. (2012). Reanalysis of phosphoproteomics data uncovers ADP-ribosylation sites. Nature Methods *9*, 771–772.

Mehrotra, P., Riley, J.P., Patel, R., Li, F., Voss, L., and Goenka, S. PARP-14 functions as a transcriptional switch for Stat6-dependent gene activation. J. Biol. Chem. *286*, 1767–1776.

Minhas, P.S., Liu, L., Moon, P.K., Joshi, A.U., Dove, C., Mhatre, S., Contrepois, K., Wang, Q., Lee, B.A., Coronado, M., et al. Macrophage de novo NAD+ synthesis specifies immune function in aging and inflammation. Nat. Immunol. *20*, 50–63.

Nicholas, D.A., Zhang, K., Hung, C., Glasgow, S., Aruni, A.W., Unternaehrer, J., Payne, K.J., Langridge, W.H.R.H., and De Leon, M. Palmitic acid is a toll-like receptor 4 ligand that induces human dendritic cell secretion of IL-1β. PLoS ONE *12*, e0176793.

Pajuelo, D., Gonzalez-Juarbe, N., Tak, U., Sun, J., Orihuela, C.J., and Niederweis, M. NAD+ Depletion Triggers Macrophage Necroptosis, a Cell Death Pathway Exploited by Mycobacterium tuberculosis. Cell Rep *24*, 429–440.

Peng, B., Thorsell, A.-G.G., Karlberg, T., Schüler, H., and Yao, S.Q. Small Molecule Microarray Based Discovery of PARP14 Inhibitors. Angew. Chem. Int. Ed. Engl. *56*, 248–253.

Rajman, L., Chwalek, K., and Sinclair, D.A. Therapeutic Potential of NAD-Boosting Molecules: The In Vivo Evidence. Cell Metab. *27*, 529–547.

Riley, J.P., Kulkarni, A., Mehrotra, P., Koh, B., Perumal, N.B., Kaplan, M.H., and Goenka, S. PARP-14 binds specific DNA sequences to promote Th2 cell gene expression. PLoS ONE *8*, e83127.

Ron-Harel, N., Santos, D., Ghergurovich, J.M., Sage, P.T., Reddy, A., Lovitch, S.B., Dephoure, N., Satterstrom, F.K., Sheffer, M., Spinelli, J.B., et al. Mitochondrial Biogenesis and Proteome Remodeling Promote One-Carbon Metabolism for T Cell Activation. Cell Metab. *24*, 104–117.

Schilling, E., Wehrhahn, J., Klein, C., Raulien, N., Ceglarek, U., and Hauschildt, S. Inhibition of nicotinamide phosphoribosyltransferase modifies LPS-induced inflammatory responses of human monocytes. Innate Immun *18*, 518–530.

Shieh, W.M., Amé, J.C., Wilson, M.V., Wang, Z.Q., Koh, D.W., Jacobson, M.K., and Jacobson, E.L. Poly(ADP-ribose) polymerase null mouse cells synthesize ADP-ribose polymers. J. Biol. Chem. *273*, 30069–30072.

Szklarczyk, D., Gable, A.L., Lyon, D., Junge, A., Wyder, S., Huerta-Cepas, J., Simonovic, M., Doncheva, N.T., Morris, J.H., Bork, P., et al. (2019). STRING v11: protein-protein

association networks with increased coverage, supporting functional discovery in genome-wide experimental datasets. Nucleic Acids Res. *47*, D607–D613.

Tak, U., Vlach, J., Garza-Garcia, A., William, D., Danilchanka, O., de Carvalho, L.P.S.P., Saad, J.S., and Niederweis, M. The tuberculosis necrotizing toxin is an NAD+ and NADP+ glycohydrolase with distinct enzymatic properties. J. Biol. Chem. *294*, 3024–3036.

Tannahill, G.M., Curtis, A.M., Adamik, J., Palsson-McDermott, E.M., McGettrick, A.F., Goel, G., Frezza, C., Bernard, N.J., Kelly, B., Foley, N.H., et al. Succinate is an inflammatory signal that induces IL-1β through HIF-1α. Nature *496*, 238–242.

Venkannagari, H., Verheugd, P., Koivunen, J., Haikarainen, T., Obaji, E., Ashok, Y., Narwal, M., Pihlajaniemi, T., Lüscher, B., and Lehtiö, L. Small-Molecule Chemical Probe Rescues Cells from Mono-ADP-Ribosyltransferase ARTD10/PARP10-Induced Apoptosis and Sensitizes Cancer Cells to DNA Damage. Cell Chem Biol *23*, 1251–1260.

Venter, G., Oerlemans, F.T., Willemse, M., Wijers, M., Fransen, J.A., and Wieringa, B. NAMPT-mediated salvage synthesis of NAD+ controls morphofunctional changes of macrophages. PLoS ONE *9*, e97378.

Verdin, E. NAD^+ in aging, metabolism, and neurodegeneration. Science *350*, 1208–1213.

Vidugiriene, J., Leippe, D., Sobol, M., Vidugiris, G., Zhou, W., Meisenheimer, P., Gautam, P., Wennerberg, K., and Cali, J.J. (2014). Bioluminescent Cell-Based NAD(P)/NAD(P)H Assays for Rapid Dinucleotide Measurement and Inhibitor Screening. Assay Drug Dev Technol *12*, 514–526.

Villén, J., and Gygi, S.P. (2008). The SCX/IMAC enrichment approach for global phosphorylation analysis by mass spectrometry. Nat Protoc *3*, 1630–1638.

Vyas, S., Matic, I., Uchima, L., Rood, J., Zaja, R., Hay, R.T., Ahel, I., and Chang, P. Family-wide analysis of poly(ADP-ribose) polymerase activity. Nat Commun *5*, 4426.

Yoneyama-Hirozane, M., Matsumoto, S.-I.I., Toyoda, Y., Saikatendu, K.S., Zama, Y., Yonemori, K., Oonishi, M., Ishii, T., and Kawamoto, T. Identification of PARP14 inhibitors using novel methods for detecting auto-ribosylation. Biochem. Biophys. Res. Commun. *486*, 626–631.

Yoshino, J., Mills, K.F., Yoon, M.J., and Imai, S. Nicotinamide mononucleotide, a key NAD(+) intermediate, treats the pathophysiology of diet- and age-induced diabetes in mice. Cell Metab. *14*, 528–536.

Zarkovic, G., Belousova, E.A., Talhaoui, I., Saint-Pierre, C., Kutuzov, M.M., Matkarimov, B.T., Biard, D., Gasparutto, D., Lavrik, O.I., and Ishchenko, A.A. Characterization of DNA ADP-ribosyltransferase activities of PARP2 and PARP3: new insights into DNA ADP-ribosylation. Nucleic Acids Res. *46*, 2417–2431.

Zhang, H., Ryu, D., Wu, Y., Gariani, K., Wang, X., Luan, P., D'Amico, D., Ropelle, E.R., Lutolf, M.P., Aebersold, R., et al. NAD^+ repletion improves mitochondrial and stem cell function and enhances life span in mice. Science *352*, 1436–1443.

Zhou, C.-C.C., Yang, X., Hua, X., Liu, J., Fan, M.-B.B., Li, G.-Q.Q., Song, J., Xu, T.-Y.Y., Li, Z.-Y.Y., Guan, Y.-F.F., et al. Hepatic NAD(+) deficiency as a therapeutic target for non-alcoholic fatty liver disease in ageing. Br. J. Pharmacol. *173*, 2352–2368.

Chapter 3: NAD^+ repletion and pan-sirtuin gene therapy in aged mice

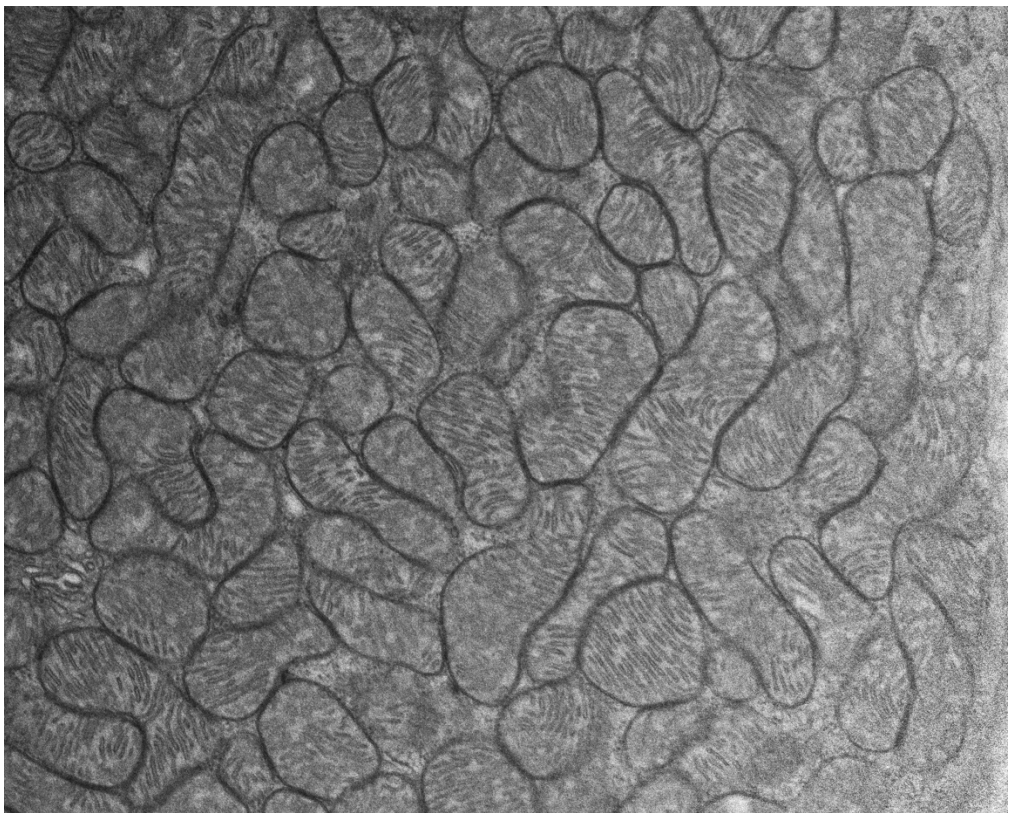

Electron micrograph of muscle mitochondria, by Michael Bonkowski and João Amorim

"Study hard what interests you the most in the most undisciplined, irreverent and original manner possible."

-Richard Feynman, 1965

Significant contributions to the chapter were made by Michael Bonkowski, Noah Davidsohn, Alice Kane, João Amorim, Yiming Cai, and Doyle Lokitiyakul

ABSTRACT

The mammalian sirtuin gene family consists of seven NAD^+-dependent deacylases that each promote health, and two of which have been shown to increase longevity. As NAD^+ levels fall during aging, sirtuin activity declines, resulting in decreased genome and epigenome stability, and increased inflammation, mitochondrial dysfunction, and a greater likelihood for many pathologies. While a reductionist approach towards studying aging has identified many contributing factors, synergies between them may be overlooked when they are studied in isolation. Here, we sought to boost the activity of the entire sirtuin gene family in tandem, and to test whether sirtuin overexpression and repletion of NAD^+ levels may be redundant, additive, or synergistic. Twenty-month old male mice were infected with adeno-associated viruses carrying each of the seven sirtuins to be overexpressed in trans, or with GFP control virus. For all seven sirtuins, viruses were confirmed to express well in the liver. Additionally, half of the sirtuin mice and half of the GFP mice were given the NAD^+ precursor NMN (300 mg/kg/day) continuously post-viral delivery. We show that NAD^+ repletion reduced age-related body weight loss, with a non-significant increase in longevity ($p=0.15$). Additionally, sirtuin overexpression appeared to protect against age-related muscle loss. The use of gene therapy-based methods to overexpress combinations of genes in pre-aged, wild-type mice may serve as a future model to more rapidly identify interactions between factors that dictate healthspan and longevity.

INTRODUCTION

Single gene manipulations have advanced our understanding of the molecular basis of aging since the first ones to impact longevity were identified (Friedman and Johnson, 1988; Kaeberlein et al., 1999; Kenyon et al., 1993). However, aging is a complex multigenic trait, and the contributions of individual genes are unlikely to be solely additive. Gene products have intricate synergies and may require one another to reveal their maximum influence on a phenotype, interactions that pure reductionist approaches, however powerful they may be, are certain to overlook (Williams and Auwerx, 2015). One example of such a synergy has been identified for longevity, in which the combination of gene mutations in *daf-2* and *rsks-1* (the homolog of S6K) led to a five-fold increase in worm lifespan, far greater than the extension from either gene alone (Chen et al., 2013). In order to push the bounds of maximum longevity, oligogeneic manipulations will likely be required. Not every gene in a manipulation need have an impact on the phenotype, as reductionist experiments can be applied subsequently to identify a minimal set. Such an approach led to the identification of the Yamanaka reprogramming factors: 24 factors were first combined to reprogram fibroblasts to induced pluripotent stem cells, and subsequently an N-1 strategy led to a curated list of four (and later three) required factors (Takahashi and Yamanaka, 2006).

The difficulty is to test combinations of genes or interventions on mammalian aging, due to the time constraints involved, especially considering that mice containing multiple transgenic or knockout alleles require multiple generations to breed, and further years to age from birth. Additionally, genes with a beneficial impact on aging may have negative pleotropic effects on embryonic and juvenile development, and might only show a benefit if expressed after reproductive age has been reached. To bypass these constraints, we pursued an experimental

framework utilizing adeno-associated viruses (AAVs) and pre-aged wild-type mice. AAVs are popular gene delivery vectors because they are considered to be non-pathogenic, do not integrate into their host genome, can infect both dividing and non-dividing cells, and usually do not generate an immune response for the first exposure (Boutin et al., 2010). By expressing transgenes or shRNAs via viral vectors in an adult wild-type animal, one may select multiple genes of interest without the need to generate and breed transgenic mice, or to worry about effects on development or growth.

The use of already aged mice further accelerates the time required to identify interventions with a positive impact on lifespan and healthspan. For example, for the outcome of longevity, median lifespan in C57Bl6/J mice is 29 months, so if one begins an experiment on mice at 20 months of age, when greater than 90% of the population is still alive, one will have an idea if an intervention is successful in less a year. Furthermore, beginning an intervention in mid to late life better mimics the course human interventions for aging would take; a treatment begun at age sixty is far more likely to meet regulatory standards and avoid compliance issues than an intervention administered from age twenty. For these reasons, the National Institute on Aging's Interventions Testing Program (ITP), which has tested over forty compounds for their effects on longevity in mice, tests some of their hits for effects beginning mid-life, such as for rapamycin and 17α-estradiol (Garratt et al., 2018; Harrison et al., 2009).

In this study, we sought to test the effects of overexpressing the entire sirtuin gene family in combination with NAD^+ supplementation with nicotinamide mononucleotide (NMN). While overexpression of sirtuins in yeast (Kaeberlein et al., 1999), worms (Tissenbaum and Guarente, 2001), and flies (Rogina and Helfand, 2004; Whitaker et al., 2013) extends lifespan by large amounts, in mammals only modest extensions of lifespan have been reported. This may be because

mammals have a greater baseline longevity, so it is more difficult to further extend it. It could also be because yeast SIR2 has diverged and specialized into seven genes in mammals, each with a more subtle impact on healthspan and lifespan. To date, whole body SIRT6, brain SIRT1, and treatment with SIRT1 activators SRT1720 and SRT2104 have been shown to extend longevity in mice on a normal diet (Kanfi et al., 2012; Mercken et al., 2014; Mitchell et al., 2014; Satoh et al., 2013). Furthermore, NAD^+ levels decline during aging, sapping sirtuins of their activity (Gomes et al., 2013; Li et al., 2017; Zhou et al., 2016). NAD^+ repletion with nicotinamide riboside has been shown to modestly extend lifespan (Zhang et al., 2016). To date, nicotinamide mononucleotide's (NMN) effect on mammalian longevity has not been shown.

To test whether the sirtuin genes overexpressed in combination, along with NAD^+ repletion, can have a dramatically positive effect on healthspan and lifespan, we injected 20-month old mice with AAV9s containing each of the seven sirtuins as transgenes, or GFP as a control. We also gave half of each group NMN (300 mg/kg) to replete NAD^+ levels throughout the remainder of lifespan. This 2x2 combinatorial experimental design allowed us to test three hypotheses: the effect of sirtuin overexpression, the effect of NMN, and whether the two interventions are redundant, additive, or synergistic (**Fig. 3.1**). While we would also have liked to test each sirtuin individually, to run such an experiment in one laboratory would be impractical unless a large effect was first observed from the combination of genes to justify the large number of animals required. Overall, we observed that NMN protected from age-related body weight loss and may have increased longevity, while sirtuin overexpression improved walking gait and enhanced skeletal muscle weight in aged animals relative to control animals. While we did not observe a striking improvement in overall healthspan or lifespan, these observations are rationale for future, more targeted studies.

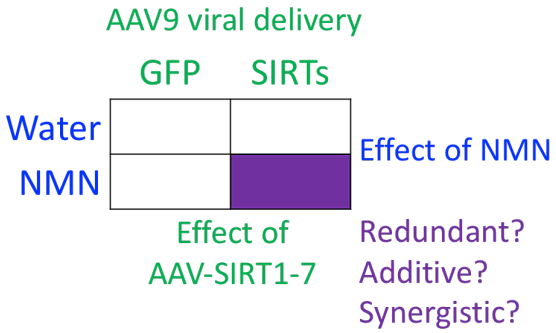

Figure 3.1: Experimental design. Two by two factorial design of experiment allows for the testing of three variables: effect of sirtuin overexpression, effect of NMN supplementation, and the interaction between these interventions.

RESULTS

Overexpression of Sirt1-7 (SIRTs)

We began by testing efficacy of expression and safety from acute toxicity in young mice before applying sirtuin gene therapy to aged mice. Eight types of AAV9 virus were generated, seven types containing the sirtuins, and one containing GFP, under the widely expressed UBC1 promoter. GFP was selected as a control gene due to its low reported immunogenicity in C57BL/6 mice, and due to its prior use in a longevity study of similar design (Bernardes de Jesus et al., 2012; Skelton et al., 2001). The first sirtuin viruses we generated, Sirt4 and Sirt7, were tested at a low dose (1×10^{10} particles) and a high dose (1×10^{11} particles) in 3-month old mice. Liver expression was examined two weeks post-injection by Western blot (**Fig. 3.2a-b**). Both constructs were well-expressed. Since AAV9 expression is manyfold higher in the liver than in other tissues, we chose to proceed with the higher titer for this study. A high dose of AAV9 containing each of the other five sirtuins was injected into young mice, and expression was similarly examined 2-weeks post injection. All constructs were found to increase liver sirtuin expression (**Fig. 3.2c-g**).

To ensure that pan-sirtuin gene therapy did not cause acute toxicity in young mice, we injected eight mice with all seven sirtuin viruses (for a total of 7×10^{11} particles). Four of these

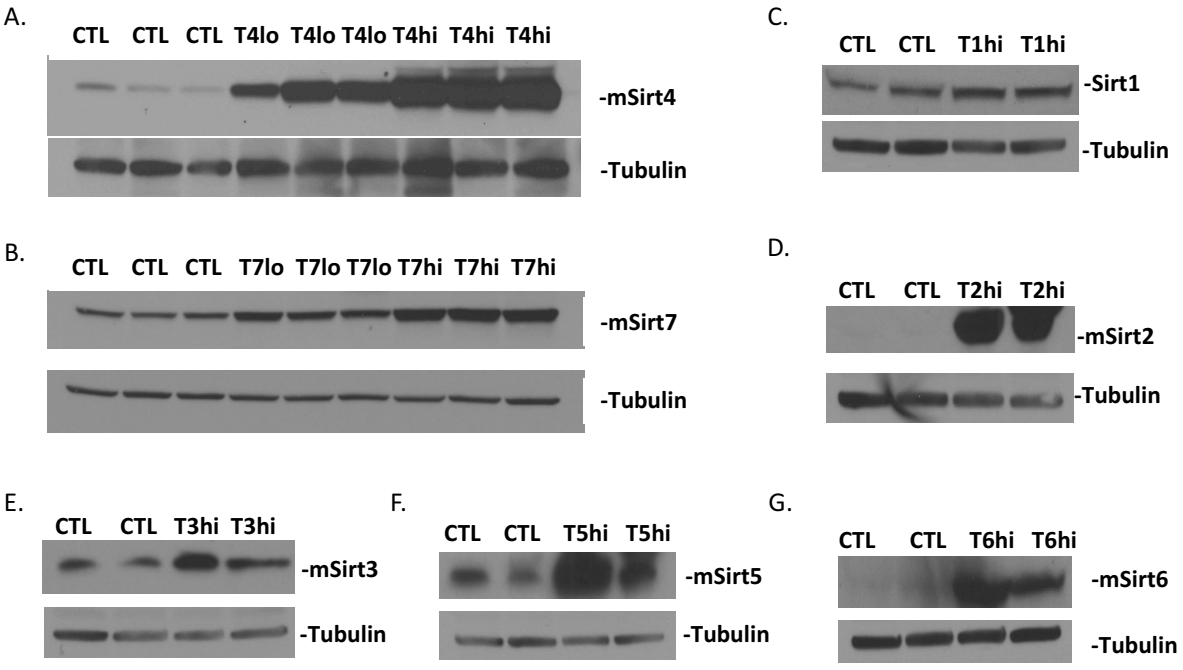

Figure 3.2: Liver expression of sirtuins. (A) Sirt4 and (B) Sirt7 expression two weeks post-injection with low dose (1 x 10^{10} particles) and a high dose (1 x 10^{11} particles) AAV9 delivery. (C) Expression of Sirt1 (D) Sirt2 (E) Sirt3 (F) Sirt5 and (G) Sirt6 two weeks post high dose injection.

mice were given supplemental NMN in their drinking water (2.4 g/L dosed for approximately 300 mg/kg/day). No loss in body weight or other signs of distress were observed in an eight week follow-up. Therefore, we concluded that sirtuin gene therapy in combination with NMN supplementation was at least acutely safe in young mice.

NMN protects from age-related body weight loss and may increase longevity

To test whether overexpressing the sirtuin gene family and supplementation of NAD^+ levels with NMN extends longevity, either alone or in combination, we delivered each of the seven sirtuins viruses at a high dose to 20-month old wild-type C57Bl6/J mice, or an equal dose of virus containing GFP. Two weeks after viral injection, NMN was provided in half of each groups' drinking water, for a total of four groups: GFP/water, GFP/NMN, SIRTs/Water, and SIRTs/NMN

(N=37 animals per group). NMN was maintained in the drinking water for the duration of the study. Water consumption was no different between cages with standard water and those with NMN-supplemented water (**Fig. 3.3a**).

Within the first few months of the study, we observed moderate weight loss in all animals, which is typically seen during aging. However, in groups receiving NMN, this weight loss was delayed by several months (**Fig. 3.3b)**. Although both water and NMN mice started with very similar weights and eventually converged after 30 months, mice on NMN did not lose weight as a population until around 28 months of age. In Chapter 4 of this dissertation, we identify weight loss as a major predictive risk factor for mortality, suggesting that this protection from age-related weight loss may improve health and survival.

We followed the four groups of mice with minimal intervention or testing until their natural deaths. We observed that the NMN/SIRTs mice had a "squaring of the curve" with enhanced survival for the earliest quartile to die. However, no group had significantly enhanced lifespan beyond that of control mice (GFP/water) (**Fig. 3.3c**). This may be because the control mice were somewhat long lived, with a median lifespan of 31 months, versus the expected 29 months (Kunstyr and Leuenberger, 1975). This may be because we began the study at 20 months, when some of mice may had already died, so we are reporting the median age of death for mice alive at 20 months. Regardless of the cause, while the lifespan of the controls demonstrates that the animals were maintained in healthy conditions, it may have reduced our sensitivity to detect efficacious interventions. When we compared the effect of NMN alone in both groups, there appears to be a positive, but non-significant ($p=0.15$) benefit on longevity (**Fig. 3.3d**).

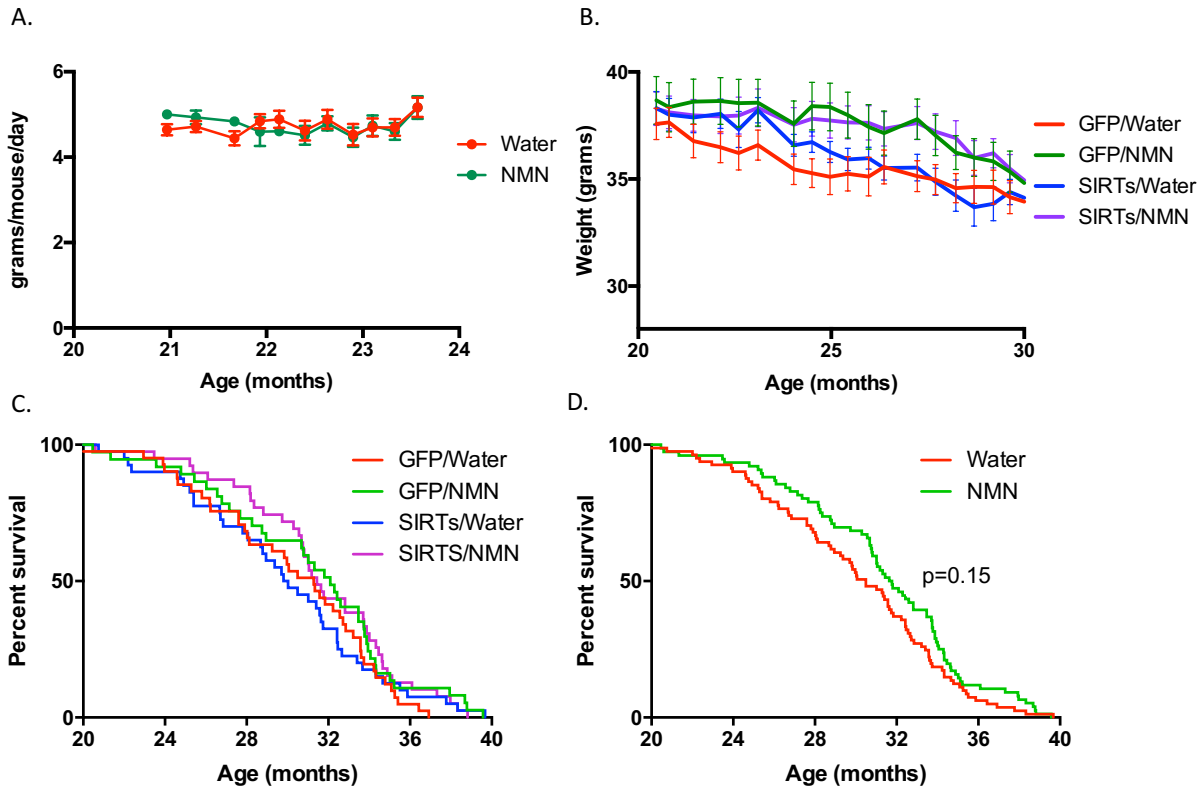

Figure 3.3: Effects of NMN and sirtuins virus on body weight and longevity. (A) Water consumption. (B) Average body weight per group. (C) Survival for all four groups. (D) Survival for combined water and NMN groups.

SIRTs and NMN improve walking gait and muscle mass

We began treatment on a second cohort of mice at the same age, with the same dose of virus and NMN. After six to nine months of treatment, we examined a host of healthspan parameters including blood cellularity, learning and memory tests, cardiac function, metabolic respiration quotient, and gait analysis. The most consistent effect we saw was an improvement in gait parameters in mice treated with sirtuins virus. For the front feet, the percentage of time spent in the swing portion of the gait was greater and the portion spent in the stance portion was smaller in mice which had received the sirtuins viruses, regardless of NMN treatment. (**Fig. 3.4a-b**). Increased stance time is observed in disease models that affect gait (Poulet et al., 2014). Mice

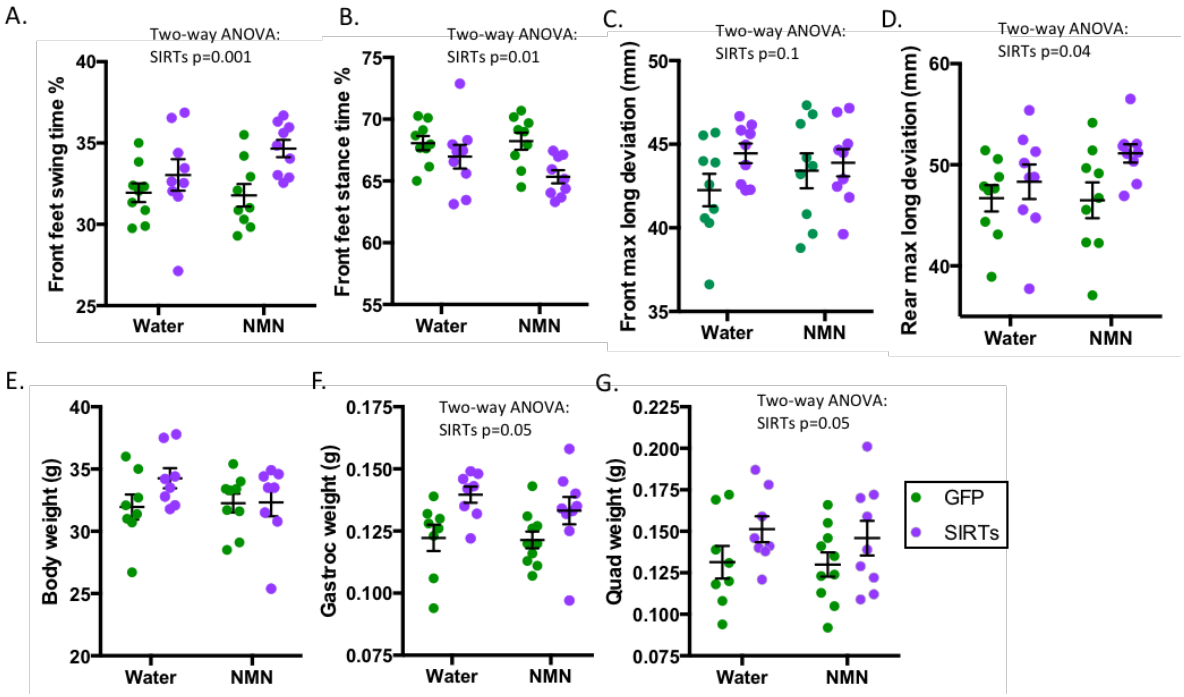

Figure 3.4: Walking gait and skeletal muscle weight. (A) Walking gait parameters front feet swing time %, (B) Front feet stance time %, (C) Front feet and (D) rear feet maximum longitudinal deviation. (E) Body weights, (F) Gastrocnemius weights, and (G) Quadriceps weights.

which had received sirtuins virus also had a greater maximum longitudinal deviation in front and rear legs, demonstrating a more dynamic gait (**Fig. 3.4c-d**).

Taken together, these data show that overexpression of sirtuins improves (or prevents decline in) walking gait in aged mice. When mice from this cohort were sacrificed at 29-months old, we observed that while there was no difference in body weight between groups (**Fig. 3.4e**), sirtuins virus mice had increased muscle mass (**Fig. 3.4f-g**). A protection from age-related muscle loss could explain the improvement in gait we observed.

DISCUSSION

In this study, we overexpressed the entire sirtuin gene family in aged mice via adeno-associated viral vectors alone or in combination with NMN supplementation and measured

lifespan and parameters of healthspan. Overall, benefits from these interventions were modest but noteworthy. NMN protected from age-related body weight loss and numerically extended longevity. Based on these results, we have begun another cohort of mice on a higher dose of NMN (600 mg/kg/day), beginning at an earlier age (12 months), and with a higher N-value, in order to increase our ability to detect a significant difference.

Overexpression of the entire sirtuin gene family was associated with improved gait parameters and increased skeletal muscle mass. Sarcopenia is the age-related loss in muscle mass and function, and our data suggest sirtuins may protect against this pathophysiology. While SIRT1 in particular is thought to have a negative impact on muscle hypertrophy through its attenuation of IGF-1 secretion and mTOR signaling, it has a positive effect on muscle cell survival via anti-inflammatory effects and suppression of p53 (reviewed in Sharples et al., 2015). While we cannot rule out a negative effect on the control animals from GFP expression, it is likely a positive effect from sirtuin overexpression, as previously, resveratrol has been shown to similarly increase muscle mass in aged rats (Bennett et al., 2013; Liao et al., 2017). We have not yet examined the muscles from our mice for histology, signaling pathways, or mitochondrial phenotypes. It is also surprising that we observed an effect on skeletal muscle, as AAV9 has relatively low expression in that tissue. Its effect may be indirect, either through promotion of endothelial cell proliferation and improved vascularization (Das et al., 2018), or through an uncharacterized endocrine effect in which sirtuins promote secretion of a molecule in a distant tissue that has a protective effect on skeletal muscle survival and function. Regardless of the mechanism, there are currently few clinical treatments for sarcopenia, so promotion of sirtuin activity may be a worthwhile avenue to explore further. Furthermore, there are very few chemical treatments which have been shown to improve longevity

in wild-type mice, and our study suggests that using NMN to boost NAD^+ levels could have a longevity benefit.

MATERIALS AND METHODS

AAV production

AAVs were produced in 293T cells using methods previously described (Grieger et al., 2006). HEK 293T cells were grown to 70-90% confluency on 15 cm plates (10 plates for approximately 5 x 10^{12} viral genomes yield). Cells were then transfected with 3 plasmids in a 2:2:1 ratio of pHelper, pCapsid, and ITR-Transgene0ITR, using polyethylenimine transfection reagent. Media was collected 3 days after transfection, and passed through a 0.2 μM filter. Cells were collected in PBS and put through 3-5x freeze-thaw cycles, then incubated with benzonase for 45 minutes at 37°C. Cells were spun at 15,000 x g for 15 min and supernatant was passed through a 0.2 μM filter and combined with the filtered media. PEG 8000 was added to a final concentration of 12%, stirred for 1 hour at 4°C and then left without stirring overnight at 4°C. The mixutrue was then centrifuged at 3000 x g for 20 minutes and supernatant was discarded. The pellet was resuspended in 7 mL of PBS and incubated with benzonase for 45 minutes at 37°C. This solution was added to a Beckman optiseal tube with a 15-60% iodixanol solution gradient, and centrifuged for 1 hour at 242,000 x g. Most of the virus concentrates in the 40% fraction, which was collected with a syringe. To this, 20 mL PBS + 0.001% F-68 was added and passed through a 0.2 μM filter, and stored at 4°C for up to one week. Viral titer was determined by qPCR.

Animals

All experiments were conducted according to protocols approved by the Institutional Animal Care and Use Committee (Harvard Medical School). Aged mice were ordered from the National Institute on Aging (Bethesda, MD). Viruses were delivered by retroorbital injection after anesthetization with isoflurane. NMN (GeneHarbor) was dissolved in drinking water at 2.4 g/L. Mice were monitored daily and weighed twice per month. Mice were only euthanized if determined to be moribund by an experienced researcher or veterinarian , likely to die within then next 48 hours, based on exhibiting at least two of the following: inability to eat or drink, severe lethargy or persistent recumbence, severe balance or gait disturbance, rapid weight loss (>20%), un ulcerated or bleeding tumor, and dyspnea or cyanosis.

Western blots

SDS-PAGE was performed by standard procedures and detected with ECL reagent (GE Healthcare). Antibodies for GAPDH (Millipore Sigma), Sirt1 (Sigma Aldrich), Sirt2 (Cell Signaling), Sirt3 (Cell Signaling), Sirt4 (non-commercial antibody, a kind gift from Marcia Haigis, Harvard Medical School, Boston, MA), Sirt5 (Cell Signaling), Sirt6 (Cell Signaling) and Sirt7 (Santa Cruz) were used at a 1:1000 dilution.

Gait Analysis

Gait analysis was measured using the TreadScan System (Clever Sys, Inc), which is comprised of a treadmill with a transparent belt and an angled mirror beneath it, via which the underside of the walking mouse is recorded with a high-speed camera. TreadScan software recognizes each paw of the mouse as it walks and calculates various measures of gait.

Statistical analysis

Data were analyzed by a Gehan-Breslow-Wilcoxon test for longevity, and by two-way ANOVAs with multiple comparisons corrections when appropriate. Statistical tests were performed with GraphPad Prism. Data are presented as means ± SEM.

REFERENCES

Bennett, B.T., Mohamed, J.S., and Alway, S.E. (2013). Effects of resveratrol on the recovery of muscle mass following disuse in the plantaris muscle of aged rats. PLoS ONE *8*, e83518.

Bernardes de Jesus, B., Vera, E., Schneeberger, K., Tejera, A.M., Ayuso, E., Bosch, F., and Blasco, M.A. (2012). Telomerase gene therapy in adult and old mice delays aging and increases longevity without increasing cancer. EMBO Mol Med *4*, 691–704.

Boutin, S., Monteilhet, V., Veron, P., Leborgne, C., Benveniste, O., Montus, M.F., and Masurier, C. (2010). Prevalence of serum IgG and neutralizing factors against adeno-associated virus (AAV) types 1, 2, 5, 6, 8, and 9 in the healthy population: implications for gene therapy using AAV vectors. Hum. Gene Ther. *21*, 704–712.

Chen, D., Li, P.W.-L., Goldstein, B.A., Cai, W., Thomas, E.L., Chen, F., Hubbard, A.E., Melov, S., and Kapahi, P. (2013). Germline signaling mediates the synergistically prolonged longevity produced by double mutations in daf-2 and rsks-1 in C. elegans. Cell Rep *5*, 1600–1610.

Das, A., Huang, G.X., Bonkowski, M.S., Longchamp, A., Li, C., Schultz, M.B., Kim, L.-J., Osborne, B., Joshi, S., Lu, Y., et al. (2018). Impairment of an Endothelial NAD+-H2S Signaling Network Is a Reversible Cause of Vascular Aging. Cell *173*, 74-89.e20.

Friedman, D.B., and Johnson, T.E. (1988). A mutation in the age-1 gene in Caenorhabditis elegans lengthens life and reduces hermaphrodite fertility. Genetics *118*, 75–86.

Garratt, M., Lagerborg, K.A., Tsai, Y., Galecki, A., Jain, M., and Miller, R.A. (2018). Male lifespan extension with 17-α estradiol is linked to a sex-specific metabolomic response modulated by gonadal hormones in mice. Aging Cell *17*.

Gomes, A.P., Price, N.L., Ling, A.J.Y., Moslehi, J.J., Montgomery, M.K., Rajman, L., White, J.P., Teodoro, J.S., Wrann, C.D., Hubbard, B.P., et al. (2013). Declining NAD(+) induces a pseudohypoxic state disrupting nuclear-mitochondrial communication during aging. Cell *155*, 1624–1638.

Grieger, J.C., Choi, V.W., and Samulski, R.J. (2006). Production and characterization of adeno-associated viral vectors. Nat Protoc *1*, 1412–1428.

Harrison, D.E., Strong, R., Sharp, Z.D., Nelson, J.F., Astle, C.M., Flurkey, K., Nadon, N.L., Wilkinson, J.E., Frenkel, K., Carter, C.S., et al. (2009). Rapamycin fed late in life extends lifespan in genetically heterogeneous mice. Nature *460*, 392–395.

Kaeberlein, M., McVey, M., and Guarente, L. (1999). The SIR2/3/4 complex and SIR2 alone promote longevity in Saccharomyces cerevisiae by two different mechanisms. Genes Dev. *13*, 2570–2580.

Kanfi, Y., Naiman, S., Amir, G., Peshti, V., Zinman, G., Nahum, L., Bar-Joseph, Z., and Cohen, H.Y. (2012). The sirtuin SIRT6 regulates lifespan in male mice. Nature *483*, 218–221.

Kenyon, C., Chang, J., Gensch, E., Rudner, A., and Tabtiang, R. (1993). A C. elegans mutant that lives twice as long as wild type. Nature *366*, 461–464.

Kunstyr, I., and Leuenberger, H.G. (1975). Gerontological data of C57BL/6J mice. I. Sex differences in survival curves. J Gerontol *30*, 157–162.

Li, J., Bonkowski, M.S., Moniot, S., Zhang, D., Hubbard, B.P., Ling, A.J.Y., Rajman, L.A., Qin, B., Lou, Z., Gorbunova, V., et al. (2017). A conserved NAD+ binding pocket that regulates protein-protein interactions during aging. Science *355*, 1312–1317.

Liao, Z.-Y., Chen, J.-L., Xiao, M.-H., Sun, Y., Zhao, Y.-X., Pu, D., Lv, A.-K., Wang, M.-L., Zhou, J., Zhu, S.-Y., et al. (2017). The effect of exercise, resveratrol or their combination on Sarcopenia in aged rats via regulation of AMPK/Sirt1 pathway. Exp. Gerontol. *98*, 177–183.

Mercken, E.M., Mitchell, S.J., Martin-Montalvo, A., Minor, R.K., Almeida, M., Gomes, A.P., Scheibye-Knudsen, M., Palacios, H.H., Licata, J.J., Zhang, Y., et al. (2014). SRT2104 extends survival of male mice on a standard diet and preserves bone and muscle mass. Aging Cell *13*, 787–796.

Mitchell, S.J., Martin-Montalvo, A., Mercken, E.M., Palacios, H.H., Ward, T.M., Abulwerdi, G., Minor, R.K., Vlasuk, G.P., Ellis, J.L., Sinclair, D.A., et al. (2014). The SIRT1 activator SRT1720 extends lifespan and improves health of mice fed a standard diet. Cell Rep *6*, 836–843.

Poulet, B., de Souza, R., Knights, C.B., Gentry, C., Wilson, A.M., Bevan, S., Chang, Y.-M., and Pitsillides, A.A. (2014). Modifications of gait as predictors of natural osteoarthritis progression in STR/Ort mice. Arthritis & Rheumatology (Hoboken, N.J.) *66*, 1832–1842.

Rogina, B., and Helfand, S.L. (2004). Sir2 mediates longevity in the fly through a pathway related to calorie restriction. Proc Natl Acad Sci U S A *101*, 15998–16003.

Satoh, A., Brace, C.S., Rensing, N., Cliften, P., Wozniak, D.F., Herzog, E.D., Yamada, K.A., and Imai, S.-I. (2013). Sirt1 extends life span and delays aging in mice through the regulation of Nk2 homeobox 1 in the DMH and LH. Cell Metab. *18*, 416–430.

Sharples, A.P., Hughes, D.C., Deane, C.S., Saini, A., Selman, C., and Stewart, C.E. (2015). Longevity and skeletal muscle mass: the role of IGF signalling, the sirtuins, dietary restriction and protein intake. Aging Cell *14*, 511–523.

Skelton, D., Satake, N., and Kohn, D.B. (2001). The enhanced green fluorescent protein (eGFP) is minimally immunogenic in C57BL/6 mice. Gene Therapy *8*, 1813.

Takahashi, K., and Yamanaka, S. (2006). Induction of pluripotent stem cells from mouse embryonic and adult fibroblast cultures by defined factors. Cell *126*, 663–676.

Tissenbaum, H.A., and Guarente, L. (2001). Increased dosage of a sir-2 gene extends lifespan in Caenorhabditis elegans. Nature *410*, 227–230.

Whitaker, R., Faulkner, S., Miyokawa, R., Burhenn, L., Henriksen, M., Wood, J.G., and Helfand, S.L. (2013). Increased expression of Drosophila Sir2 extends life span in a dose-dependent manner. Aging (Albany NY) *5*, 682–691.

Williams, E.G., and Auwerx, J. (2015). The Convergence of Systems and Reductionist Approaches in Complex Trait Analysis. Cell *162*, 23–32.

Zhang, H., Ryu, D., Wu, Y., Gariani, K., Wang, X., Luan, P., D'Amico, D., Ropelle, E.R., Lutolf, M.P., Aebersold, R., et al. (2016). NAD^+ repletion improves mitochondrial and stem cell function and enhances life span in mice. Science *352*, 1436–1443.

Zhou, C.-C., Yang, X., Hua, X., Liu, J., Fan, M.-B., Li, G.-Q., Song, J., Xu, T.-Y., Li, Z.-Y., Guan, Y.-F., et al. (2016). Hepatic NAD(+) deficiency as a therapeutic target for non-alcoholic fatty liver disease in ageing. Br. J. Pharmacol. *173*, 2352–2368.

Chapter 4 - FrightAge and AFRAID Score for age and life expectancy prediction from frailty

Illustration by Kevin Krull

"It is possible that death may be the consequence of two generally co-existing causes; the one, chance, without previous disposition to death or deterioration; the other, a deterioration, or an increased inability to withstand destruction."

-Benjamin Gompertz, 1825

Significant contributions to this chapter were made by Alice Kane and Michael Bonkowski. A manuscript based on this work is in preparation.

ABSTRACT

The identification of biomarkers for biological age would accelerate research into interventions that alter the aging process. Molecular biomarkers such as DNA methylation and blood parameters hold great promise, but have the detriment of being invasive and expensive. The Frailty Index (FI) is a score based on a battery of measurements of gross external parameters of health, and has the advantage of being fast, cheap, and non-invasive. Previous studies have demonstrated that FI correlates with mortality risk in mice and humans. However, no models currently exist for using FI to directly predict biological age or life expectancy. Here, we track a group of aging mice until their natural deaths, scoring them longitudinally with the FI. We observe that specific parameters of FI are well-correlated with chronologic age while others are not, the best of which include tail stiffening, breathing rate/depth, gait disorders, hearing loss, kyphosis, and tremor. In order to better predict chronological age, we performed an ElasticNet regression on the FI components, the model from which we call FRIGHT (Frailty Inferred Geriatric Health Timeline) Age. While FRIGHT Age is a strong predictor of chronological age ($r^2 = 0.732$, median error = 47.5 days), it is not superior to chronological age in at predicting mortality. We further built a model to predict life expectancy, a random forest regression model termed the AFRAID (Analysis of Frailty and Death) score, which is able to predict survival at multiple ages ($r^2=0.375$, median error = 46.4 days). The largest contributing factors to the AFRAID score are chronological age and recent weight loss. Both FRIGHT and AFRAID models can detect the effects of an intervention that improves healthspan. Our findings underscore the value of assessing non-invasive biomarkers for aging research.

INTRODUCTION

The discovery of well validated biomarkers for aging would greatly accelerate research into aging's underlying causes. Interventional studies could proceed apace, with biomarker readouts as early, reliable indications for an experiment's prospects. However, identification of such biomarkers has proven difficult, in no small part because a consensus on the definition of aging is lacking. Thus, for a biomarker of aging to be robust, it must serve multiple roles and meet multiple corresponding criteria: it should track roughly with chronological age, in order to predict at what point an individual is in their total lifespan; it should predict remaining longevity, even at an age when most of a population is still alive; it should serve as a better predictor of longevity than does chronological age alone; and its measurement should be non-invasive as to allow for repeated measurements without altering the health or lifespan of the animal measured (Butler et al., 2004). Proposed biomarkers include physiological measurements (e.g. grip strength, gait), DNA-damage readouts (e.g. γ-H2AX levels, PARP-1 activity), epigenetic measures (e.g. DNA methylation, histone levels), telomere length, immunological biomarkers (e.g. levels of serum immunoglobulins or cytokines), and markers based on protein modifications and oxidative stress (e.g. glycosylation products) (Bürkle et al., 2015). No single biomarker yet challenges the preeminence of maximum longevity as the standard to assess aging interventions.

Of the biomarkers that have been identified so far, those which are more predictive of aging have been modeled in the form of aging "clocks," in which the biomarker data are fed into a statistical framework to generate a numerical prediction of biological age. A biological age prediction generated from a clock should roughly follow chronological age, but should serve as a better predictor of mortality and disease risk than does chronological age. The most popular such set of clocks are those based on the methylation status of a few to hundreds of DNA loci. Such

clocks have been generated for humans (Hannum et al., 2013; Horvath, 2013) and mice (Meer et al., 2018; Petkovich et al., 2017; Wang et al., 2017). They are able to predict lifespan and age-related diseases better than does chronological age alone, and are altered by interventions known to affect health and longevity (Cole et al., 2017; Hahn et al., 2017; Horvath et al., 2015, 2016; Levine et al., 2015; Maierhofer et al., 2017; Petkovich et al., 2017; Quach et al., 2017; Stubbs et al., 2017; Wang et al., 2018). While these clocks are trained on chronological age, other methylation clocks have been trained specifically to predict life expectancy, either directly (Zhang et al., 2017), indirectly via surrogate biomarkers for mortality (PhenoAge) (Levine et al., 2018) or in combination with clinical biomarkers (GrimAge) (Lu et al., 2019). Recently, another biomarker has been used to generate a clock based on the relative frequencies of immune cell types, termed IMM-AGE, which also predicts mortality better than does chronological age (Alpert et al., 2019). The major drawback of these clocks is that collecting blood or tissue must be done infrequently if at all, especially in mice, if it is not to affect the subjects' aging trajectories, and that acquiring and analyzing methylation clock or IMM-AGE data can be time consuming and expensive.

The Frailty Index (FI) is a compound biomarker of aging which tallies physiological deficits as they accumulate (**Fig 4.1**). First developed for humans, FI has been "reverse translated" to mice, where it is quick and essentially free to assess and analyze (Kane et al., 2017; Parks et al., 2012; Whitehead et al., 2014). In mice, 31 deficits are scored as zero (absent), half (moderate), or one (severe). As conceived, frailty captures the heterogeneity in health parameters among individuals of the same age, which impacts their mortality (Vaupel et al., 1979). Indeed, FI is associated with mortality, but has not yet been used to build a predictive model of biological age or life expectancy (Blodgett et al., 2017; Hao et al., 2016). In this study, we track FI longitudinally in a cohort of aging mice from 21 months of age until their natural deaths. With these data, we

A.

B.

C.

D.

E.

F.

G.

Integument				Notes	Ocular/Nasal				Notes
Alopecia	0	H	1		Cataracts	0	H	1	
Fur color loss	0	H	1		Corneal opacity	0	H	1	
Dermatitis	0	H	1		Eye discharge/swelling	0	H	1	
Loss of whiskers	0	H	1		Microphthalmia	0	H	1	
Coat condition	0	H	1		Vision loss	0	H	1	
Physical/Musuloskeletal					Menace reflex	0	H	1	
Tumors	0	H	1		Nasal discharge	0	H	1	
Distended abdomen	0	H	1		**Digestive/Urogenital**				
Kyphosis	0	H	1		Malocclusions	0	H	1	
Tail stiffening	0	H	1		Renal prolapse	0	H	1	
Gait disorders	0	H	1		Vaginal/uterine/ penile prolapse	0	H	1	
Tremor	0	H	1		Diarrhoea	0	H	1	
Grip strength	0	H	1		**Respiratory system**				
Body condition	0	H	1		Breathing rate/depth	0	H	1	
Vestibulocochlear/Auditory					**Discomfort**				
Vestibular disturb.	0	H	1		Mouse grimace	0	H	1	
Hearing loss	0	H	1		Piloerection	0	H	1	

Figure 4.1: Overview of frailty index. (A) Vision loss is assessed by lowering a mouse until it reaches its arms towards a surface, signifying its visual distance capacity. (B) Menace reflex, which is lost during aging, is assessed by poking an object towards the mouse's face and observing aggressive behavior. (C) Tail stiffening, which increases during aging, is assessed by the capacity for the tail to curve around an object. (D) Example of alopecia. (E) Grip strength is assessed by lifting a mouse while it grasps a grate with its front paws. (F) Gait is assessed by observing a mouse walk down an incline. Hair greying (fur color loss) and piloerection are also visible. (G) Data entry sheet for frailty analysis, which is amenable to be read by a scantron-like program.

built predictive "clocks" for chronological age, termed FRIGHT Age, and life expectancy, termed the AFRAID score. We intend for these tools to be used, and further refined, to accelerate the pace of aging research.

RESULTS

Frailty correlates with and is predictive of age

We measured frailty longitudinally as a part of unpublished longevity studies. The datasets used for the analyses in this chapter are from two sets of control animals. Both sets of animals had normal median (954 and 922 days) and maximal (1126 and 1142 days) lifespans, slightly surpassing those cited by Jackson Labs (median 878 days, maximum 1200 days) (Festing, 1979; Kunstyr and Leuenberger, 1975), demonstrating that the mice were maintained and aged in healthy conditions (**Fig. 4.2a**). The distributions of frailty scores were also consistent between the groups (**Fig. 4.2b**).

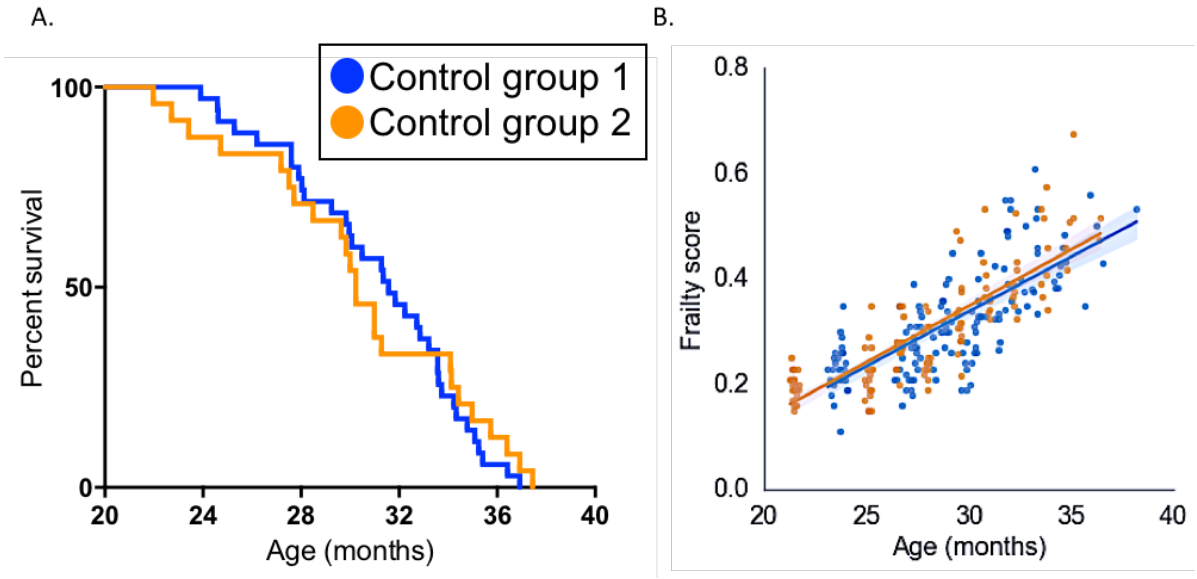

Figure 4.2: Comparison of control cohorts used for analysis. (A) Survival curves of both groups. (B) Longitudinal frailty index scores of both groups.

FI score, which is the unweighted average of the individual deficit scores, increased approximately linearly with age from 21 to 36 months at the population level (**Fig. 4.3a**). At the individual level, frailty trajectories displayed significant variance, possibly representative of the variability in how individuals experience aging (**Fig 4.3b-c**). As FI score is well correlated with chronological age, we wondered to what degree FI score was predictive of chronological and biological age. We performed a simple least squares linear regression on FI score for age with a training data set and evaluated its accuracy on a testing data set (**Fig. 4.4a-b**). FI score was able to predict chronological age with a median error of 65.5 days and an r-squared value of 0.64. The error may be representative of biological age, with individuals having a predicted age younger than their true age being healthier than those with a predicted age older than their true age. We refer to this difference as delta age. Delta age did indeed have a negative correlation with survival, with "younger" mice living longer, at every individual age, longitudinally (**Fig. 4.4c**). However, when predictions at all ages were aligned against the median survival time for a given age, the correlation was shown to be weak, with an r-squared value of only 0.092 (**Fig. 4.4d**). Additionally, the model consistently predicted younger mice (e.g. at 21 months) to be older than they are, and older mice

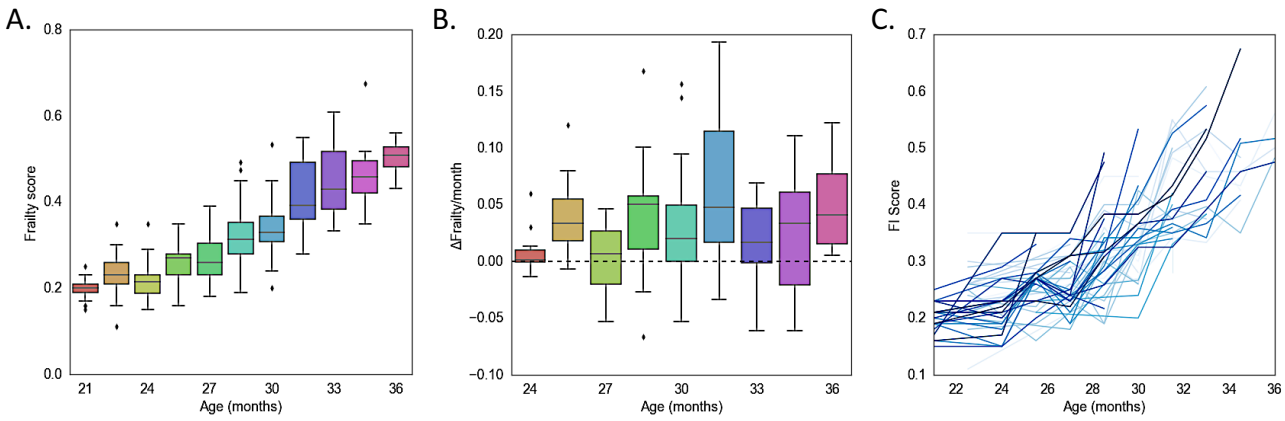

Figure 4.3: Longitudinal frailty scores. (A) Boxplot of FI scores as a function of age. (B) Boxplot of change in FI score between measurement periods for each mouse. (C) Individual trajectories of FI scores for each mouse.

(e.g. at 36 months) to be younger than they are, an apparent artifact of the regression towards the mean age. It also assigned relatively few assessments ages of younger than 25 months.

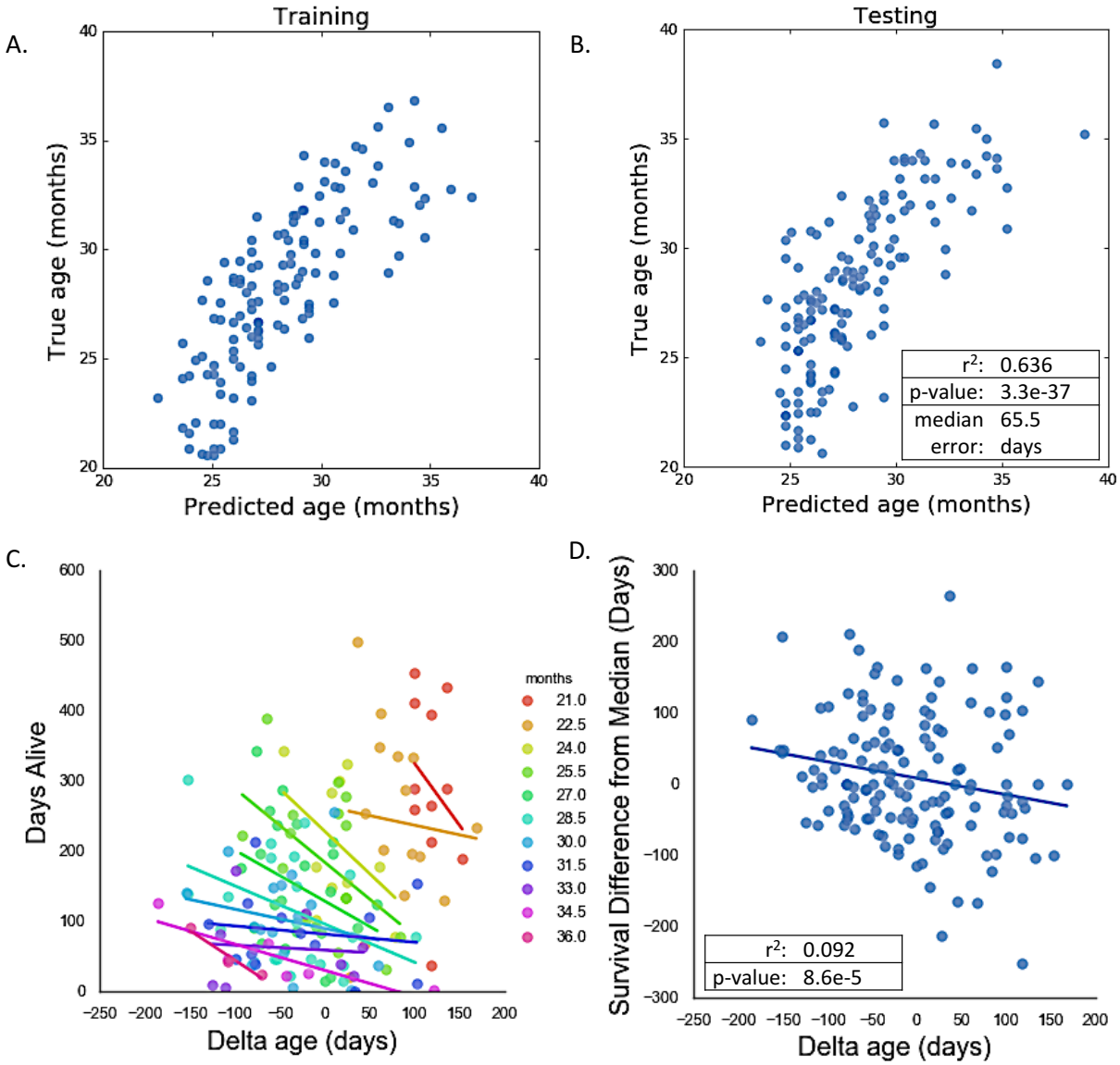

Figure 4.4: Linear regression model of frailty for chronological age. (A) Correlation between predicted age for training data and (B) testing data. (C) Correlation between delta age (predicted age – true age) and days alive, the number of days between the date of the frailty assessment and the date of the animal's death, colored by the animal's age at the time of assessment. (D) Correlation between delta age days alive relative to the median days alive for a given age, allowing for visualization of a trend across all ages.

Individual scores vary in their correlation with age

While a simple linear regression on overall frailty score was somewhat predictive of age, we hypothesized that by differentially weighting individual metrics, we could build a more predictive model. To this end, we calculated the correlation between each individual parameter and chronological age (**Table 4.1, Fig. 4.5**). Some parameters, such as tail stiffening, breathing rate/ depth, gait disorders, hearing loss, kyphosis, and tremor, were remarkably well correlated with age. The fact that some parameters were very well correlated and others poorly correlated suggested that by weighting scores, we could build an improved model for age prediction.

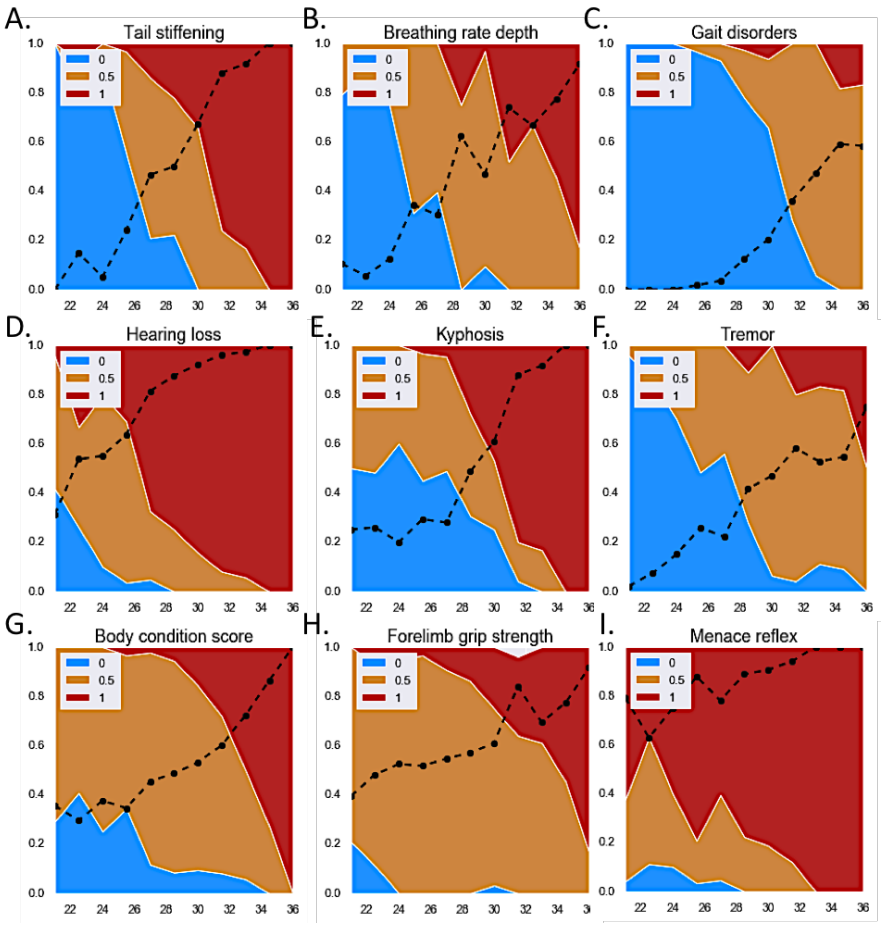

Figure 4.5: Correlations between individual parameters and age. The top nine parameters with categorical scores were (A) tail stiffening, (B) breathing rate depth, (C) gait disorders, (D) hearing loss, (E) kyphosis, (F) tremor, (G) body condition score, (H) forelimb grip strength, and (I) menace reflex. The proportion at a given age that scored zero is colored in blue, 0.5 orange, and one in red. The mean score is plotted in black. A "downward diagonal" pattern of the three scores is observed for parameters that are well correlated with age.

Table 4.1: Correlation between individual parameters and age.

Parameter	r^2	p-value
Tail stiffening	0.584	3.50E-53
Breathing rate/depth	0.499	2.80E-42
Gait disorders	0.419	1.37E-33
Hearing loss	0.382	6.71E-30
Kyphosis	0.381	7.15E-30
Tremor	0.378	1.49E-29
Body condition	0.262	1.83E-19
Grip strength	0.117	7.86E-09
%twc	0.115	1.05E-08
Menace reflex	0.114	1.15E-08
Alopecia	0.104	5.93E-08
Tumors	0.081	2.04E-06
Diarrhea	0.054	1.09E-04
Penile prolapse	0.052	1.42E-04
Microphthalmia	0.048	2.70E-04
Dermatitis	0.048	2.71E-04
Rectal prolapse	0.041	8.02E-04
Distended abdomen	0.039	1.14E-03
Eye discharge/swelling	0.037	1.46E-03
Coat condition	0.035	1.85E-03
Body Weight Score	0.023	1.25E-02
Thresh %rwc	0.014	5.11E-02
Loss of fur color	0.014	5.53E-02
Piloerection	0.012	6.87E-02
Mouse grimace scale	0.011	7.97E-02
Vestibular disturbance	0.007	1.57E-01
Vision loss	0.004	3.05E-01
Loss of whiskers	0.004	3.27E-01
%rwc	0.002	4.95E-01
Cataracts	0.001	6.78E-01
Corneal capacity	0	7.22E-01
Nasal discharge	0	1.00E+00

R-squared and p-value are reported for the correlation between each parameter vs. chronological age. Abbreviations: total weight change from 20 months (%twc), recent weight change from previous month (%rwc). Weight change beyond a threshold in either direction (thresh %rwc).

Multivariate regressions of individual scores to predict age (FRIGHT Age)

We compared FI as a single variable and four different types of multivariate linear regression using five-fold cross validation on the training set: simple least squares regression, ridge regression, elastic net regression, and random forest regression. Only parameters that had a significant, even if weak, correlation with age ($p<0.05$) were included in the analysis. The multivariate models appear superior to FI as a single variable. We observed no significant difference among the multivariate models in predictive accuracy (**Fig. 4.6a-c).** For further analysis, we selected the elastic net regression (ELN) model, as it reduces the number of covariates required for the model.

We term this model FRIGHT Age for Frailty Inferred Geriatric Health Timeline. When assessed on the testing dataset, FRIGHT Age had a strong correlation with chronological age, with a median error of 47.5 days and an r-squared value of 0.73 (**Fig. 4.6d-f).** However, while FRIGHT Age was superior to overall frailty score at predicting chronological age, the residuals from the predictions (delta age) were not well correlated with mortality (**Fig. 4.6g**). This may be because the individual parameters that correlate well with chronological age are different than those that correlate well with mortality. So while FRIGHT Age is a better predictor of chronological age than is FI, it is yet unclear as to whether it is a better predictor of biological age, however defined.

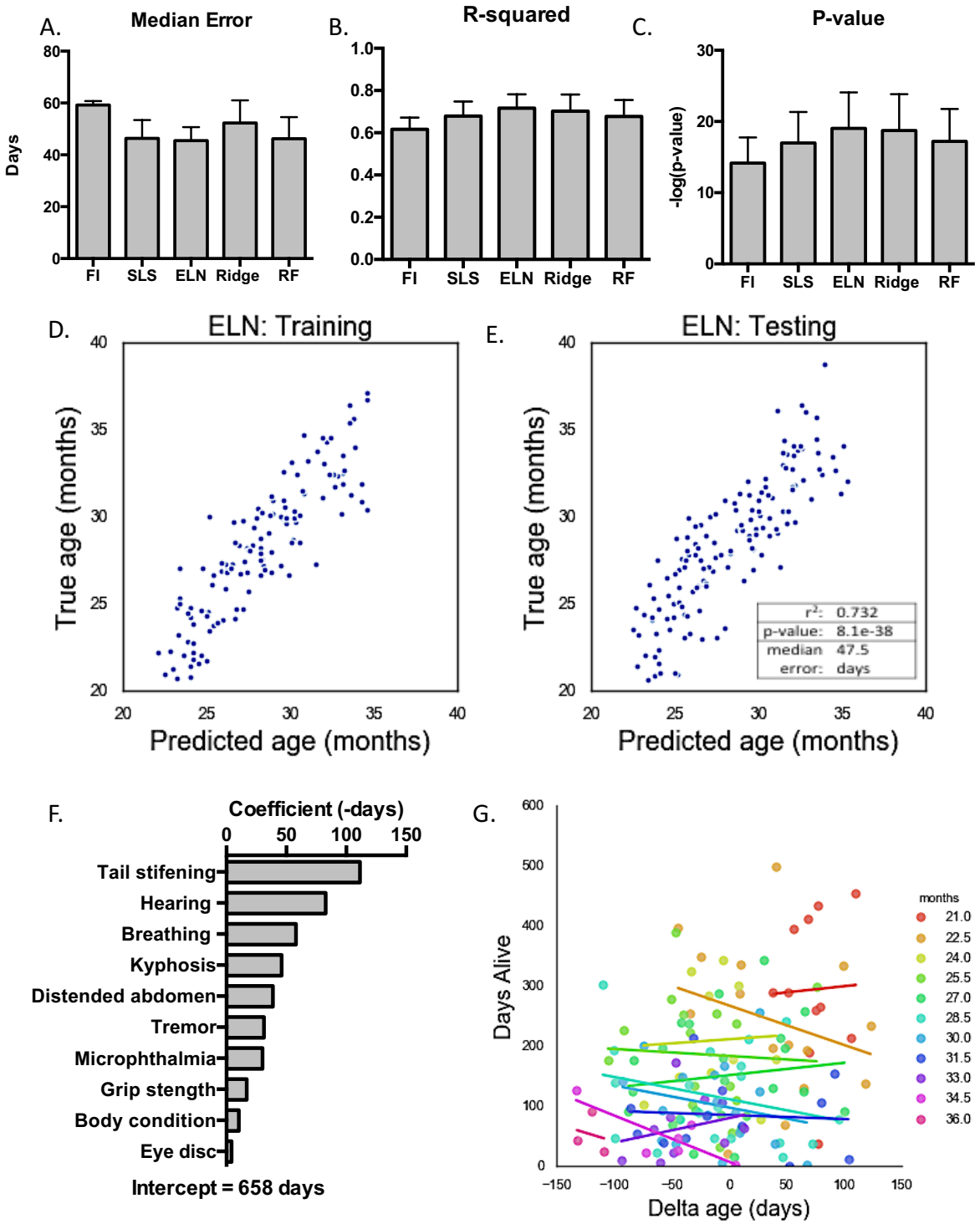

Figure 4.6: FIGHT Age for prediction of chronological age from frailty. (A) Median error, (B) r-squared, and (C) p-value results from five-fold cross validation of training data for frailty index as a single variable (FI), simple least squares (SLS), elastic net (ELN), ridge, and random forest (RF) regressions. (D) Training, and (E) testing data and (F) coefficients for the ELN model, termed FRIGHT Age. (G) Error in FRIGHT Age correlated to survival, colored by age on date of assessment.

Multivariate regressions of individual scores to predict life expectancy (AFRAID Clock)

As FRIGHT Age appears to be no better a predictor of mortality than is chronological age, we sought to build a model that directly predicts for life expectency. We began by calculating the correlation between each individual parameter and survival (number of days from date of assessment to date of death). Unsurprisingly, chronological age was the best predictor of mortality, followed by tremor, body condition score, and gait disorders (**Table 4.2**). However, many of these parameters appear to be better predictors than they are. Since age is a fair predictor of survival, and many of these parameters correlate with age, their correlation with survival is largely only for mice of different ages, and not of the same age. Indeed, when analyzed for only mice of the same age, the only parameters that reached a p-value of less than 0.05 were those measuring weight change.

As a compound biomarker, unweighted FI was correlated with survival, with an overall r^2 value of 0.308. Importantly, FI was also correlated to survival at individual ages (**Fig. 4.7a**). To build a model to predict mortality, we compared a regression of FI as a single variable, and four types of multivariate regressions with five-fold cross-validation. For prediction of survival, a random forest regression model was the superior model (**Fig. 4.7b-d**). We term this model the AFRAID score for Analysis of Frailty and Death. In the testing dataset, the AFRAID score is well correlated with survival (r^2=0.375, median error = 46.4 days). The AFRAID score is also correlated with survival at individual ages, making it potentially useful for comparing the effects of interventional studies (**Fig. 4.7e-h**). It appears to be better at making predictions at older ages, as average life expectency decreases.

The most important variable in the model was, perhaps unsurprisingly, chronological age, followed by total weight loss, recent weight loss, distended abdomen, and tremor (**Fig. 4.7i**). (In

Table 4.2: Correlation between individual parameters and survival.

Parameter	r^2	p-value
Age (days)	0.349	7.48E-27
Tremor	0.246	3.18E-18
Body condition	0.195	2.18E-14
Gait disorders	0.187	9.11E-14
Tail stiffening	0.185	1.15E-13
Breathing rate/depth	0.172	1.01E-12
Hearing loss	0.169	1.72E-12
Kyphosis	0.123	2.73E-09
Distended abdomen	0.109	2.68E-08
Menace reflex	0.078	3.14E-06
%twc	0.073	5.99E-06
Grip strength	0.069	1.14E-05
Alopecia	0.047	3.45E-04
Thresh %rwc	0.041	7.45E-04
Microphthalmia	0.033	2.63E-03
Body Weight Score	0.032	2.97E-03
Coat condition	0.031	3.71E-03
Diarrhea	0.025	9.38E-03
Grimace scale	0.024	1.12E-02
Loss of fur color	0.023	1.28E-02
Dermatitis	0.018	2.79E-02
Piloerection	0.017	3.04E-02
%rwc	0.013	6.02E-02
Rectal prolapse	0.012	7.03E-02
Penile prolapse	0.01	1.08E-01
Tumors	0.009	1.26E-01
Eye discharge/swelling	0.007	1.74E-01
Vestibular disturbance	0.006	1.91E-01
Vision loss	0.005	2.69E-01
Cataracts	0.003	3.85E-01
Corneal capacity	0.002	4.37E-01
Loss of whiskers	0.002	5.06E-01
Nasal discharge	0	1.00E+00

R-squared and p-value are reported for the correlation between each parameter vs. survival.

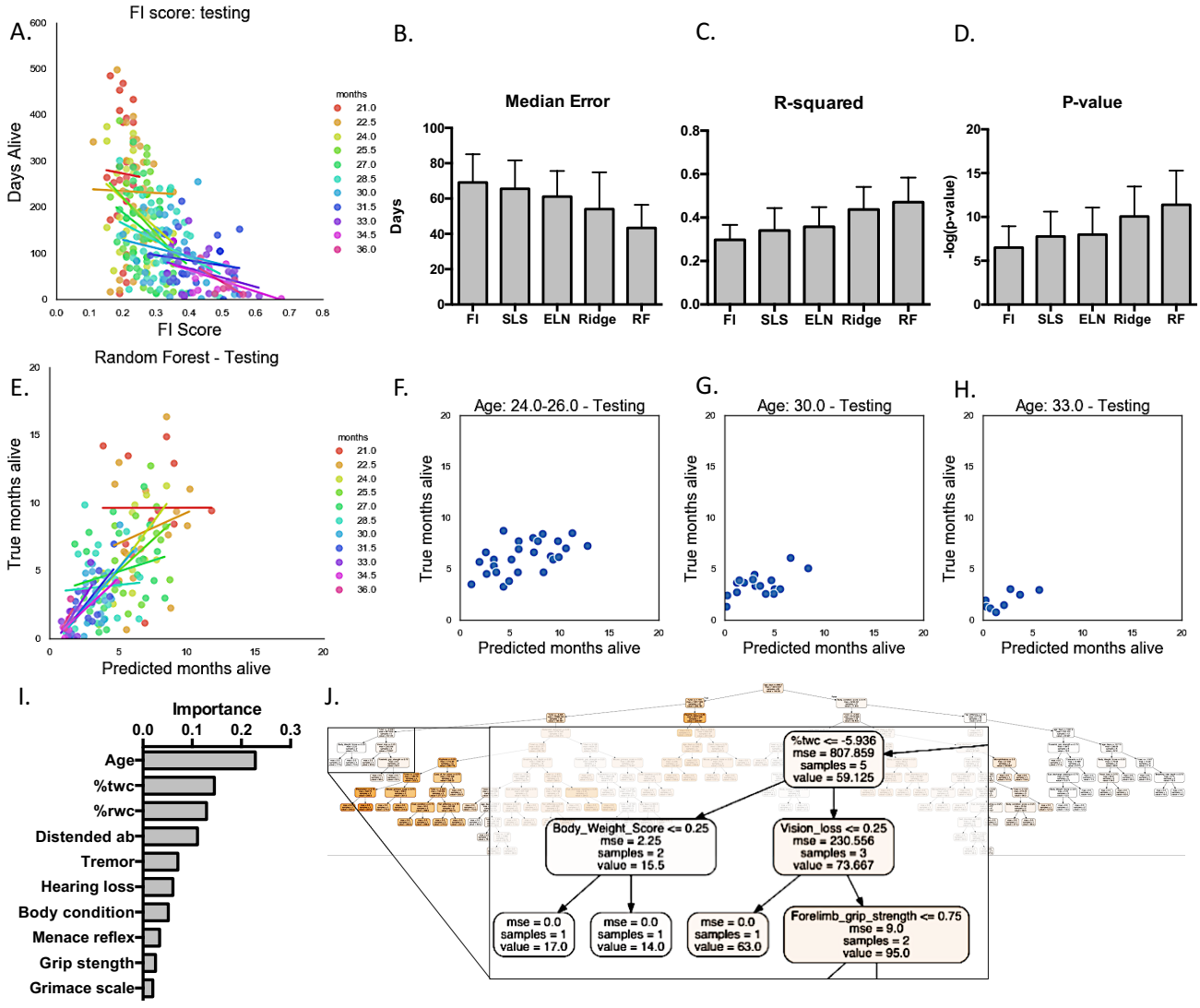

Figure 4.7: AFRAID score for prediction of life expectancy from frailty. (A) Correlation between frailty score and survival (days alive) colored by age on date of assessment. (B) Median error, (C) r-squared, and (D) p-value results from five-fold cross validation of training data for frailty index as a single variable (FI), simple least squares (SLS), elastic net (ELN), ridge, and random forest (RF) regressions. (E) Predictions and true values of survival in the testing data set from the AFRAID clock, a random forest regression model, colored by age on the date of assessment. (F) Predictions and true values of survival in the testing dataset for mice at ages 24-26 months (G) 30 months and (H) 33 months. (I) The importance weights of the ten variables in the model. (J) An illustration of one decision tree, out of one thousand that comprise the model.

a random forest, importance is calculated by a combination of the relative frequency of a variable and its ability to reduce variance at a split.) While it is debatable whether such a model should include chronological age as a prediction variable, it makes good sense in a random forest model, which can account for complex relationships between predictor variables, based on the branching structure of the model (**Fig. 4.7j**). This is in contrast to linear models, where all variables are treated independently.

Analysis of responses to an intervention

One ultimate ultility for such models would be to serve as early biomarkers for the effects of interventional treatments, which are expected to extend or reduce healthspan and lifespan. To date, few interventional studies have measured FI. However, a recently published study measured FI in 24-month old mice treated with the angiotensin converting enzyme (ACE) inhibitor enalapril from 16 months of age (Keller et al., 2018). As previously shown, enalapril the averge FI score (**Fig. 4.8a**). When the data were converted to a prediction of chronological age, enalapril reduced FRIGHT Age by 32 days relative to control mice (**Fig. 4.8b**). When the data were converted to a prediction of survival, enalapril extended predicted survival by 19 days, a non-significant

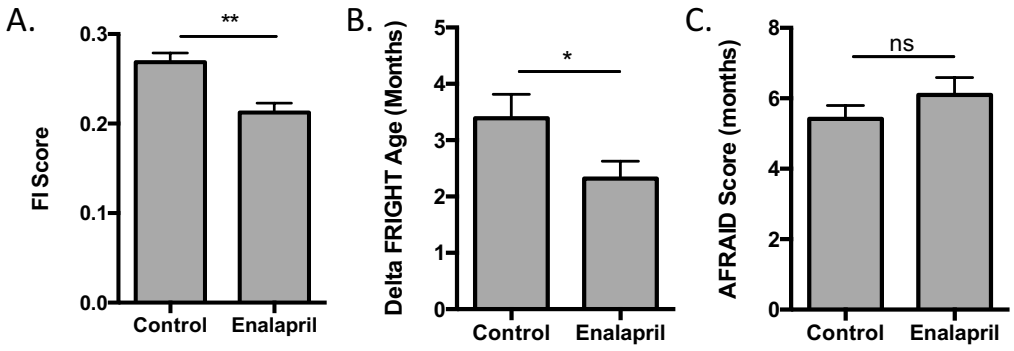

Figure 4.8: Effect of enalapril treatment. (A) Frailty index score on control and enalapril-treated male mice at 24 months of age, from (Keller et al., 2018). (B) Reanalysis of FI data for predictions of delta FRIGHT Age and (C) AFRAID score.

difference between the groups (**Fig. 4.8c**). As enalapril improves healthspan but has not been shown to significantly extend lifespan, the accuracy of these predicitons is yet untested (Harrison et al., 2009). While it will be useful to test these models in interventional studies with compounds that have been shown to extend lifespan, such as rapamycin and STACs, these analyses nonetheless show that these models are likely also responsive to more potent interventions.

DISCUSSION

This is the first study to measure frailty longitudinally in a population of naturally aging mice and to track those mice until their natural deaths, in order to connect FI to life expectancy. We show that FI is not only correlated with age but is also predictive of survival, even for animals of the same age. We further generate two models based on FI: FRIGHT age, which is a prediction of chronological age, and the AFRAID score, which is a prediction of life expectancy. These models have median errors of 47 and 46 days, respectively. FRIGHT age was responsive to long-term enalapril administration, showing that it is capable of responding to a pharmacological intervention. The AFRAID score was less responsive to enalapril administration. It is not currently clear whether this is due to a deficiency in the model, or because enalapril does not extend lifespan.

The major advantage of FI as biomarker for aging is its ease of use. It is relatively quick and essentially free to assess, and has no negative impact on the health of the animals. We encourage future longevity studies to incorporate periodic FI assessment as a routine measure. This will help further determine its utility for predicting outcomes of interest, and may eventually

Figure 4.9: The relationship between chronological age, mortality, and biological age. FRIGHT age is a model to predict chronological age, which is strongly associated with biomarkers such as tail stiffening and hearing loss, that increase during aging but may not impact mortality. The AFRAID clock is a model to predict life expectancy, which is associated with weight loss, and theoretically with disease-specific markers such as tumors. Biological age falls in the area of overlap between chronological age and mortality.

be used as a screening tool to decide whether to continue expensive longevity studies after a short duration with a prospective intervention.

The models discussed in this study could benefit from the incorporation of additional input variables, especially from relatively non-invasive molecular biomarkers. Much can be inferred from tallying gross physiological deficits. However, these deficits have molecular origins which may add predictive value at much earlier time points if they can be identified (Kane et al., 2019).

The aim of all three frailty metrics, FI, FRIGHT age, and AFRAID score, is a robust method for appraisal of biological age. Yet in the absence of a clear definition of biological age, and without a lodestar biomarker with which to compare, assessment of the relative value of these metrics is difficult. In one sense, FRIGHT age is the best metric, as it tracks most closely with chronological age, in spite of its lack of sensitivity to predict mortality. One would expect an intervention that slows aging to suppress all aspects of aging, even those that don't impinge on life expectancy. In another sense, the AFRAID score is the superior metric, because an increase in life expectancy, median and maximum, is the ultimate benchmark for an aging intervention. One could also argue that overall unweighted FI is the best metric, because while it is not best at predicting either chronological age or mortality, it is better than either FRIGHT age or AFRAID score at predicting both. Perhaps true biological age is tangential to both chronological age and mortality

(**Fig 4.9**). Certainly it is not exactly akin to chronological age, or there would be no use in having both definitions; nor is it the same as mortality, or all fatal diseases would also be diseases of aging, something which is obviously not the case. This study highlights the deficit in our understanding of what aging fundamentally is, which hinders our ability to identify robust biomarkers for it. The development and further refinement of biomarkers of aging will get us closer to such a definition and understanding.

MATERIALS AND METHODS

Animals

All experiments were conducted according to protocols approved by the Institutional Animal Care and Use Committee (Harvard Medical School). Aged mice were ordered from the National Institute on Aging (Bethesda, MD). Group 1 had been injected with AAV vectors containing GFP as a control group for a longevity experiment. This did not affect their frailty or longevity in comparison to group 2, which were completely untreated. Mice were only euthanized if determined to be moribund by an experienced researcher or veterinarian , likely to die within then next 48 hours, based on exhibiting at least two of the following: inability to eat or drink, severe lethargy or persistent recumbence, severe balance or gait disturbance, rapid weight loss (>20%), un ulcerated or bleeding tumor, and dyspnea or cyanosis.

Frailty analysis

Frailty was assessed longitudinally by the same researcher (A.K.), as previously described (Kane et al., 2017). Individual FI parameters are reported inf **Fig. 4.1g**. Malocclusions and body temperature were not assessed. For regression analyses, prediction variables were added to

represent body weight change: total percent weight change, from 20 months of age; recent percent weight change, from one month before the assessment; and threshold recent weight change – mice scored positive if they gained more than eight grams or lost more than ten grams in the previous month.

Machine learning

Data were analyzed in Python using algorithms provided in the Scikit-learn package. Training and testing datasets were separated by mouse rather than by assessment.

REFERENCES

Alpert, A., Pickman, Y., Leipold, M., Rosenberg-Hasson, Y., Ji, X., Gaujoux, R., Rabani, H., Starosvetsky, E., Kveler, K., Schaffert, S., et al. (2019). A clinically meaningful metric of immune age derived from high-dimensional longitudinal monitoring. Nat. Med. *25*, 487–495.

Blodgett, J.M., Theou, O., Howlett, S.E., and Rockwood, K. (2017). A frailty index from common clinical and laboratory tests predicts increased risk of death across the life course. Geroscience *39*, 447–455.

Bürkle, A., Moreno-Villanueva, M., Bernhard, J., Blasco, M., Zondag, G., Hoeijmakers, J.H.J., Toussaint, O., Grubeck-Loebenstein, B., Mocchegiani, E., Collino, S., et al. (2015). MARK-AGE biomarkers of ageing. Mech. Ageing Dev. *151*, 2–12.

Butler, R.N., Sprott, R., Warner, H., Bland, J., Feuers, R., Forster, M., Fillit, H., Harman, S.M., Hewitt, M., Hyman, M., et al. (2004). Biomarkers of aging: from primitive organisms to humans. J. Gerontol. A Biol. Sci. Med. Sci. *59*, B560-567.

Cole, E., Brown, T.A., Pinkerton, K.E., Postma, B., Malany, K., Yang, M., Kim, Y.J., Hamilton, R.F., Holian, A., and Cho, Y.H. (2017). Perinatal exposure to environmental tobacco smoke is associated with changes in DNA methylation that precede the adult onset of lung disease in a mouse model. Inhal Toxicol *29*, 435–442.

Festing, M.F.W. (1979). Inbred Strains in Biomedical Research (Macmillan International Higher Education).

Gompertz, B. (1815). On the Nature of the Function Expressive of the Law of Human Mortality, and on a New Mode of Determining the Value of Life Contingencies. Proceedings of the Royal Society of London *2*, 252–253.

Hahn, O., Grönke, S., Stubbs, T.M., Ficz, G., Hendrich, O., Krueger, F., Andrews, S., Zhang, Q., Wakelam, M.J., Beyer, A., et al. (2017). Dietary restriction protects from age-associated DNA methylation and induces epigenetic reprogramming of lipid metabolism. Genome Biol. *18*, 56.

Hannum, G., Guinney, J., Zhao, L., Zhang, L., Hughes, G., Sadda, S., Klotzle, B., Bibikova, M., Fan, J.-B., Gao, Y., et al. (2013). Genome-wide methylation profiles reveal quantitative views of human aging rates. Mol. Cell *49*, 359–367.

Hao, Q., Song, X., Yang, M., Dong, B., and Rockwood, K. (2016). Understanding Risk in the Oldest Old: Frailty and the Metabolic Syndrome in a Chinese Community Sample Aged 90+ Years. J Nutr Health Aging *20*, 82–88.

Harrison, D.E., Strong, R., Sharp, Z.D., Nelson, J.F., Astle, C.M., Flurkey, K., Nadon, N.L., Wilkinson, J.E., Frenkel, K., Carter, C.S., et al. (2009). Rapamycin fed late in life extends lifespan in genetically heterogeneous mice. Nature *460*, 392–395.

Horvath, S. (2013). DNA methylation age of human tissues and cell types. Genome Biol. *14*, R115.

Horvath, S., Pirazzini, C., Bacalini, M.G., Gentilini, D., Di Blasio, A.M., Delledonne, M., Mari, D., Arosio, B., Monti, D., Passarino, G., et al. (2015). Decreased epigenetic age of PBMCs from Italian semi-supercentenarians and their offspring. Aging (Albany NY) *7*, 1159–1170.

Horvath, S., Langfelder, P., Kwak, S., Aaronson, J., Rosinski, J., Vogt, T.F., Eszes, M., Faull, R.L.M., Curtis, M.A., Waldvogel, H.J., et al. (2016). Huntington's disease accelerates epigenetic aging of human brain and disrupts DNA methylation levels. Aging (Albany NY) *8*, 1485–1512.

Kane, A.E., Ayaz, O., Ghimire, A., Feridooni, H.A., and Howlett, S.E. (2017). Implementation of the mouse frailty index. Can. J. Physiol. Pharmacol. *95*, 1149–1155.

Kane, A.E., Keller, K.M., Heinze-Milne, S., Grandy, S.A., and Howlett, S.E. (2019). A Murine Frailty Index Based on Clinical and Laboratory Measurements: Links Between Frailty and Pro-inflammatory Cytokines Differ in a Sex-Specific Manner. J. Gerontol. A Biol. Sci. Med. Sci. *74*, 275–282.

Keller, K., Kane, A., Heinze-Milne, S., Grandy, S.A., and Howlett, S.E. (2018). Chronic treatment with the ACE inhibitor enalapril attenuates the development of frailty and differentially modifies pro-and anti-inflammatory cytokines in aging male and female C57BL/6 mice. J. Gerontol. A Biol. Sci. Med. Sci.

Kunstyr, I., and Leuenberger, H.G. (1975). Gerontological data of C57BL/6J mice. I. Sex differences in survival curves. J Gerontol *30*, 157–162.

Levine, M.E., Hosgood, H.D., Chen, B., Absher, D., Assimes, T., and Horvath, S. (2015). DNA methylation age of blood predicts future onset of lung cancer in the women's health initiative. Aging (Albany NY) *7*, 690–700.

Levine, M.E., Lu, A.T., Quach, A., Chen, B.H., Assimes, T.L., Bandinelli, S., Hou, L., Baccarelli, A.A., Stewart, J.D., Li, Y., et al. (2018). An epigenetic biomarker of aging for lifespan and healthspan. Aging (Albany NY) *10*, 573–591.

Lu, A.T., Quach, A., Wilson, J.G., Reiner, A.P., Aviv, A., Raj, K., Hou, L., Baccarelli, A.A., Li, Y., Stewart, J.D., et al. (2019). DNA methylation GrimAge strongly predicts lifespan and healthspan. Aging (Albany NY) *11*, 303–327.

Maierhofer, A., Flunkert, J., Oshima, J., Martin, G.M., Haaf, T., and Horvath, S. (2017). Accelerated epigenetic aging in Werner syndrome. Aging (Albany NY) *9*, 1143–1152.

Meer, M.V., Podolskiy, D.I., Tyshkovskiy, A., and Gladyshev, V.N. (2018). A whole lifespan mouse multi-tissue DNA methylation clock. Elife *7*.

Parks, R.J., Fares, E., Macdonald, J.K., Ernst, M.C., Sinal, C.J., Rockwood, K., and Howlett, S.E. (2012). A procedure for creating a frailty index based on deficit accumulation in aging mice. J. Gerontol. A Biol. Sci. Med. Sci. *67*, 217–227.

Petkovich, D.A., Podolskiy, D.I., Lobanov, A.V., Lee, S.-G., Miller, R.A., and Gladyshev, V.N. (2017). Using DNA Methylation Profiling to Evaluate Biological Age and Longevity Interventions. Cell Metab. *25*, 954-960.e6.

Quach, A., Levine, M.E., Tanaka, T., Lu, A.T., Chen, B.H., Ferrucci, L., Ritz, B., Bandinelli, S., Neuhouser, M.L., Beasley, J.M., et al. (2017). Epigenetic clock analysis of diet, exercise, education, and lifestyle factors. Aging (Albany NY) *9*, 419–446.

Stubbs, T.M., Bonder, M.J., Stark, A.-K., Krueger, F., BI Ageing Clock Team, von Meyenn, F., Stegle, O., and Reik, W. (2017). Multi-tissue DNA methylation age predictor in mouse. Genome Biol. *18*, 68.

Vaupel, J.W., Manton, K.G., and Stallard, E. (1979). The impact of heterogeneity in individual frailty on the dynamics of mortality. Demography *16*, 439–454.

Wang, T., Tsui, B., Kreisberg, J.F., Robertson, N.A., Gross, A.M., Yu, M.K., Carter, H., Brown-Borg, H.M., Adams, P.D., and Ideker, T. (2017). Epigenetic aging signatures in mice livers are slowed by dwarfism, calorie restriction and rapamycin treatment. Genome Biology *18*, 57.

Wang, X., Liu, A.-H., Jia, Z.-W., Pu, K., Chen, K.-Y., and Guo, H. (2018). Genome-wide DNA methylation patterns in coronary heart disease. Herz *43*, 656–662.

Whitehead, J.C., Hildebrand, B.A., Sun, M., Rockwood, M.R., Rose, R.A., Rockwood, K., and Howlett, S.E. (2014). A clinical frailty index in aging mice: comparisons with frailty index data in humans. J. Gerontol. A Biol. Sci. Med. Sci. *69*, 621–632.

Zhang, Y., Wilson, R., Heiss, J., Breitling, L.P., Saum, K.-U., Schöttker, B., Holleczek, B., Waldenberger, M., Peters, A., and Brenner, H. (2017). DNA methylation signatures in peripheral blood strongly predict all-cause mortality. Nat Commun *8*, 14617.

Chapter 5: Concluding Remarks

Illustration by Oldřich Kulhánek

"The credit belongs to the man who is actually in the arena, whose face is marred by dust and sweat and blood; who strives valiantly; who errs, who comes short again and again, because there is no effort without error and shortcoming; but who does actually strive to do the deeds; who knows great enthusiasms, the great devotions; who spends himself in a worthy cause; who at the best knows in the end the triumph of high achievement, and who at the worst, if he fails, at least fails while daring greatly."

-Theodore Roosevelt, 1910

PARP14 hydrolyzes NAD^+ during TLR-induced inflammation

Inflammation and aging both have underlying metabolic bases and the metabolite NAD^+ plays a significant role in both processes. In Chapter 2 of this dissertation, I describe the kinetics of steady state NAD^+ and NADH levels in response to various stimuli in macrophages, as an *in vitro* model system for inflammation. We observed a drop in NAD^+ levels in response to LPS, P3CSK4, and palmitic acid, all stimuli for toll-like receptors, whereas no drop is associated with IFNγ or IL-4. We ruled out reduction as a cause for the drop in levels of NAD^+, as NADH levels do not increase, and turned our attention to NAD^+ hydrolases as potentially causal. Multiple lines of evidence, including the use of macrophages from knockout mice, eliminated prominent NAD^+ hydrolases CD38 and PARP1 as necessary for the phenomenon. Profiling of RNA levels revealed that multiple members of the PARP family of ADPRTs are transcribed at levels inversely related to NAD^+ levels. We knocked out each of the top six PARPs in immortalized macrophages using Cas9, and observed that only in PARP14 knockout cell lines were NAD^+ levels flat in response to LPS stimulation. We have further shown that PARP14 inhibition or deletion prevents splenic NAD^+ levels from dropping during LPS-induced septic shock and in normal aging.

Several open questions remain in this line of research. First, we have shown that PARP14 was necessary in all conditions measured for this TLR-induced NAD^+ depletion. However, its expression was not sufficient in all contexts. IFNγ-stimulated macrophages upregulated PARP14 levels similar to those seen with LPS; however, this did not engender a depletion of NAD^+. Such an observation suggests that there must be some second permissive signal required for NAD^+ depletion, perhaps a post-translational modification on PARP14 itself, or the presence of a binding partner. This second permissive signal must be constitutively activated in HEK 293T cells, as PARP14 overexpression was sufficient in that context to deplete NAD^+ levels. However, in

macrophages, we were unable to overexpress PARP14 to cause an NAD^+ depletion. This could be because (1) expression was not sufficiently high enough, (2) the lentiviruses used to deliver PARP14 changed the behavior of the macrophages, or (3) this permissive signal was not present. Our inability to date to generate a highly active recombinant PARP14 in *E. coli* for *in vitro* studies may also be due to a lack of activation.

Secondly, the mechanism by which NAD^+ is depleted is currently unclear. PARP14 is a mono-ADP- ribosyltransferase and requires a peptide substrate, so it is an unlikely culprit to be a major consumer of NAD^+. We have shown in 293T cells that its macro domains are not necessary for activity, but its PARP catalytic domain is required. As PARP14 also contains and RNA recognition motif (RRM), and many putative PARP14 ADP-ribosylation targets are RNA binding proteins, we hypothesize that PARP14 may be ADP-ribosylating RNA. Ongoing experiments with RRM deletion mutants and with immunoprecipitated PARP14 from 293T cells are focused on unraveling such a mechanism.

Additionally, we would like to characterize further biological effects of this temporal NAD^+ depletion. We have already identified that the drop in NAD^+ levels robs PARP1 of its substrate and activity, which can be restored via PARP14-specific inhibition with OUL35 or with NAD^+ repletion via NRH. We currently seek to measure whether the activity of sirtuins is similarly altered. This is more difficult to measure than is PARP1 activity as it requires immunoprecipitating sirtuin targets and immunostaining with an acetyl-lysine antibody. Furthermore, we would like to identify physiological consequences of this depletion, either in macrophages or *in vivo*, especially in the spleen where we see a large effect. Previous studies have depleted NAD^+, e.g. with the NAMPT inhibitor FK866, for much longer periods of time (Cameron et al., 2019; Halvorsen et al., 2015; Schilling et al., 2012; Van Gool et al., 2009; Venter et al.,

2014). As the biologically-activated depletion which we have described is eventually reversed through putative feedback mechanisms, its effects are likely less severe than are than are the effects of longer term depletion.

One future direction of this work is to explore whether PARP14 has a role in regulating NAD^+ levels under a high fat diet, which has previously been shown to suppress NAD^+ levels relative to those in mice on a lean diet (Cantó et al., 2012; Yoshino et al., 2011). In this study, I have shown that palmitic acid causes such a depletion of NAD^+. It is plausible that similar saturated fatty acids from a high fat diet induce inflammation via TLR signaling and PARP14 expression. Perhaps mice given PARP14 inhibitors or PARP14 knock-out mice are protected from some of the detrimental effects of a high fat diet and metabolic syndrome.

Another future direction is research into improved PARP14 inhibitors, which has also been a focus for other research groups (Holechek et al., 2018; Peng et al., 2017; Schuller et al., 2017; Yoneyama-Hirozane et al., 2017). OUL35 was identified originally as a PARP10 inhibitor, with off-target activity against PARP14 at micromolar concentrations (Venkannagari et al., 2016). Worse, while OUL35 is sufficiently soluble in dimethyl sulfoxide for *in vitro* cell culture experiments, it is scarcely soluble in any solvent amenable for *in vivo* studies. In order to deliver it in sufficient concentrations, it had to be first dissolved in a solubilization agent, HP-β-cyclodextrin, with heat, as well as the thickening agent carboxymethylcellulose (CMC), to prevent it from crashing out of solution. This insolubility limited the concentration at which it could be delivered, and inclusion of the CMC made injection of a viscous solution difficult. To date, our lab has made two analogs of OUL35 (synthesized by M. Parvez Alam). One such analog is slightly less active against PARP14 than is OUL35, but still inhibits it in the micromolar range, and importantly is soluble in cyclodextrin at twice the concentrations and without any need for CMC

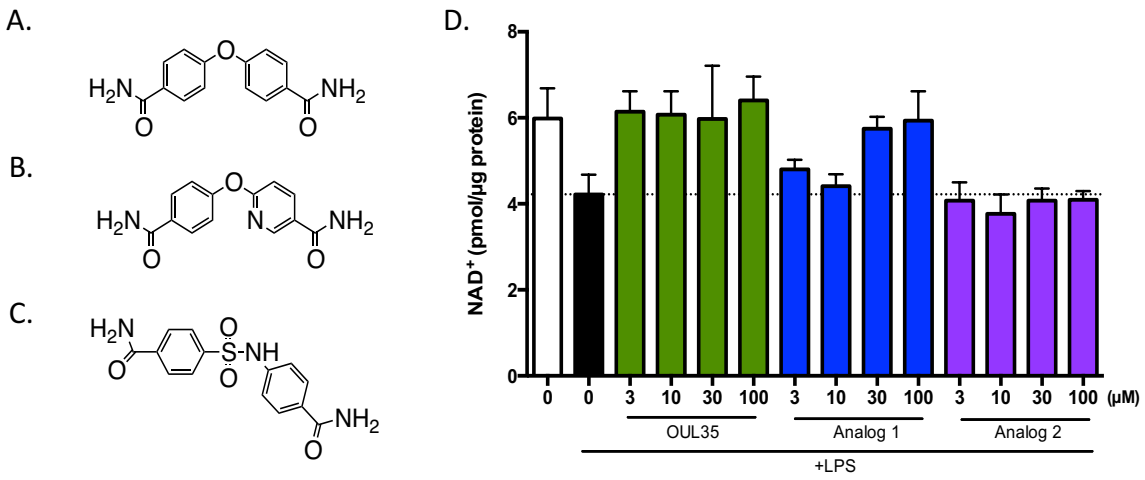

Figure 5.1: Activity of OUL35 analogs. (A) Structure of OUL35, (B) analog 1, and (C) analog 2. (D) Effect of analogs on NAD^+ levels in LPS-treated RAW264.7 cells.

(**Figure 5.1**). Development of PARP14 inhibitors with improved pharmacodynamic and pharmacokinetic profiles would be of benefit for future *in vivo* studies and for potential translation towards clinical indications.

We also showed that NRH is a remarkably effective small molecule NAD^+ booster. It is likely so because it is a synthetic metabolite and may not be governed by normal feedback and clearance mechanisms, or because it is less polar than its natural analogs and therefore crosses the cell membrane much more rapidly, perhaps even without the need for a transporter. While NRH did not prove to be effective at preventing death from LPS-induced septic shock, such a potent molecule may have beneficial effects in other disease models with less severe symptoms.

NAD^+ repletion and pan-sirtuin gene therapy in aged mice

In Chapter 3 of this dissertation, I discuss the implementation of an approach to test combinations of potential longevity-promoting interventions in pre-aged wild-type mice. Using AAV vectors, we overexpressed sirtuins 1-7, in combination with NAD^+-boosting via NMN in the drinking water. We observed that NMN protected from age-related weight loss and engendered a

numerical extension in median and maximum lifespan. However, our study was not sufficiently powered to detect a statistically significant difference in longevity of that magnitude. In another cohort of mice in which we assessed aging-associated phenotypes, we observed an improvement in multiple parameters of walking gait, and an increase in skeletal muscle mass relative to controls. We did not report any interaction between sirtuin overexpression and NMN treatment for any of the phenotypes we measured.

One possible reason for why we did not see larger effects from delivery of AAV vectors is because while the serotype we utilized, AAV9, has a wider tissue distribution than other serotypes, it nonetheless predominantly infects liver and heart (Zincarelli et al., 2008). Peripheral tissues, which certainly contribute to healthspan and lifespan, may not have received a sufficient amount of virus to engender physiological effects. Furthermore, we sought to test the effects of combining expression of all seven sirtuins. While it would not be possible to assemble all seven on the same vector, due to the genome size limit for AAV vectors to be packaged, in theory this would be a more ideal approach. Unpublished data from our lab show that *in vivo* Yamanaka reprogramming effects are much more apparent when factors are assembled on the same AAV vector than when they are delivered on separate vectors (Lu et al., in preparation). Future studies which seek to test the combinatorial effects of genes delivered by this approach should endeavor to combine them in the same vector whenever possible.

One future direction of this research is to delve further into characterizing the sarcopenia-like protection effect of the sirtuin overexpression at the cellular and molecular level. We may examine the skeletal muscles by histology for fiber cross-sectional area, vascularization by CD31 staining, mitochondrial size by electron microscopy, mitochondrial copy number by PCR, gene expression by qPCR, and markers of apoptosis and inflammation by qPCR and Western blot.

Another future direction is to validate the putative NMN longevity effect. The sensitivity in our study was decreased by our control mice, which had a slightly longer than expected lifespan, and by the fact that we only began our study at 20 months of age. We are currently planning to test NMN's effects at a higher dose, beginning at 12 months of age. As NMN is a molecule of great research and clinical interest, it is important to further establish its long-term effects on healthspan and lifespan.

FRIGHT Age and AFRAID Score for age and life expectancy prediction from frailty

In Chapter 4 of this dissertation, I discuss the development of statistical models to infer chronological age and mortality from quick, non-invasive assessments of frailty in aging mice. To produce these models, we measured the parameters of the mouse frailty index (FI) longitudinally in two naturally aging cohorts of wild-type mice. We then applied various machine learning algorithms, trained to predict either chronological age or life expectancy. Our models for both chronological age, termed FRIGHT age, and for mortality, termed AFRAID score, were relatively accurate when analyzed on a per animal basis. FRIGHT age was also retrospectively able to detect the effect of an intervention, enalapril treatment. However, the cross-versality of these models was low – FRIGHT age did not predict mortality any better than did chronological age, while the AFRAID score is more accurate when animals are older and closer to the end of their lifespans.

Future studies should consider measuring FI and applying these models prospectively. Not only will this contribute valuable healthspan information, it will also help to judge the utility of these models for detecting successful aging interventions at early points in time. Incorporation of additional non-invasive biomarkers, especially non-invasive molecular biomarkers if they can be

identified, may further increase the sensitivity and predictive ability of these models, with the goal of developing more accurate biomarkers for biological age.

Metabolite-focused molecular biology

The major focus of this dissertation is the metabolite NAD^+: on dynamic changes in its steady state levels in response to stimuli, on the enzymes that govern this regulation, on approaches to modulate these levels, and on its biological effects. Research focused on a metabolite, rather than on a gene or protein, poses unique challenges. Since the formulation of the central dogma of molecular biology, many biochemical techniques have been developed to assess DNA, RNA, and proteins, which can be applied to nearly any target. DNA and RNA techniques are especially versatile since there is relative uniformity in polymers with only four building blocks; and protein techniques are fairly well developed, given the existence of antibodies against a target with satisfactory performance. However, there is much more diversity around the chemistry necessary to measure and modulate metabolites. Mass spectrometry is the only truly versatile technique, yet it is time consuming and expensive. Beyond this, any given metabolite will require unique assays in order to measure its levels. Luckily in the case of NAD^+ and NADH, multiple assays have been developed, including a very sensitive enzymatic assay, without which much of the research described here would not have been practicable. In addition, further challenges are added when measuring labile metabolites, and if one wishes to measure metabolic flux rather than steady state levels.

Mechanisms to modulate a metabolite are also more individualized than those for a protein, which can be overexpressed or knocked out with now standard molecular biology techniques. Modulation of a metabolite generally cannot be done directly, and requires providing a cell-

permeable, stable precursor (e.g. NRH or NMN), or inhibitor, or overexpressing an enzyme that regulates that metabolite (e.g. NAMPT or PARP14). In spite of these challenges, research continues to progress on the biology of endogenous small molecule metabolites, including but not limited to NAD^+, H_2S, acetyl-coA, and 2-hydroxyglutarate, to name a few (Dang et al., 2009; Hine et al., 2018; Mews et al., 2017). Further developments in techniques to measure and modulate the diverse array of small molecules that inhabit a cell will likely open up new fields of investigation in the future.

Aging as a disease

The unifying theme of this dissertation is on identifying novel mechanisms, interventions, and biomarkers of aging. Although it is certainly valuable to investigate the aging process solely for the benefit of human understanding, it would be a shame if this increased understanding did not also contribute to the benefit of human health. While some previously FDA-approved drugs like metformin and rapamycin seem to slow the aging process, to date no interventions discovered by the aging field have yet to be translated to FDA-approved pharmaceuticals. This will hopefully change in the coming decade as the aging field matures, yet candidate molecules will almost certainly be approved to treat specific age-related indications, rather than for aging as a whole. There are indeed vast regulatory and financial barriers to getting a drug approved for use in all healthy individuals to slow all age-related diseases. Yet, the first barrier may be one of imagination.

The concept of a drug to treat aging is still foreign for many in the medical field, because aging is not considered a disease. As aging affects everyone, it is viewed as a natural process, which it certainly is; but it is no more natural a process than dysregulated physiological states that

are universally recognized as diseases. Ultimately, the question of 'what is a disease' is one of semantics. The practical question is, if aging can be slowed, is it not a goal worth pursuing? From the lens of natural selection, aging occurs as a byproduct of optimizing for growth and reproduction, not as an end in itself. As humanity moves further into the 21st century, the older among us ought not to suffer from age-related diseases needlessly due to an unquestioning acceptance of the healthspans and lifespans bequeathed to us. Wider recognition of the fact that the aging process is something which can be altered, and the translation of discoveries from the lab to the clinic, will be of benefit to human health and welfare.

References

Cameron, A.M., Castoldi, A., Sanin, D.E., Flachsmann, L.J., Field, C.S., Puleston, D.J., Kyle, R.L., Patterson, A.E., Hässler, F., Buescher, J.M., et al. (2019). Inflammatory macrophage dependence on NAD+ salvage is a consequence of reactive oxygen species-mediated DNA damage. Nat. Immunol. *20*, 420–432.

Cantó, C., Houtkooper, R.H., Pirinen, E., Youn, D.Y., Oosterveer, M.H., Cen, Y., Fernandez-Marcos, P.J., Yamamoto, H., Andreux, P.A., Cettour-Rose, P., et al. (2012). The NAD(+) precursor nicotinamide riboside enhances oxidative metabolism and protects against high-fat diet-induced obesity. Cell Metab. *15*, 838–847.

Dang, L., White, D.W., Gross, S., Bennett, B.D., Bittinger, M.A., Driggers, E.M., Fantin, V.R., Jang, H.G., Jin, S., Keenan, M.C., et al. (2009). Cancer-associated IDH1 mutations produce 2-hydroxyglutarate. Nature *462*, 739–744.

Halvorsen, B., Espeland, M.Z., Andersen, G.Ø., Yndestad, A., Sagen, E.L., Rashidi, A., Knudsen, E.C., Skjelland, M., Skagen, K.R., Krohg-Sørensen, K., et al. (2015). Increased expression of NAMPT in PBMC from patients with acute coronary syndrome and in inflammatory M1 macrophages. Atherosclerosis *243*, 204–210.

Hine, C., Zhu, Y., Hollenberg, A.N., and Mitchell, J.R. (2018). Dietary and Endocrine Regulation of Endogenous Hydrogen Sulfide Production: Implications for Longevity. Antioxid. Redox Signal. *28*, 1483–1502.

Holechek, J., Lease, R., Thorsell, A.-G., Karlberg, T., McCadden, C., Grant, R., Keen, A., Callahan, E., Schüler, H., and Ferraris, D. (2018). Design, synthesis and evaluation of potent and selective inhibitors of mono-(ADP-ribosyl)transferases PARP10 and PARP14. Bioorg. Med. Chem. Lett. *28*, 2050–2054.

Mews, P., Donahue, G., Drake, A.M., Luczak, V., Abel, T., and Berger, S.L. (2017). ACETYL-COA SYNTHETASE REGULATES HISTONE ACETYLATION AND HIPPOCAMPAL MEMORY. Nature *546*, 381–386.

Peng, B., Thorsell, A.-G., Karlberg, T., Schüler, H., and Yao, S.Q. (2017). Small Molecule Microarray Based Discovery of PARP14 Inhibitors. Angew. Chem. Int. Ed. Engl. *56*, 248–253.

Schilling, E., Wehrhahn, J., Klein, C., Raulien, N., Ceglarek, U., and Hauschildt, S. (2012). Inhibition of nicotinamide phosphoribosyltransferase modifies LPS-induced inflammatory responses of human monocytes. Innate Immun *18*, 518–530.

Schuller, M., Riedel, K., Gibbs-Seymour, I., Uth, K., Sieg, C., Gehring, A.P., Ahel, I., Bracher, F., Kessler, B.M., Elkins, J.M., et al. (2017). Discovery of a Selective Allosteric Inhibitor Targeting Macrodomain 2 of Polyadenosine-Diphosphate-Ribose Polymerase 14. ACS Chem. Biol. *12*, 2866–2874.

Van Gool, F., Gallí, M., Gueydan, C., Kruys, V., Prevot, P.-P., Bedalov, A., Mostoslavsky, R., Alt, F.W., De Smedt, T., and Leo, O. (2009). Intracellular NAD levels regulate tumor necrosis factor protein synthesis in a sirtuin-dependent manner. Nat. Med. *15*, 206–210.

Venkannagari, H., Verheugd, P., Koivunen, J., Haikarainen, T., Obaji, E., Ashok, Y., Narwal, M., Pihlajaniemi, T., Lüscher, B., and Lehtiö, L. (2016). Small-Molecule Chemical Probe Rescues Cells from Mono-ADP-Ribosyltransferase ARTD10/PARP10-Induced Apoptosis and Sensitizes Cancer Cells to DNA Damage. Cell Chem Biol *23*, 1251–1260.

Venter, G., Oerlemans, F.T.J.J., Willemse, M., Wijers, M., Fransen, J.A.M., and Wieringa, B. (2014). NAMPT-mediated salvage synthesis of NAD+ controls morphofunctional changes of macrophages. PLoS ONE *9*, e97378.

Yoneyama-Hirozane, M., Matsumoto, S.-I., Toyoda, Y., Saikatendu, K.S., Zama, Y., Yonemori, K., Oonishi, M., Ishii, T., and Kawamoto, T. (2017). Identification of PARP14 inhibitors using novel methods for detecting auto-ribosylation. Biochem. Biophys. Res. Commun. *486*, 626–631.

Yoshino, J., Mills, K.F., Yoon, M.J., and Imai, S. (2011). Nicotinamide mononucleotide, a key NAD(+) intermediate, treats the pathophysiology of diet- and age-induced diabetes in mice. Cell Metab. *14*, 528–536.

Zincarelli, C., Soltys, S., Rengo, G., and Rabinowitz, J.E. (2008). Analysis of AAV serotypes 1-9 mediated gene expression and tropism in mice after systemic injection. Mol. Ther. *16*, 1073–1080.